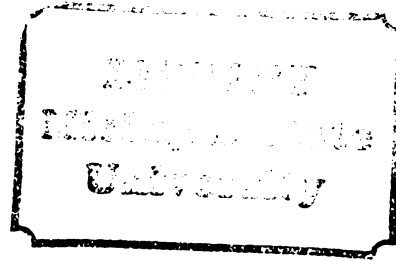


THESIS



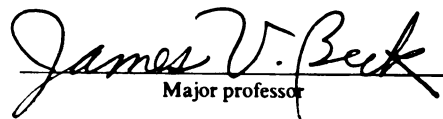
This is to certify that the
dissertation entitled
SURFACE ELEMENT METHOD IN TRANSIENT
HEAT CONDUCTION PROBLEMS

presented by

BAHMAN LITKOUHI

has been accepted towards fulfillment
of the requirements for

PH. D. degree in MECHANICAL ENGINEERING


Major professor

Date 8-11-82



RETURNING MATERIALS:
Place in book drop to
remove this checkout from
your record. FINES will
be charged if book is
returned after the date
stamped below.

--	--	--

SURFACE ELEMENT METHOD IN TRANSIENT
HEAT CONDUCTION PROBLEMS

By

Bahman Litkouhi

A DISSERTATION

Submitted to
Michigan State University
in partial fulfillment of the requirements
for the degree of

DOCTOR OF PHILOSOPHY

Department of Mechanical Engineering

1982

ABSTRACT

SURFACE ELEMENT METHOD IN TRANSIENT HEAT CONDUCTION PROBLEMS

By

Bahman Litkouhi

The heat transfer between two (or more) bodies with perfect or imperfect contact at the interface is of fundamental importance in heat transfer studies and it has accordingly received considerable attention over the last two or three decades. It is important in the problems involving electric contact, electronic cooling, welding, fins, contact conductance and many other applications for which two (or more) similar or dissimilar bodies are attached one to the other over a small part of their surface boundaries. In general, it is difficult to obtain analytical solutions to such problems.

The transient surface element method (SEM) is a new numerical method for solution of linear transient two- and three-dimensional heat transfer problems. The method is well-suited for the above mentioned problems compared with the other numerical procedures such as finite difference (FD), finite element (FE) or boundary integral equation (BIE) methods. In the SEM only the interface between the two geometries requires discretization as opposed to discretization of the whole domain needed in the FD and FE or discretization of the whole boundary in the BIE method. This in turns reduces the size of numerical calculation and computer time.

In this dissertation a multinode transient surface element method for two-dimensional heat conduction problems with linear boundary conditions has been developed and formulated. The method uses Duhamel's integral and involves the inversion of a set of Volterra integral equations, one for each surface element. Computer programs were written and the following three different problems were solved: i) two semi-infinite bodies initially at two different temperatures suddenly brought together over a small circular area and insulated elsewhere, ii) the intrinsic thermocouple problem, and iii) a semi-infinite body with mixed boundary condition if a step change of the surface temperature over an infinite strip.

For each of these problems the multinode SEM performed well. The results showed excellent agreement with those obtained by other investigators. It was found that very high accuracy is attainable with a relatively small number of surface elements. This feature makes the method superior to the alternative numerical procedures such as FD, FE, or BIE methods for the type of problems considered.

ACKNOWLEDGEMENT

The author wishes to express his deepest appreciation and gratitude to his major advisor, Chairman of his Guidance Committee, Professor James V. Beck for his contributions, guidance and encouragement during the course of this research and also for his friendship and painstaking review of this dissertation.

The author is also grateful to the other members of the Committee, Professor Mahlon C. Smith, Professor Larry J. Segerlind, and Professor K. Jayaraman for their guidance and valuable discussions.

Financial support for this research was provided by the National Science Foundation under grant number CME 79-20103 which is greatly appreciated. Gratitude is also extended to the Department of Mechanical Engineering and the Division of Engineering Research for their financial support and cooperations.

To his wife Mahshad, the author dedicates this dissertation for her understanding and moral support during the graduate study and research.



TABLE OF CONTENTS

	Page
LIST OF TABLES	v
LIST OF FIGURES	vii
LIST OF SYMBOLS	xi
CHAPTER 1. INTRODUCTION AND DEVELOPMENT OF INTEGRAL EQUATIONS	1
1.1 Introduction	1
1.2 Mathematical Description	7
1.3 Duhamel's Integral	12
1.4 Derivation Of Duhamel's Integral Equation for Arbitrary Time and Space Variable Heat Flux Boundary Condition in a Two-Dimensional Region	13
1.5 Integral Equation Formulation	18
CHAPTER 2. SURFACE ELEMENT METHOD FOR TWO BODIES IN CONTACT	22
2.1 Introductory Remarks	22
2.2 Problems to be Considered	23
2.3 Discretization Over Space	23
2.4 Surface Element Formulation for Two-Bodies in Contact	26
2.5 Solution of Simultaneous Integral Equations	32
CHAPTER 3. TWO SEMI-INFINITE BODIES IN CONTACT OVER A CIRCULAR AREA	40
3.1 Introduction	40
3.2 Statement of the Problem	43
3.3 Surface Element Solution	44
3.4 Temperature at the Surface of a Semi-Infinite Body with a Disk Heat Source	46
3.5 Thermal Constriction Resistance of the Two Solids	52

	Page
3.6 Results and Discussion	53
CHAPTER 4. INTRINSIC THERMOCOUPLE PROBLEM	75
4.1 Introduction	75
4.2 Statement of the Problem	83
4.3 Solution	83
4.4 Results and Discussion	86
CHAPTER 5. SEMI-INFINITE BODY WITH MIXED BOUNDARY CONDITIONS	98
5.1 Introduction	98
5.2 Statement of the Problem	100
5.3 Solution	107
5.4 Solution to the Interior Region	107
5.5 Results and Discussion	107
CHAPTER 6. TEMPERATURES IN SEMI-INFINITE BODY HEATED BY CONSTANT FLUX q_0 OVER HALF SPACE	117
6.1 Introduction	117
6.2 Mathematical Description	118
6.3 Derivation of the Solution	118
6.4 Other cases of Boundary Condition	132
CHAPTER 7. SUMMARY AND CONCLUSIONS	144
APPENDIX A DERIVATION OF EQUATIONS (2.5.11a) and (2.5.11b) ..	148
APPENDIX B EVALUATION OF $I(r^+, b^+)$ GIVEN BY (3.4.5b)	150
APPENDIX C EVALUATION OF THE INTEGRAL IN EQUATION (6.3.11) ..	154
REFERENCES	156



LIST OF TABLES

Table	Page
3.1 Values of the influence function, ϕ_{kjM} , for semi-infinite body at dimensionless time $t_M^+ = .001$	54
3.2 Values of the influence function, ϕ_{kjM} , for semi-infinite body at dimensionless time $t_M^+ = 1$	54
3.3 Values of the influence function, ϕ_{kjM} , for semi-infinite body at dimensionless time $t_M^+ = 1000$	55
3.4 Results for elemental heat flux q_j , for an isothermal disk region on the surface of a semi-infinite body ($t^+ = \alpha t/a^2$).	57
3.5 Normalized spatial variation of the surface heat flux at different times for the geometry of Case a, see Fig. 3.1. ($q^+ = q/q_{CL}$ vs $r^+ = r/a$).	58
3.6 Normalized area averaged interface heat flux for the geometry of Case a, see Fig. 3.1. $\bar{q}^+ = \bar{q} / \bar{q}_\infty$	58
3.7 Results for elemental heat flux, q_j , for a disk-shaped interface of two semi-infinite bodies, one of copper and the other of glass ($t^+ = \alpha_1 t/a^2$).	65
3.8 Results for dimensionless constriction resistance, for an isothermal disk region on the surface of a semi-infinite body $R_C^+ = R_C \cdot a \cdot k$	70
3.9 Results for dimensionless constriction resistance for a disk-shaped interface of two semi-infinite bodies, one of copper and the other of glass $R_C^+ = R_C / R_C(\infty)$	71
4.1 Normalized values of elemental interface temperature, T_j^+ , as a function of dimensionless time $t^+ = \alpha_2 t/a^2$	87

Table	Page
4.2 Normalized area averaged temperature histories for chromel substrate and alumel wire.	94
5.1 Comparison between the results obtained from the local- ϕ solution and the averaged- ϕ solution.	115
6.1 Values of Function $H(X,p)$	128
6.2 Values of the functions $H(X,p)$, and $ERFC(pX)$ for various X values.	128
6.3 Number of terms in series of function $H(X,p)$ given by equations (6.3.20a) and (6.3.23a) to obtain 8 decimal places accuracy.	128
6.4 Values of dimensionless temperature for the solution given by equation (6.3.18), for different values of X and Z	133
6.5 Values of dimensionless temperature for various values of x^+ and z^+ due to a strip source at time $t^+ = .25$	128

LIST OF FIGURES

Figure		Page
1.1	Some geometries for intrinsic thermocouple problem	2
1.2	Some geometries for contact conductance problem	2
1.3	Some geometries illustrating mixed boundary conditions.	2
1.4	Geometry showing a two-dimensional heat conduction problem.	8
1.5	Geometries illustrating various types of boundary conditions in a two-dimensional region	8
1.6	Geometry showing a two-dimensional region heated by an arbitrary heat flux only over a portion of its boundary.	14
2.1	Geometry showing a discretization over the heated portion of the surface boundary.	24
2.2	Uniform heat flux assumption over each element.	24
2.3	Geometry of semi-infinite slab attached to a semi-infinite body.	28
2.4	Possible distribution of surface elements for connected semi-infinite body and slab.	28
2.5	Basic building blocks for the geometries of semi-infinite body and semi-infinite slab.	31
2.6	Geometry illustrating uniform heat flux assumption over each time interval.	31
3.1	Geometry of a semi-infinite body with a step change of the surface temperature over a circular area.	42
3.2	Distribution of surface elements for two semi-infinite bodies in contact over a circular area. .	42
3.3	Semi-infinite body heated over an annular-shaped region $a_{j-1} < r < a_j$ and $z=0$	47

Figure	Page
3.4 Semi-infinite body heated over a circular area $0 < r < a$ and $z = 0$	47
3.5 Geometry describing the influence functions for a semi-infinite body.	48
3.6 Geometry of semi-infinite insulated cylinder with constant disk heat source.	48
3.7 Normalized heat flux distributing across the interface at various times for the geometry of Case a, see Fig. 3.1.	60
3.8 Normalized area averaged interface heat flux versus dimensionless time for the geometry of Case a, see Fig. 3.1.	61
3.9 Percent of relative error in the area averaged interface heat flux with respect to SEM solution as a function of time for Case a, see Fig. 3.1.	62
3.10 Normalized interface temperature distribution for the geometry of Case b, see Fig. 1.2a. (Normalized with respect to initial temperature of body 2, copper).	66
3.11 Dimensionless area averaged interface heat flux versus dimensionless time for the geometry of Case b, see Fig. 1.2a. (Normalized with respect to the steady state of value \bar{q}).	67
3.12 Dimensionless area averaged interface temperature versus dimensionless time for the geometry of Case b, see Fig. 1.2a. (Normalized with respect to the steady state value of \bar{T}).	68
3.13 Normalized thermal constriction resistance across the interface versus time for the geometry of Case b.	72
3.14 Percent of relative error in thermal constriction resistance, R_C^+ , with respect to SEM solution as function of time, Case a.	73
4.1 The geometry for Burnett's problem.	77
4.2 Henning and Parker's idealized geometry for an intrinsic thermocouple problem.	77

Figure	Page
4.3 Finite difference mesh for Model II considered in reference [27].	80
4.4 Finite difference mesh for Model III considered in reference [27].	81
4.5 Discretization of the interface between the semi-infinite thermocouple wire and the semi-infinite substrate.	85
4.6 Normalized interface temperature distribution for intrinsic thermocouple with chromel half-space and alumel wire.	88
4.7 Normalized heat flux distribution across the interface at various values of time for intrinsic thermocouple. .	91
4.8 Normalized area averaged interface temperature histories for intrinsic thermocouple problem.	92
4.9 Percent of relative error (with respect to SEM solution) in interface temperature as function of time for intrinsic thermocouple problem.	96
4.10 Normalized area averaged interface heat flux histories for intrinsic thermocouple problem.	97
5.1 Geometry for Sadhal's problem.	99
5.2 Possible distribution of surface elements for the problem of semi-infinite body with constant surface temperature, T_c , over an infinite strip.	101
5.3 Variation of the normalized area averaged interface heat flux with number of time steps used in the calculations.	109
5.4 Variation of the normalized area averaged interface heat flux with the size of elements.	111
5.5 Results of average interface heat flux using different number of elements along the interface (local ϕ 's used).	112
5.6 Normalized heat flux distribution across the strip at various values of time.	113

Figure	Page
5.7 Comparison of the multinode surface element solution and the approximate analytical single node solutions for the early and the late times.	116
6.1 Geometry of a semi-infinite region heated by a uniform heat flux, q_0 , over half space $-\infty < x < 0$ and $z=0$	119
6.2 Geometry showing various regions of $ p <1$, $ p =1$, and $ p >1$	125
6.3 Function $H(X,p)$ versus X for different values of p	129
6.4 Dimensionless temperature $T(X,Z)$ versus X for different values of Z in semi-infinite body heated by a uniform heat flux over half space $x<0$, $z=0$	134
6.5 Lines of dimensionless isotherms in semi-infinite body heated by a uniform heat flux over half space $x < 0$	135
6.6 Various possible cases that can be treated using the solution given for figure 6.1 as a building block.	137
6.7 Geometry of a semi-infinite body heated by a uniform heat flux, q_0 , over an infinite strip with width $2a$	138
6.8 Dimensionless temperatures $T(x^+,z^+,t^+)$ versus x^+ , for various values of z^+ at $t^+=.25$	140
6.9 Dimensionless surface temperature $T(x^+,0,t^+)$ versus dimensionless x^+ , for various values of dimensionless times.	141
6.10 Dimensionless isotherms in semi-infinite body heated by a uniform heat flux over an infinite strip at $z^+=0$, for $t^+=1$	142

LIST OF SYMBOLS

a	Raduis of the Contact area
A_c	Contact area
A_j	Area of the surface element j
b	Raduis of cylinder
b^+	Dimensionless value of b given by (3.4.5c)
\bar{B}	Matrix defined by (2.5.12)
C_p	Specific heat
\bar{C}	Matrix defined by (2.5.8a)
$C_i(\cdot)$	Cosine integral
\bar{D}	Vector defined by (2.5.8b)
$e_n(\cdot)$	Truncated exponential function
$\text{erf}(\cdot)$	Error function
$\text{erfc}(\cdot)$	Complementary error function
\bar{E}	Vector defined by (2.5.8c)
$E(\cdot)$	Complete elliptic integral of the 2nd kind defined by (3.4.4b)
$E_1(\cdot)$	Exponential integral
\bar{F}	Vector defined by (2.5.8d)
$F(t)$	Time-varying input function
h_s	Heat transfer coefficient
\bar{H}_M	Conductance matrix at time $t_M = M \cdot \Delta t$
$H(X,P)$	Function defined by (6.3.17)
$\text{ierfc}(\cdot)$	Iterated error function

$I(r^+, b^+)$	Function defined by (3.4.5b)
$J_k(\cdot)$	Bessel function of the kth order
k	Thermal conductivity
$K(\cdot)$	Complete elliptic integral of the 1st kind defined by (3.4.4a)
M	Time index
n_s	Outward normal direction
N	Number of surface elements
p	Variable defined by (6.3.10c)
q	Heat flux
q_0	Constant surface heat flux
q_{cL}	Center line heat flux
\bar{q}	Area averaged interface heat flux
\bar{q}_M	Heat flux vector at time $t_M = M \cdot \Delta t$
$Q_C(t)$	Total heat flow through the contact area as a function of time
\bar{r}	position vector
r	Radial coordinate
r^+	Dimensionless radial coordinate
R	Interior region
R_C	Thermal constriction resistance
R_C^+	Normalized thermal constriction resistance
s	Coordinate along the boundary
S	Surface boundary
$S_i(\cdot)$	Sine integral
t	Time
t^+	Dimensionless time
T	Temperature
T_s	Surface temperature

T_{∞}	Ambient temperature
T_i, T_0	Initial temperatures
\bar{T}	Area average interface temperature
\bar{T}_i	Initial temperature vector
$\bar{T}_c(t)$	Average temperature of the contact area as a function of time
T_c^+	Normalized contact area temperature
\hat{T}	Instantaneous temperature
T	Dimensionless temperature defined by (6.3.10d)
u	Variable defined by (6.3.8)
w	Width of the slab (see Fig. 2.3)
x	Cartesian coordinate
x^+	Dimensionless x defined by (6.4.2a)
X	Dimensionless x defined by (6.3.10a)
y	Cartesian coordinate
z	Axial and Cartesian coordinates
z^+	Dimensionless z defined (6.4.2b)
Z	Dimensionless z defined by (6.3.10b)
α	Thermal diffusivity
β	Variable defined by (4.4.2)
γ	Euler's Constant
$\Gamma(.,.)$	Incomplete gamma function
η	A point along the surface boundary
θ_{kji}^M	Temperature rise due to unit heat flux defined by (3.3.4)
λ	Dummy variable
ρ	Density
ϕ	Temperature rise for unit heat flux (influence function)

$\hat{\phi}$	Instantaneous temperature for unit heat flux
ϕ_{kji}^m	Temperature rise at element k due to unit heat flux over element j at time $t_i = i \cdot \Delta$ for body m.
$\phi_M^{(x,y)}$	Temperature rise at interior position (x,y) due to unit heat flux at element j at time $t_M = M \cdot \Delta t$
$\bar{\phi}_i$	Influence Matrix at time $t_i = i \cdot \Delta t$
$\psi(\bar{r}, t)$	Fundamental solution
ψ_Q	Flux based fundamental solution
ψ_T	Temperature based fundamental solution

CHAPTER 1

INTRODUCTION AND DEVELOPMENT OF INTEGRAL EQUATIONS

1.1 Introduction

The transient surface element method (SEM) is a new numerical method for solution of linear transient two- and three-dimensional heat transfer problems. Its development originated with the need of solving certain transient composite body problems. There are numerous cases for which similar or dissimilar bodies are attached one to the other over a part of their surface boundaries. Some examples in conduction are problems associated with the intrinsic thermocouple, contact conductance and fins when the transient temperature distribution of the fin including the base is of interest. Other related problems are those with mixed boundary conditions. See Figures 1.1-1.3. In general it is difficult to obtain analytical solutions for such problems. The SEM described and developed in this dissertation is particularly suited for such problems compared with other numerical procedures.

The most widely used numerical method in heat transfer is the finite difference method (FDM) [1,2]. It involves approximating the partial differential equations by simpler, localized algebraic ones valid at a series of nodes within the region. The method is extremely valuable for problems involving composite bodies, nonhomogeneous boundary conditions, and nonlinearity in the differential equations or boundary conditions.

The finite element method (FEM) is similar to the FDM. The main difference between the FEM and the FDM is in the way of constructing the algebraic equations. The FDM involves approximating derivatives in differential equations, while in the FEM the approximating equations

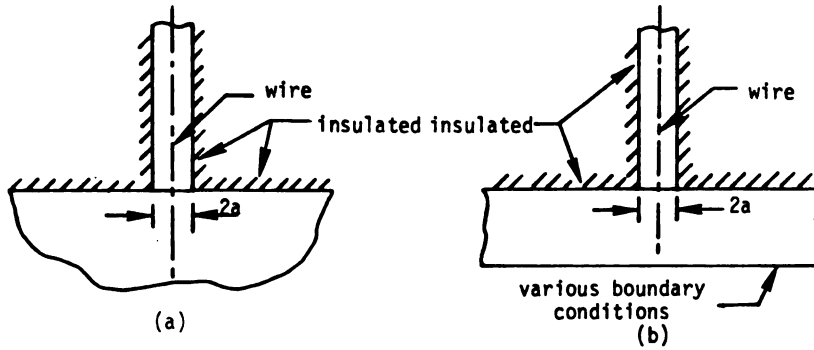


Figure 1.1 Some geometries for intrinsic thermocouple problem.

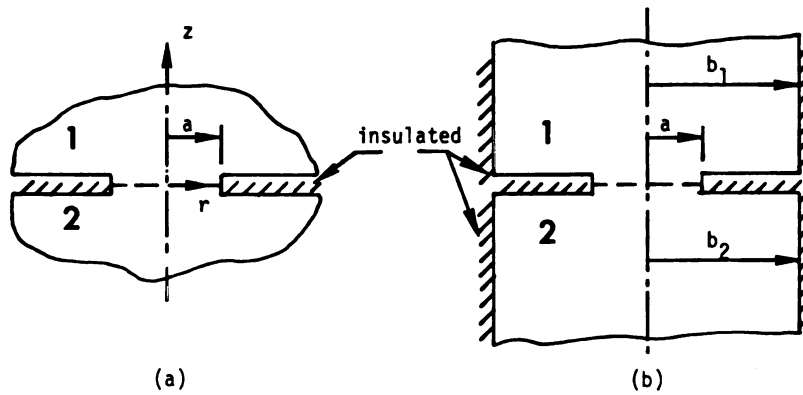


Figure 1.2 Some geometries for contact conductance problem.

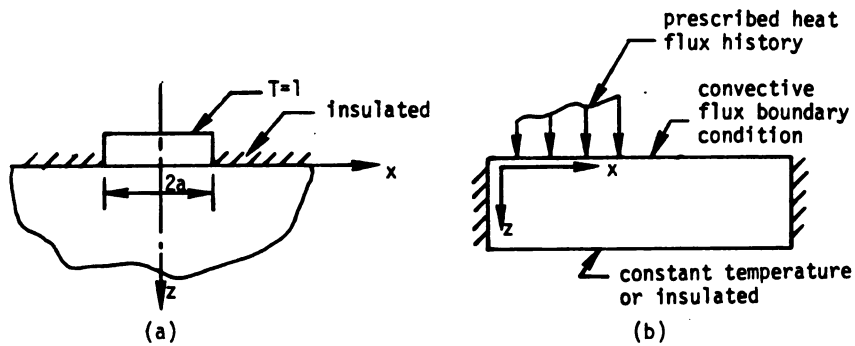


Figure 1.3 Some geometries illustrating mixed boundary conditions.

are cast in an integral form [3]. This approximation results from a minimization process based upon the theories of variational calculus. In general, the FEM is best designed to handle complex boundaries, while the FDM is superior for complex equations.

For the problems mentioned above, the use of the FDM or the FEM is not entirely satisfactory. This is partly due to the necessity of setting up extremely fine grids near the interface, and many large grids further from the interface. Further, both methods involve whole-body discretization schemes which require, finally, the solution of very large system of algebraic equations, especially for two- and three-dimensional problems. These methods unavoidably generate the solution at all internal nodes, whether or not this information is needed. This causes significant economic disadvantages for many applications where only interface results are of interest.

Closely related to the SEM is the boundary integral equation method (BIEM), also referred as boundary element method (BEM) which has become very popular in recent years. It has been used in a variety of engineering problems such as solid mechanics, fluid flow, seepage, soil mechanics, water waves, heat conduction, electrical problems and a broad range of other applications [4-8]. The method utilizes Green's theorem to formulate the problem described by a partial differential equation in a given region with some specific boundary conditions as an integral equation which applies only to the boundary of the region. Basic building blocks used in the BIEM are source solutions (Green's functions) for infinite homogeneous bodies. The main advantage of the method over alternative numerical methods such as the FDM or FEM is the reduction by one of the dimensionality of the problem under consideration, i.e. two-dimensional problems are reduced to one-dimensional

problems and similarly three-dimensional to two-dimensional ones. This results in considerable savings in the input data and the computer time required to run the problem. A disadvantage of the BIEM is the presence of singularities at the boundaries.

The BIEM is well-suited for solving steady state problems with infinite domain and irregular shaped boundaries. A number of papers have been written for steady state heat conduction problems [9-12]. Schneider [9] examined the constriction resistance problem using the BIEM for isothermal rectangular, hollow rectangular, and circular-annular contacts located on a semi-infinite body. He further (in a joint paper with LeDain [10]), introduced the method to solution of steady state heat conduction problems with special attention given to the corner problem[†]. Khader [11] and Khader and Hanna [12] employed BIEM in conjunction with Kirchhoff's transformation to solve nonlinear steady state heat conduction problems.

Application of the BIEM to transient problems have received less attention compared to the steady state problems. This is due to the complexity resulted by having the independent variable of time. There are two basic ways of handling the effects of time. One is to temporarily eliminate time as an independent variable by utilizing the Laplace transform and then solving the problem in the transform space by using BIEM. The time solution is then obtained by numerical transform inversion. This was the approach taken by Rizzo and Shippy [13] to solve the problem of heat conduction in an infinite cylinder of

[†] This situation arises in the problems with mixed boundary conditions and at geometric corners [10].

an isotropic medium. The other approach (similar to the one used in this dissertation) is to treat the time directly in the same manner as the spatial coordinates are treated, integrating numerically over the time as well as over the boundary of the body [14-16]. Shaw [14] utilized the direct approach to investigate the heat conduction in a circular sector of an isotropic medium. A similar approach was taken by Chang, et al. [15] to treat anisotropic heat conduction in the transient case with heat generation. As a test they applied their method of solution to three specific problems of i) a long square prism, ii) a long circular cylinder, and iii) a hollow eccentric cylinder. Recently, Wrobel and Brebbia [16] employed BIEM to solve three-dimensional axisymmetric transient heat conduction problems of i) a solid circular cylinder with convection, ii) a prolate spheroidal solid with zero initial temperature subjected to a unit surface temperature at time zero, and iii) a solid sphere with time dependent boundary conditions. The time integrations were performed directly by dividing the entire time domain into small intervals. Temperature and heat flux were assumed to be constant over each interval. This assumption made possible the analytical evaluations of the time integrals by using series expansions.

For the problems shown in Figures 1.1 through 1.3 (bodies connected over relatively small area) the SEM is superior to the FDM, FEM or BIEM. In the SEM only the interface between the two geometries required discretization as opposed to the discretization of the whole domain required in the FDM and FEM or discretization of the whole boundary in the BIEM. This in turn reduces the size of numerical calculations and computer time. Further, the SEM does not require any modifications or special handling of points near the domain boundaries unlike the above mentioned alternative methods.

The SEM uses Duhamel's integral and involves the inversion of a set of Volterra integral equations, one for each surface element. Though the method is limited to linear regions it can be used for nonlinear boundary conditions.

Two types of kernels (building blocks or fundamental solutions) can be employed in the SEM; temperature-based and heat flux-based. The SEM requires that these "building blocks" or kernels be known for the basic geometries under consideration. For example, for the contact conductance problem (see Fig. 1.1a) solved in Chapter 3, solution for a constant heat flux over a disk-shaped area on a semi-infinite body is needed. For many geometries the kernels are known or can be obtained simply by analytical or numerical procedures.

Yovanovich [17] suggested the name "surface element" and did early work on a steady state form of SEM. Keltner and Beck [18] and later Beck and Keltner [19], were the first to employ the SEM for transient problems. They have considered only one element along the interface and utilized the Laplace transform technique to obtain "early" and "late" time analytical solutions for certain cases [18,19]. Both types of kernels have been used in their solutions.

In this dissertation a multinode transient surface element method for two-dimensional heat conduction problems with linear boundary conditions is developed and formulated. Only heat flux-based kernels are considered. three different problems are solved and the results are compared with those obtained by the other investigators.

In Chapter 1 mathematical descriptions for two-dimensional heat conduction problems with various types of boundary conditions are presented first. Next, the Duhamel's theorem is introduced

and its application to arbitrary time and space variable heat flux boundary conditions in a two-dimensional region is developed. Finally, integral equations with temperature-based kernel and heat flux-based kernel are discussed.

In Chapter 2, the multinode surface element method formulations for two arbitrary geometries in perfect (or imperfect) contact over part of their boundaries are developed and described. In Chapters 3 and 4, the SEM presented in Chapter 2, is employed to solve the problem of two semi-infinite bodies initially at two different temperatures suddenly brought together over a small circular region and insulated elsewhere (contact conductance problem), and the intrinsic thermocouple problem, respectively.

In Chapter 5, the SEM is further utilized to solve the problem of a semi-infinite body with mixed boundary condition of a step change of the surface temperature over an infinite strip and insulated elsewhere. The kernels required in this chapter are obtained from the exact solution for the problem of a semi-infinite body heated by a constant heat flux over half the surface which is presented in Chapter 6.

Finally, the closure and conclusions are given in Chapter 7.

1.2 Mathematical Description

In this section the equation and the different types of boundary conditions associated with the boundary value problems of heat conduction for two-dimensional bodies are stated and briefly discussed.

Consider the boundary value problem of heat conduction for a two dimensional region R , with the boundary S as shown in Fig. 1.4. The body is assumed to have temperature-independent thermal properties and to be homogeneous and isotropic with no heat generation. The

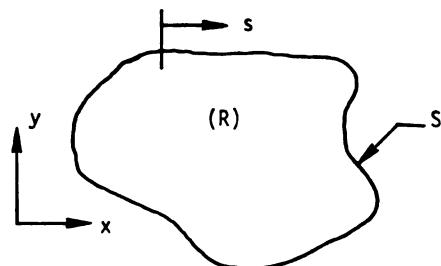


Figure 1.4 Geometry showing a two-dimensional heat conduction problem.

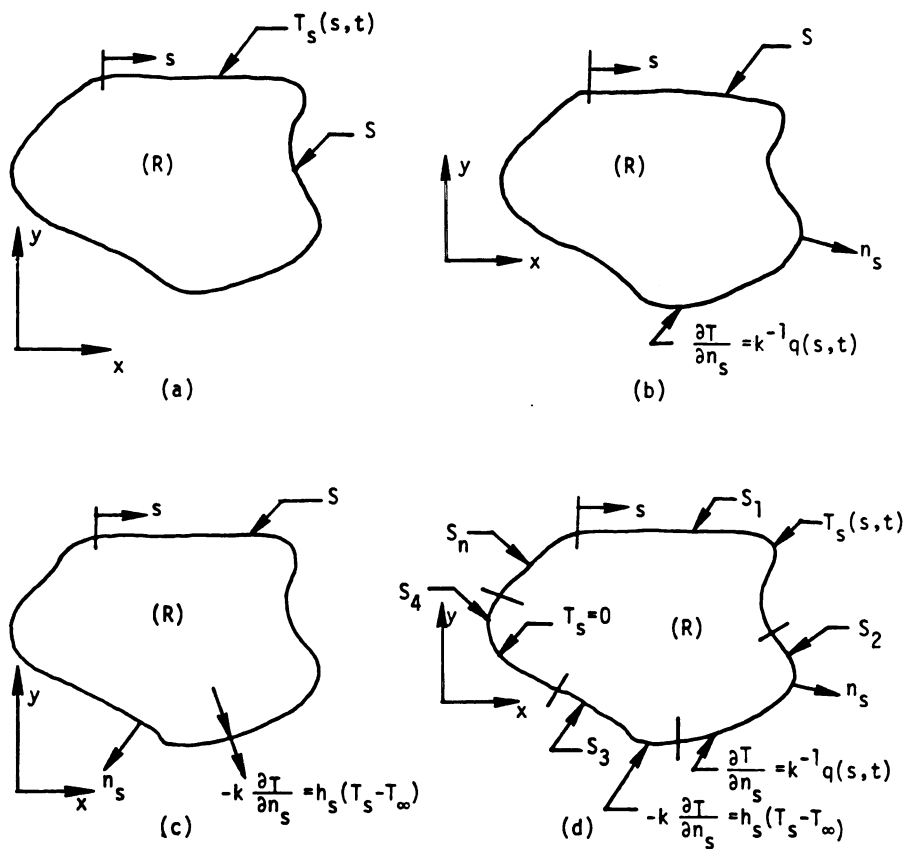


Figure 1.5 Geometries illustrating various types of boundary conditions in a two-dimensional region.

differential equation is,

$$\nabla^2 T(x,y,t) = \frac{1}{\alpha} \frac{\partial T(x,y,t)}{\partial t} \quad (1.2.1)$$

with the initial condition of

$$\begin{aligned} T(x,y,t) &\rightarrow T_i(x,y) \\ \text{as } t &\rightarrow 0 \end{aligned} \quad (1.2.2)$$

where T is the temperature, x and y are the space variables, t is the time, and α is the thermal diffusivity.

Type of Boundary Conditions

In this thesis the primary concern is with linear boundary conditions. Linear boundary conditions, in general, can be separated into four different types.

I. Prescribed Surface Temperature (First Kind)

The surface temperature of the boundaries can be specified to be a constant, a function of time or position, or a function of both position and time,

$$T = T_s(s,t) \quad \text{on } S \quad (1.2.3a)$$

where s denotes location along the surface boundary S . See Fig. 1.5a. If the temperature at the boundary surface vanishes, the homogeneous boundary condition of the first kind is obtained,

$$T = 0 \quad \text{on } S \quad (1.2.3b)$$

II. Prescribed Heat Flux Across the Surface (Second Kind)

In the second type of boundary conditions the normal derivative of temperature is specified to be a constant, or function of time t ,

or position s , or both s and t at the boundary,

$$\frac{\partial T(s,t)}{\partial n_s} = k^{-1}q(s,t) \quad \text{on } S \quad (1.2.4a)$$

where $\frac{\partial}{\partial n_s}$ denotes differentiation with respect to outward pointing normal to the surface boundary S . See Fig. 1.5b. This boundary condition is equivalent to prescribing the magnitude of the heat flux along the boundary. If the normal derivative of the temperature at the boundary surface vanishes, the homogeneous boundary condition of the second kind is obtained (insulation),

$$\frac{\partial T(s,t)}{\partial n_s} = 0 \quad \text{on } S \quad (1.2.4b)$$

III. Heat Transfer to the Ambient by Convection (Third Kind)

If the flux across the surface boundary is proportional to the temperature difference between the surface boundary and the ambient, the boundary condition is,

$$-k \frac{\partial T(s,t)}{\partial n_s} = h_s [T_s(s,t) - T_\infty(s,t)] \quad (1.2.5a)$$

where T_∞ is the ambient temperature and h_s , the proportionality constant, is the heat transfer coefficient. See Fig. 1.5c. This equation can also be written as,

$$\begin{aligned} k \frac{\partial T(s,t)}{\partial n_s} + h_s T_s(s,t) \\ = h_s T_\infty(s,t) \equiv f(s,t) \quad \text{on } S \end{aligned} \quad (1.2.5b)$$

As $h_s \rightarrow 0$ this case tends to the boundary condition of case II, and as

$h_s \rightarrow \infty$ it tends to the boundary condition of case I. If the ambient temperature is zero, the homogeneous boundary condition of the third kind is obtained,

$$k \frac{\partial T(s,t)}{\partial n_s} + h_s T_s(s,t) = 0 \quad \text{on } S \quad (1.2.5c)$$

IV. Mixed Boundary Condition

In this case all or some of the previous types of boundary conditions may be specified over different portions of the boundary S .

$$\begin{aligned} T &= T_s(x,t) && \text{on } S_1, \\ k \frac{\partial T(s,t)}{\partial n_s} &= q(s,t) && \text{on } S_2, \\ k \frac{\partial T(s,t)}{\partial n_s} + h_s T_s(s,t) &= h_s T_\infty(s,t) && \text{on } S_3, \\ T &= 0 && \text{on } S_4, \end{aligned} \quad (1.2.6)$$

and so on. See Fig. 1.5d.

The boundary conditions described above cover most cases of physical problems. There are also the radiative boundary conditions with heat flux obeying the fourth-power temperature law, the natural convection boundary condition, and the interface conditions associated with phase change. Such boundary conditions are nonlinear and are not considered. However, it should be noted that the surface element method is capable of treating nonlinearities at the boundaries and approximately inside domains for certain cases.

1.3 Duhamel's Theorem

Duhamel's theorem provides a means for solving boundary value problems of heat conduction with time dependent boundary conditions. It utilizes the solution to a corresponding fundamental problem with time-independent boundary conditions. This method is a useful tool for obtaining the solution of problems with transient boundary conditions whenever the solution to the corresponding fundamental problem is available.

Duhamel's theorem has been expressed in different forms. Briefly it states that if $\psi(\bar{r}, t)$ is the solution to a linear system initially at zero temperature, due to a unit stepwise input, then the solution to the same system initially, at zero temperature due to a time-varying input $F(t)$ (instead of a unit step) is,

$$T(\bar{r}, t) = \frac{\partial}{\partial t} \int_0^t F(\lambda) \psi(\bar{r}, t-\lambda) d\lambda \quad (1.3.1)$$

where \bar{r} is the position vector, t is the time, and λ is a dummy variable. The input function, $F(t)$, can be any type of time-dependent boundary condition (for instance, prescribed surface temperature, ambient temperature or heat flux), or heat generation. Using Leibnitz's rule for differentiation of an integral, an alternative form of (1.3.1) can be obtained,

$$T(\bar{r}, t) = \int_0^t F(\lambda) \frac{\partial \psi(\bar{r}, t-\lambda)}{\partial t} d\lambda \quad (1.3.2)$$

It also has been conventional to treat problems with arbitrary space-variable conditions by using Duhamel's method with integrating over space [20]. In the following section it is shown that Duhamel's method can be extended to simultaneous variation of both time and space

conditions.

1.4 Derivation of Duhamel's Integral Equation for Arbitrary Time and Space Variable Heat Flux Boundary Conditions in a Two-Dimensional Region

Consider the two-dimensional heat conduction problem given in Section 1.2 with the heat flux boundary conditions given by equation (1.2.4a) for an arbitrary geometry as shown in Fig. 1.5b. This investigation is restricted to systems initially at zero temperatures ($T_i = 0$), because most practical problems can be reduced to this case.

For simplicity it is assumed that $q(s,t)$ is non-zero only over the portion of the boundary S from $s = 0$ to $s = L$, and the other portion of the boundary is insulated ($q(s,t)=0$, for $s > L$). See Fig. 1.6. The objective is to find the expression for the solution of the above problem using Duhamel's integral method.

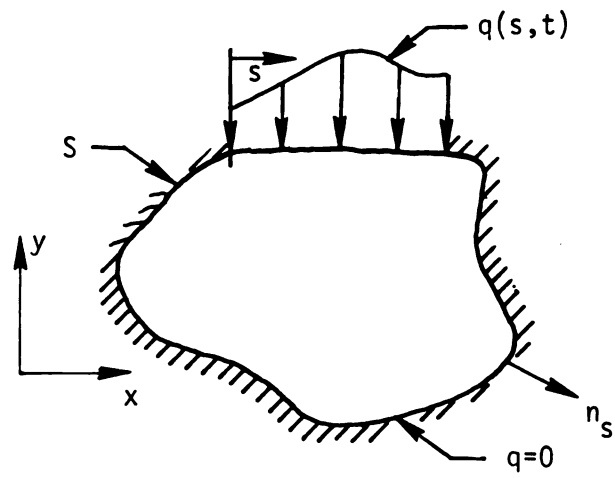
In the first step the solution to the fundamental problem is found. The fundamental problem is identical to the above problem with the exception that the variable flux boundary condition $q(s,t)$ is replaced by a special unit step function. It is described by the following equations:

$$\nabla^2 \psi_q = \frac{1}{\alpha} \frac{\partial \psi_q}{\partial t} \quad (1.4.1)$$

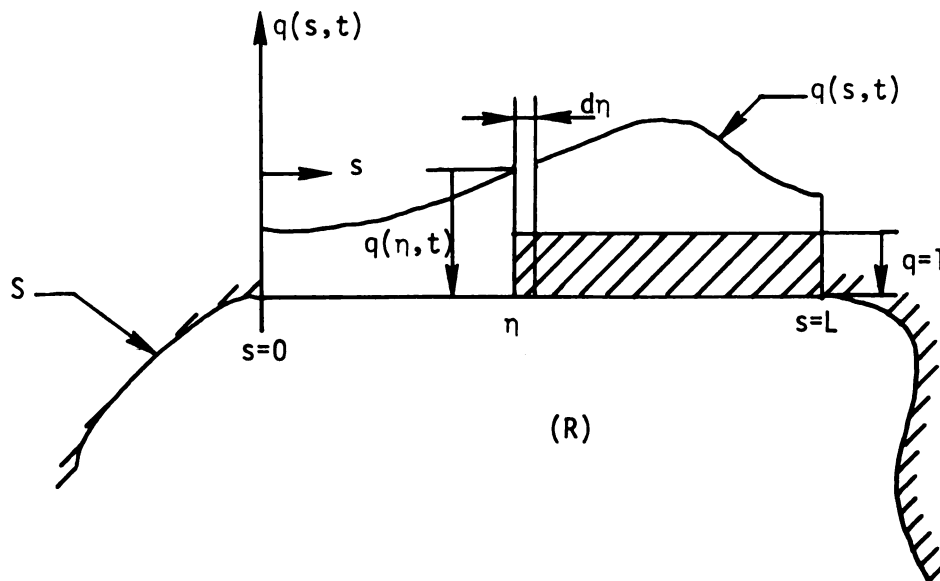
$$\psi_q(x,y,0) = 0 \quad (1.4.2)$$

$$k \frac{\partial \psi_q}{\partial n_s} = \begin{cases} 0 & \text{for } t < 0 \text{ or } s < \eta \\ 1 & \text{for } t > 0 \text{ and } \eta < s < L \end{cases} \quad (1.4.3)$$

where η is a point along S between $s = 0$ to $s = L$, and $\psi_q(x,y,\eta,t)$ is the temperature rise at position (x,y) and time t caused by a unit



(a)



(b)

Figure 1.6 Geometry showing a two-dimensional region heated by an arbitrary heat flux only over a portion of its boundary.

step change of heat flux at time $t = 0$, from η to L ($\eta < s < L$), which is called the Flux Based Fundamental Solution (FBFS). It is indicated in Fig. 1.6 by the cross-hatched portion. Notice that, for fixed (x,y) and t , $\psi_q(x,y,\eta,t)$ decreases as η increases,

$$\psi_q(x,y,\eta,t) > \psi_q(x,y,\eta+d\eta,t) \quad (1.4.4)$$

Temporarily let, η be fixed and consider the variation of the heat flux with time only. From the fundamental solution the temperature rise at position (x,y) and time t due to a unit step change of heat flux at time λ is,

$$\psi_q(x,y,\eta,t-\lambda) \quad (1.4.5)$$

where $(t-\lambda)$ is the time that has elapsed since the step at λ . Also the temperature rise at time t due to a unit step change of heat flux at time $\lambda+d\lambda$ is,

$$\psi_q[x,y,\eta,t-(\lambda+d\lambda)] \quad (1.4.6)$$

Then from (1.4.5) and (1.4.6), the temperature rise at position (x,y) and time t due only to a unit step change in q for $\lambda < t < \lambda+d\lambda$ is

$$-d_\lambda \psi_q(x,y,\eta,t-\lambda) = \psi_q(x,y,\eta,t-\lambda) - \psi_q[x,y,\eta,t-(\lambda+d\lambda)] \quad (1.4.7)$$

where d_λ is a differentiation operator for λ . Notice that $\psi_q(x,y,\eta,t-\lambda)$ is greater than $\psi_q[x,y,\eta,t-(\lambda+d\lambda)]$. Using (1.4.7), the temperature rise at position (x,y) and time t due to the value $q(\eta,t)$ for $\lambda < t < \lambda+d\lambda$ and η being fixed is given by

$$-q(\eta,\lambda) d_\lambda \psi_q(x,y,\eta,t-\lambda) = -q(\eta,\lambda) \frac{\partial \psi_q(x,y,\eta,t-\lambda)}{\partial \lambda} d\lambda \quad (1.4.8)$$

for small $d\lambda$. Since the problem is linear, superposition can be employed and the total effect of all step changes of heat flux over small $d\lambda$'s from time zero to time t is simply found by integrating (1.4.8) from 0 to t . Hence one can write,

$$\psi'_q(x, y, \eta, t) = - \int_0^t q(\eta, \lambda) \frac{\partial \psi_q(x, y, \eta, t-\lambda)}{\partial \lambda} d\lambda \quad (1.4.9a)$$

Since,

$$\frac{\partial \psi_q(x, y, \eta, t-\lambda)}{\partial \lambda} = - \frac{\partial \psi_q}{\partial (t-\lambda)}$$

and

$$\frac{\partial \psi_q(x, y, \eta, t-\lambda)}{\partial t} = \frac{\partial \psi_q}{\partial (t-\lambda)}$$

it is evident that,

$$\frac{\partial \psi_q(x, y, \eta, t-\lambda)}{\partial \lambda} = - \frac{\partial \psi_q(x, y, \eta, t-\lambda)}{\partial t}$$

Therefore (1.4.9a) may be written as,

$$\psi'_q(x, y, \eta, t) = \int_0^t q(\eta, \lambda) \frac{\partial \psi_q(x, y, \eta, t-\lambda)}{\partial t} d\lambda \quad (1.4.9b)$$

where ψ'_q is the temperature rise for the case that q is zero for $s < \eta$, and is uniformly distributed over space for $\eta < s < L$.

Further, one can show that the temperature rise for the case that the heat flux, q , is zero for $s < \eta + d\eta$ and is uniformly distributed for $\eta + d\eta < s < L$, is,

$$\psi'_q(x, y, \eta + d\eta, t) = \int_0^t q(\eta, \lambda) \frac{\partial \psi_q(x, y, \eta + d\eta, t - \lambda)}{\partial t} d\lambda \quad (1.4.10)$$

Using (1.4.9b) and (1.4.10), the temperature rise due to a uniform heat flux q , between $s = \eta$ and $s = \eta + d\eta$ and for $t > 0$ is,

$$\begin{aligned} -d_\eta \psi'_q(x, y, \eta, t) &= \psi'_q(x, y, \eta, t) - \psi'_q(x, y, \eta + d\eta, t) \\ &= - \frac{\partial \psi'_q(x, y, \eta, t)}{\partial \eta} d\eta \end{aligned} \quad (1.4.11)$$

where d_η is a differentiation operator for η . (Notice that $\psi'_q(x, y, \eta, t)$ is greater than $\psi'_q(x, y, \eta + d\eta, t)$.) Introducing (1.4.9b) and (1.4.10) into (1.4.11), one can show,

$$-d_\eta \psi'_q(x, y, \eta, t) = - \int_0^t q(\eta, \lambda) \frac{\partial^2 \psi_q(x, y, \eta, t - \lambda)}{\partial t \partial \eta} d\lambda d\eta \quad (1.4.12)$$

Again superposition can be employed and the total effect of the variation of heat flux from $s = 0$ to $s = L$ can be found by integrating (1.4.12) over space from $s = 0$ to $s = L$.

$$T(x, y, t) = - \int_0^L \int_0^t q(\eta, \lambda) \frac{\partial^2 \psi_q(x, y, \eta, t - \lambda)}{\partial t \partial \eta} d\lambda d\eta \quad (1.4.13)$$

In this problem it was assumed that only a portion of the surface boundary is exposed to heat flux with the remainder being insulated. However, if none of the boundary S is insulated, the first integral in (1.4.13) extends over entire boundary S . Furthermore, if the initial temperature of the system is T_i instead of being zero, the solution becomes

$$T(x,y,t)-T_i = - \int_S \int_0^t q(\eta,\lambda) \frac{\partial^2 \psi_q(x,y,\eta,t-\lambda)}{\partial t \partial \eta} d\lambda d\eta \quad (1.4.14)$$

In the above problem the input function is the heat flux along the boundary which varies with both space and time, and the solution is in terms of the FBFS, ψ_q . If, however, the surface temperature were known along the boundary as the input function, (instead of heat flux), then in a similar manner to that described above, the solution in terms of the Temperature Based Fundamental Solution (TBFS), ψ_T , can be obtained as,

$$T(x,y,t)-T_i = - \int_S \int_0^t [T_s(\eta,\lambda)-T_i] \frac{\partial^2 \psi_T(x,y,\eta,t-\lambda)}{\partial \eta \partial t} d\lambda d\eta \quad (1.4.15)$$

Equations (1.4.14) and (1.4.15) are rather general expressions for the case that the input function varies with both space and time in a two-dimensional region. To the author's knowledge, they do not appear anywhere in the open literature. Colladay [21] has shown the Duhamel's integral equation with flux-based kernel for flow between heated parallel plates. His equation, however, is different from what is given here. In the next section the application of the above equations to the solution of two-dimensional transient heat conduction problems is discussed.

1.5 Integral Equation Formulation

The Duhamel's integral equations given in Section 1.4 are now employed to obtain the solution to equation (1.2.1) subject to the various types of boundary conditions discussed in Section 1.2. The solution can be determined in two different ways, either a) using ψ_T ,

the TBFS, or b) using ψ_q , the FBFS. To compare the two approaches and discuss their utility for each particular type of boundary condition, both form of solutions given by (1.4.14) and (1.4.15) are considered.

For the problems with the boundary conditions of the first type, where the temperature is solely specified everywhere along the boundary, (1.2.3a), the right hand side of (1.4.15) is known, and one can solve for the temperature history of any interior point of R, by direct integration. If, however, (1.4.14) is employed instead of (1.4.15), the direct evaluation of $T(x,y,t)$ is not possible, because of the unknown heat flux, q , in the right hand side of this equation. In this case an inverse problem must be first solved for the unknown surface heat flux which is the required information needed by (1.4.14) to find $T(x,y,t)$ at any interior point. (The inverse problem is discussed further in the solution of the mixed boundary-value problems.) Therefore, in the problems with the first type of boundary condition, (1.4.15), is more appropriate than (1.4.14).

On the other hand if the boundary condition is of the second type where q is solely specified along the boundary S, (1.2.4a), then the right hand side of (1.4.14) is known which leads to evaluation of a direct integral. In this case (1.4.14) is more appropriate than (1.4.15).

For the boundary conditions of the third and fourth type where neither surface temperature nor its normal derivative are completely known over the entire boundary S, none of the above equations can be used directly to obtain temperature history for any interior point. An example is given to illustrate this case better.

Consider the homogeneous convective boundary condition given by (1.2.5c) where the temperature and its normal derivative are related through a linear expression along the boundary as,

$$k \frac{\partial T(s,t)}{\partial n_s} + h_s T_s(s,t) = 0 \quad \text{on } S \quad (1.2.5c)$$

substituting for q in (1.4.14) from (1.2.5c) one can write,

$$T(x,y,t) - T_i = - \int_S \int_0^t h_s T_s(\eta,\lambda) \frac{\partial^2 \psi_q(x,y,\eta,t-\lambda)}{\partial t \partial \eta} d\lambda d\eta \quad (1.4.16)$$

Equation (1.4.16) cannot directly be integrated for $T(x,y,t)$, since $T_s(s,t)$ inside the integral is unknown. In other words the number of unknown functions in (1.4.16) is more than one, $T_s(s,t)$ and $T(x,y,t)$. However, for a point along the boundary S , (1.4.16) reduces to,

$$T_s(s,t) - T_i = - \int_S \int_0^t h_s T_s(\eta,\lambda) \frac{\partial^2 \psi_q(\eta,t-\lambda)}{\partial t \partial \eta} d\lambda d\eta \quad (1.4.17)$$

which is a Volterra integral equation of the second kind with the only unknown function, $T_s(s,t)$, both inside and outside the integral. As an inverse problem (1.4.17) can be solved numerically for $T_s(s,t)$. Once the surface temperature, $T_s(s,t)$, has been determined, the solution to the interior temperature history, $T(x,y,t)$, can be obtained by substituting $T_s(s,t)$ into (1.4.16).

Hence, for the problems with mixed or convective boundary conditions the temperature history at any interior point (x,y) can be determined in two steps:

- a) Find the boundary information by solving an inverse integral equation, and
- b) using the boundary data obtained in a), find the interior temperature history by using a direct integration.

In this thesis the solution of two-dimensional heat conduction

problems only based upon ψ_q (FBFS) is considered. Equation (1.4.14) is the basic starting point in the development of the SEM formula in the following sections. Furthermore, the problems with the first and second type of boundary conditions are not discussed herein, since their solutions can be found explicitly by direct integration.

CHAPTER 2

SURFACE ELEMENT METHOD FOR TWO BODIES IN CONTACT

2.1 Introductory Remarks

The heat transfer between two bodies with perfect or imperfect contact at the interface is of fundamental importance and it has accordingly received considerable attention over the last two or three decades. It is important in the problems involving electric contact, electronic cooling, welding, fins, contact conductance, and many other applications for which two similar to dissimilar bodies are attached one to the other over small parts of their surface boundaries. Some examples are given in Chapter 1. In general it is difficult to obtain analytical solutions to such problems.

In this chapter a transient multinode surface element method for two arbitrary geometries contacting over part of their surface boundaries is developed and formulated. Both cases of perfect contact and imperfect contact are considered. The method starts with the Duhamel's integral equation given by (1.4.14) which is then approximated numerically in a piecewise manner over time, and the boundaries and the interfaces of interest.

The method is superior to the other numerical procedures such as FDM, FEM, or BIEM, for the particular problems mentioned above. In this method only certain parts of boundaries (interface) need to be discretized as opposed to the whole body discretization required in the FDM and the FEM or discretization of the whole boundaries needed in the BIEM.

2.2 Problems to be Considered

To illustrate the capability and limitations of the method, the three different geometries given below are investigated.

The first geometry involves two semi-infinite bodies initially at two different temperatures suddenly brought together over a small circular region and insulated elsewhere (contact conductance problem). See Fig. 1.1a.

The second geometry has a semi-infinite insulated cylinder attached to a semi-infinite body (the intrinsic thermocouple problem). See Fig. 1.2a.

The third geometry is a semi-infinite body with the mixed boundary condition of a step change of the surface temperature over an infinite strip and insulated elsewhere. See Fig. 1.3a.

In each case the solution to the interfacial heat flux is emphasized. For the third geometry, however, the solution to the interior temperature history is also formulated.

2.3 Discretization over Space

In order to solve numerically the integral equation given by (1.4.14), the surface boundary is divided into N finite surface elements Δs_j , as shown in Fig. 2.1. (Notice that only the parts of the boundary with non-zero values of heat flux need to be discretized). Equation (1.4.14) can be written as,

$$T(x,y,t) - T_i = - \int_0^t \left[\sum_{j=1}^N \int_{\Delta s_j} q(n,\lambda) \frac{\partial^2 \psi_q(x,y,n,t-\lambda)}{\partial t \partial n} dn \right] d\lambda \quad (2.3.1)$$

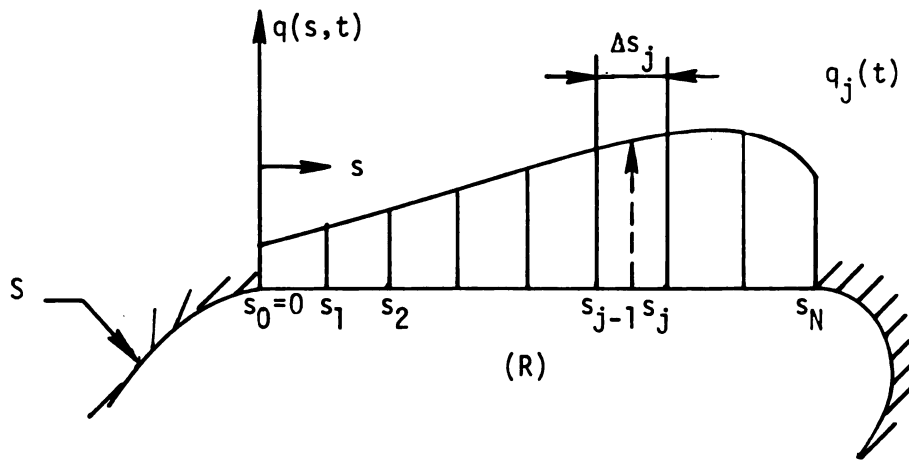


Figure 2.1 Geometry showing discretization over the heated portion of the surface boundary.

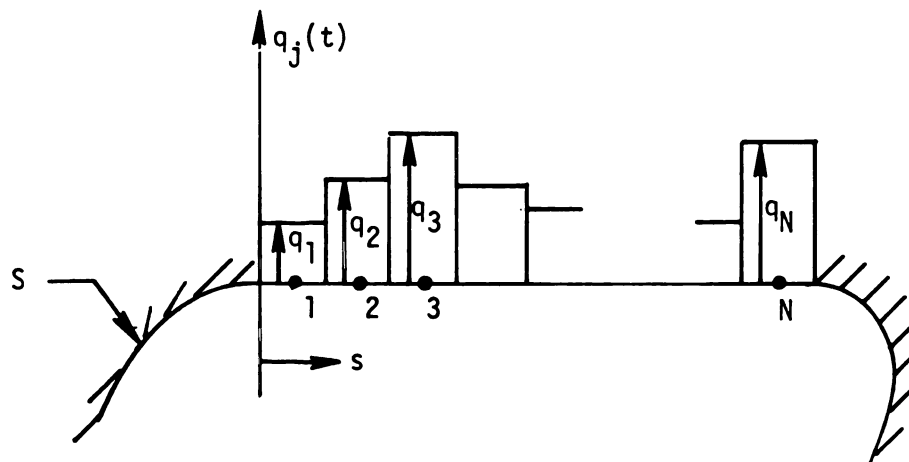


Figure 2.2 Uniform heat flux assumption over each element.

In the simplest form of approximation, the heat flux is assumed uniform over each element (but different, in general, at each element. See Fig. 2.2), so that,

$$\begin{aligned} T(x,y,t)-T_i &= - \int_0^t \left\{ \sum_{j=1}^N q_j(\lambda) \frac{\partial}{\partial t} [\psi_q(x,y,s,t-\lambda) \Big|_{s_{j-1}}^{s_j}] \right\} d\lambda \\ &= - \int_0^t \left\{ \sum_{j=1}^N q_j(\lambda) \frac{\partial}{\partial t} [\Delta\psi_{q_j}(x,y,t-\lambda)] \right\} d\lambda \end{aligned} \quad (2.3.2)$$

where

$$\Delta\psi_{q_j}(x,y,t) = \psi_q(x,y,s_j,t) - \psi_q(x,y,s_{j-1},t) \quad (2.3.3)$$

Further, if the temperature rise at position (x,y) due to a unit step increase in heat flux q at the element j is denoted $\phi_j(x,y,t)$, it can be shown that

$$-\Delta\psi_{q_j}(x,y,t) = \phi_j(x,y,t) \quad (2.3.4)$$

(See Sec. 1.4). Using (2.3.4) in (2.3.2) results in

$$T(x,y,t)-T_i = \sum_{j=1}^N \int_0^t q_j(\lambda) \frac{\partial \phi_j(x,y,t-\lambda)}{\partial t} d\lambda \quad (2.3.5)$$

which gives the temperature rise at location (x,y) and time t due to the effect of N heat flux histories $q_1(t)$, $q_2(t)$, ..., $q_N(t)$. The function $\phi_j(x,y,t)$ is the basic building block solution needed in the above expression and is termed an influence function.

2.4 Surface Element Formulation for Two-Bodies in Contact

In this section the surface element method formulations for two arbitrary geometries in contact over part of their boundaries are developed and described.

a) Perfect Contact

Two different geometries of a semi-infinite body and a semi-infinite slab initially at uniform but different temperatures are brought together into perfect contact over the interface of width w . One side of the slab, $x = 0$, is held at zero temperature and the other parts of the boundaries are assumed to be insulated. See Fig. 2.3. The bodies may have different thermal conductivities, k , and density-specific heats, ρc_p . The upper body is referred to as region 1 ($y > 0$) and the other body as region 2 ($y < 0$). The initial temperatures are denoted by T_{i1} and T_{i2} for regions 1 and 2, respectively. In the rest of the analysis the subscripts 1 and 2 are used in references to the properties of the corresponding regions. The describing differential equations are,

$$\frac{\partial^2 T_1}{\partial x^2} + \frac{\partial^2 T_1}{\partial y^2} = \frac{1}{\alpha_1} \frac{\partial T_1}{\partial t} \quad (2.4.1)$$

$$\frac{\partial^2 T_2}{\partial x^2} + \frac{\partial^2 T_2}{\partial y^2} = \frac{1}{\alpha_2} \frac{\partial T_2}{\partial t}$$

subject to,

$$\begin{aligned} T_1 &= T_{i1} && \text{for } t=0, |x| \geq 0, y \geq 0 \\ T_2 &= T_{i2} && \text{for } t=0, 0 \leq x \leq w, y \leq 0 \end{aligned} \quad (2.4.2)$$

and

$$T_1 = T_{i1} \quad \text{for } t > 0, \text{ as } |x| \rightarrow \infty \quad (2.4.3a)$$

$$\begin{aligned} T_2 &= 0 & \text{for } t > 0, x=0, y < 0 \\ \frac{\partial T_2}{\partial x} &= 0 & \text{for } t > 0, x=w, y < 0 \end{aligned} \quad (2.4.3b)$$

$$\begin{aligned} T_1 &= T_2 \\ k_1 \frac{\partial T_1}{\partial y} &= k_2 \frac{\partial T_2}{\partial y} & \text{for } t > 0, 0 \leq x \leq w, y=0 \end{aligned} \quad (2.4.4a)$$

$$\frac{\partial T_1}{\partial y} = 0 \quad \text{for } t > 0, x < 0 \text{ and } x > w, y=0$$

$$\begin{aligned} T_1 &= T_{i1} & \text{for } t > 0, \text{ as } y \rightarrow \infty \\ T_2 &= T_{i2} & \text{for } t > 0, \text{ as } y \rightarrow -\infty \end{aligned} \quad (2.4.4b)$$

where T_1 and T_2 denote the temperature distributions, k_1 and k_2 represent the thermal conductivities, α_1 and α_2 refer to the thermal diffusivities, x and y are the space coordinates, and t is the time.

Analysis

First, the interface is divided into N finite surface elements (each being an infinite strip), Δx_j , as shown in Fig. 2.4. (If the system is symmetric only half of the interface needs to be discretized.) It is assumed that there is no spatial variation of temperature or heat flux over each element (uniform approximation). The heat fluxes $q_1(t)$, $q_2(t)$, ..., $q_N(t)$ are arbitrary functions to be found. The heat flux $q_j(t)$ which leaves body 2 in Fig. 2.4 is the same heat flux that enters body one over the region $x=x_{j-1}$ to $x=x_j$, that is,

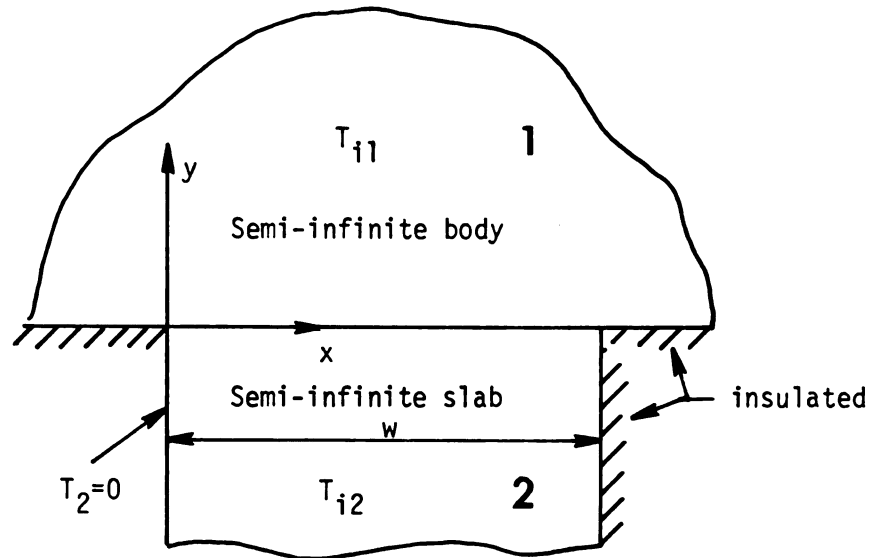


Figure 2.3 Geometry of semi-infinite slab attached to a semi-infinite body.

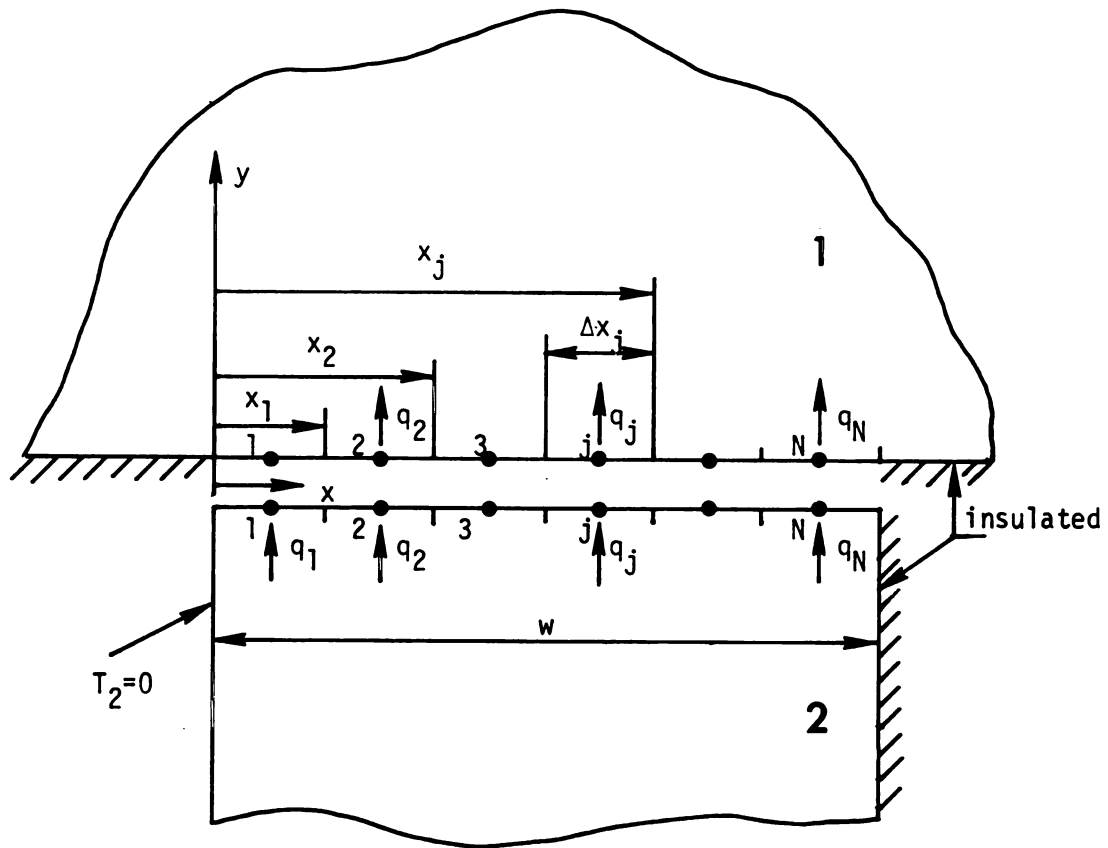


Figure 2.4 Possible distribution of surface elements for connected semi-infinite body and slab.

$$-k_1 \frac{\partial T_1}{\partial y} = -k_2 \frac{\partial T_2}{\partial y} = q_j(t) \quad \text{for } t > 0, x_{j-1} \leq x \leq x_j, y=0 \quad (2.4.5)$$

Using (2.3.5), the temperature at element k in body one and at time t can be given by,

$$T_{k1}(t) = T_{i1} + \sum_{j=1}^N \int_0^t q_j(\lambda) \frac{\partial \phi_{kj}^{(1)}(t-\lambda)}{\partial t} d\lambda \quad (2.4.6a)$$

where

$$T_{k1} \equiv T(x'_k, 0, t), \quad x'_k = x_k - \Delta x_k / 2 \quad (2.4.6b)$$

and

$$\phi_{kj}^{(1)}(t-\lambda) \equiv \phi_j^{(1)}(x'_k, 0, t-\lambda) \quad (2.4.6c)$$

is the temperature rise at element k and time t due to a unit step heat flux at element j of surface 1. $\phi_{kj}^{(1)}(t)$ is the basic building block needed for body 1. It can be found from the known solution given in Chapter 6, for a constant heat flux over an infinite strip of a semi-infinite body. See Fig. 2.5a.

Similar to (2.4.6a), an integral equation can be given for the k th surface element of body 2,

$$T_{k2}(t) = T_{i2} - \sum_{j=1}^N \int_0^t q_j(\lambda) \frac{\partial \phi_{kj}^{(2)}(t-\lambda)}{\partial t} d\lambda \quad (2.4.7a)$$

where

$$T_{k2} \equiv T_2(x'_k, 0, t) \quad (2.4.7b)$$

and

$$\phi_{kj}^{(2)}(t-\lambda) \equiv \phi_j^{(2)}(x_k', 0, t-\lambda) \quad (2.4.7c)$$

is the temperature rise at element k and time t due to a unit step heat flux at element j of surface 2. The minus sign before the summation in (2.4.7a) is used because the heat flux is pointing outward from body 2. The basic building block for body 2, $\phi_{kj}^{(2)}(t)$, can be found from the solution of a semi-infinite slab heated over an infinite strip with zero temperature on one side and insulated on the other side. See Fig. 2.5b. This solution can be obtained from the known solution for a constant heat flux over an infinite strip of a semi-infinite body by using the method of images (see Chapter 6, and [22].)

For the case where the bodies are in perfect contact, one can write,

$$T_{k1}(t) = T_{k2}(t) \quad \text{for } k=1, 2, \dots, N \quad (2.4.8)$$

By introducing (2.4.6a) and (2.4.7a) into (2.4.8), a set of integral equations for $k=1, 2, \dots, N$ can be found,

$$T_{i2} - T_{i1} = \sum_{j=1}^N \int_0^t q_j(t) \frac{\partial \phi_{kj}(t-\lambda)}{\partial t} d\lambda \quad (2.4.9)$$

where

$$\phi_{kj}(t) = \phi_{kj}^{(1)}(t) + \phi_{kj}^{(2)}(t) \quad (2.4.10)$$

Equation (2.4.9) represents a set of Volterra equations of the first kind which can be solved simultaneously for N unknown heat flux histories $q_1(t)$, $q_2(t)$, ..., $q_N(t)$.

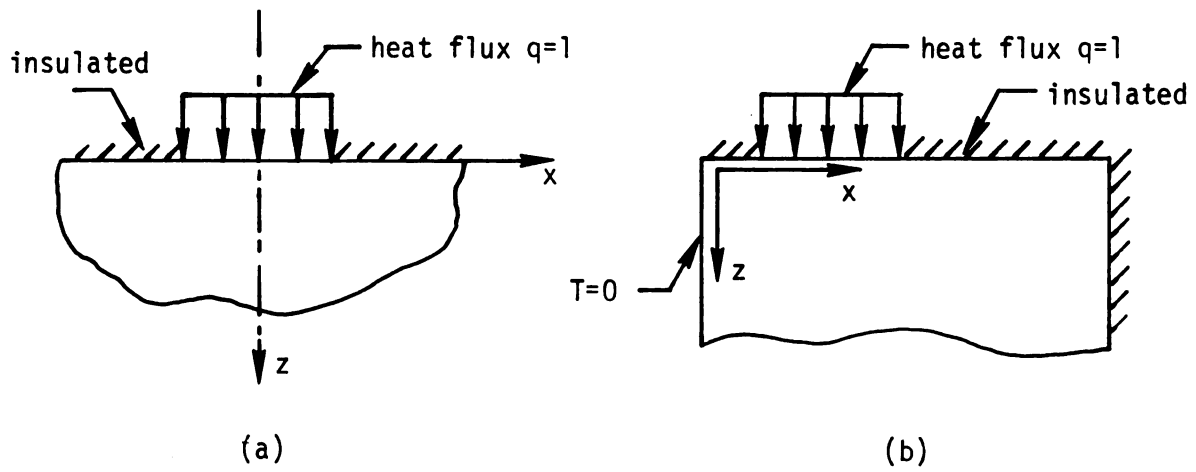


Figure 2.5 Basic building blocks for the geometries of semi-infinite body and semi-infinite slab.

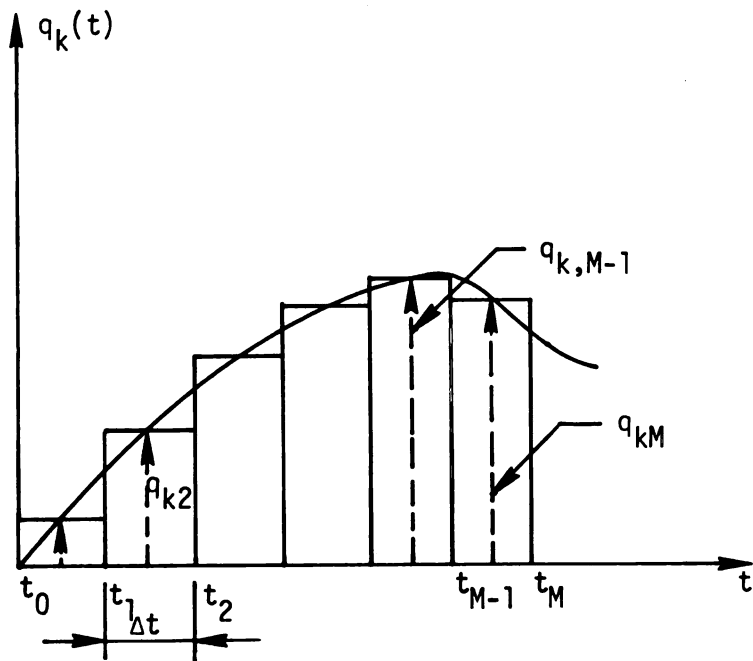


Figure 2.6 Geometry illustrating uniform heat flux assumption over each time interval.

b) Imperfect Contact

Even though the perfect contact is a common interface assumption, it will only be valid for very intimate contact, such as a soldered joint. For imperfect contact (2.4.8) is replaced by

$$q_k(t) = h_k(t) [T_{k2}(t) - T_{k1}(t)] \quad \text{for } k=1, 2, \dots, N \quad (2.4.11)$$

where $h_k(t)$ is the time-variable contact conductance for surface element k . The above relation tends to the case of perfect contact (given by (2.4.8)), as $h_k \rightarrow \infty$. It also includes the cases of convection, prescribed heat flux and prescribed temperature. By introducing (2.4.6a) and (2.4.7a) into (2.4.11), a set of integral equations for heat fluxes $q_k(t)$, $k=1, 2, \dots, N$, can be obtained,

$$T_{i2} - T_{i1} = \frac{q_k(t)}{h_k(t)} + \sum_{j=1}^N \int_0^t q_j(t) \frac{\partial \phi_{kj}(t-\lambda)}{\partial t} d\lambda \quad (2.4.12)$$

$$\text{for } k=1, 2, \dots, N$$

Equation (2.4.12) represents a set of Volterra equations of the second kind with the unknown heat fluxes, $q_k(t)$'s, appearing both inside and outside the integrals. These integral equations can be solved simultaneously in an inverse fashion for the unknown heat fluxes. The method of the solution is described for the case of imperfect contact which includes the other cases as well.

2.5 Solution of the Simultaneous Integral Equations

The Volterra equation (2.4.12) can be approximated by a system of linear algebraic equations by replacing the integrals with suitable quadrature formulas. As the first step, the time region 0 to t is

divided into M equal small time intervals, Δt , so that t_M represents the value of t at the end point of the Mth interval,

$$t \equiv t_M = M\Delta t \quad (2.5.1)$$

Equation (2.4.12) can be written as

$$T_{i2} - T_{i1} = \frac{q_k(t_M)}{h_k(t_M)} + \sum_{j=1}^N \sum_{t=1}^M \int_{t_{i-1}}^{t_i} q_j(\lambda) \frac{\partial \phi_{kj}(t_M - \lambda)}{\partial t} d\lambda \quad (2.5.2a)$$

for $k=1, 2, \dots, N$

where

$$t_0 \equiv 0 \quad (2.5.2b)$$

In the simplest form of approximation the heat flux histories $q_j(t)$ are assumed to have constant values in each time interval (see Fig. 2.6) so that

$$T_i = \frac{q_{kM}}{h_{kM}} + \sum_{j=1}^N \sum_{i=1}^M q_{ji} \Delta \phi_{kj, M-i} \quad \text{for } k=1, 2, \dots, N \quad (2.5.3a)$$

where

$$T_i = T_{i2} - T_{i1} \quad (2.5.3b)$$

$$q_{ji} \equiv q_j[(i-1/2)\Delta t] \quad (2.5.3c)$$

$$\Delta \phi_{kj, M-i} = \phi_{kj, M+1-i} - \phi_{kj, M-i} \quad (2.5.3d)$$

In the form given by (2.5.3a), the heat fluxes q_{jM} 's (for $j=1, 2, \dots, N$) can be determined at different time intervals one after another,

by marching forward in time for,

$$M = 1, 2, 3, \dots$$

While calculating each new time component, the fluxes at previous times,

$$q_{j1}, q_{j2}, q_{j3}, \dots, q_{j,M-2}, q_{j,M-1}$$

are known for $j=1, 2, \dots, N$. Thus for each time step, equation (2.5.3a) represents a system of N equations with N unknowns $q_{1M}, q_{2M}, q_{3M}, \dots, q_{NM}$. The objective is to solve this system for the unknowns q_{jM} , for $j=1, 2, \dots, N$. For convenience define,

$$\phi_{kji} \equiv \phi_j(x'_k, 0, t_i) \quad (2.5.4)$$

Introducing this definition into (2.5.3a) and noting that, $\phi_{kj0}=0$, gives

$$\begin{aligned} \frac{q_{kM}}{h_{KM}} + \sum_{j=1}^N q_{jM} \phi_{kj1} = T_i + \sum_{j=1}^N \sum_{i=1}^{M-1} q_{ji} \phi_{kj,M-1} \\ - \sum_{j=1}^N \sum_{i=1}^{M-1} q_{ji} \phi_{kj,M+1-i} \quad \text{for } k=1, 2, \dots, N \end{aligned} \quad (2.5.5)$$

Equation (2.5.5) is written in standard form with unknowns on the left and knowns on the right.

Expressing (2.5.5) in matrix form gives,

$$(\bar{H}_M + \bar{\Phi}_1) \bar{q}_M = \bar{T}_i + \sum_{i=1}^{M-1} \bar{\Phi}_{M-i} \bar{q}_i - \sum_{i=1}^{M-1} \bar{\Phi}_{M+1-i} \bar{q}_i \quad (2.5.6)$$

with

$$\bar{\Phi}_i \equiv \begin{bmatrix} \phi_{11i} & \phi_{12i} & \dots & \phi_{ini} \\ \phi_{21i} & \phi_{22i} & & \phi_{2Ni} \\ \vdots & & & \\ \phi_{N1i} & \phi_{N2i} & & \phi_{NNi} \end{bmatrix} \quad (2.5.7a)$$

$$\bar{H}_M \equiv \text{diag} \left[\frac{1}{h_{1M}} \quad \frac{1}{h_{2M}} \quad \dots \quad \frac{1}{h_{NM}} \right] \quad (2.5.7b)$$

$$\bar{q}_i \equiv \begin{bmatrix} q_{1i} \\ q_{2i} \\ \vdots \\ q_{Ni} \end{bmatrix}, \quad \bar{T}_i \equiv \begin{bmatrix} T_i \\ T_i \\ \vdots \\ T_i \end{bmatrix} \quad (2.5.7c,d)$$

where $\bar{\Phi}_i$ and \bar{H}_M are called the influence matrix and the conductance matrix, respectively. If further \bar{C} , and \bar{D} are defined to be the matrices,

$$\bar{C} = \bar{H}_M + \bar{\Phi}_1 \quad (2.5.8a)$$

$$\bar{D} = \bar{T}_i + \bar{E} - \bar{F} \quad (2.5.8b)$$

where

$$\bar{E} = \sum_{i=1}^{M-1} \bar{\Phi}_{M-i} \bar{q}_i \quad (2.5.8c)$$

$$\bar{F} = \sum_{i=1}^{M-1} \bar{\Phi}_{M+1-i} \bar{q}_i \quad (2.5.8d)$$

Then (2.5.6) can be written as,

$$\bar{C} \bar{q}_M = \bar{D} \quad (2.5.9)$$

The solution of (2.5.9) is

$$\bar{q}_M = \bar{C}^{-1} \bar{D} \quad (2.5.10)$$

The \bar{C} matrix, multiplier of \bar{q}_M , has to be calculated at each time step if the diagonal matrix \bar{H}_M , is a function of time. However, for the case that the contact conductances do not change with time, the \bar{C} matrix needs to be calculated only once during the entire solution and an alternative form of solution can be given as, (see Appendix A)

$$q_1 = \bar{C}^{-1} \bar{T}_i \quad (2.5.11)$$

$$\bar{q}_M = M\bar{q}_1 + \bar{B} \left[\sum_{i=1}^{M-1} \bar{q}_i \right] - \bar{C}^{-1} \bar{F} \quad \text{for } M=2, 3, \dots \quad (2.5.11b)$$

where

$$\bar{B} = \bar{H}^{-1} \bar{\Phi}_1 \quad (2.5.12)$$

(Since \bar{H} is not a function of time in (2.5.12), the subscript M is dropped.) For the case of perfect contact where $h_{kM} \rightarrow \infty$, the diagonal conductance matrix, \bar{H}_M , becomes zero which implies that,

$$\bar{C} = \bar{\Phi}_1 \quad (2.5.13)$$

Introducing (2.5.8a,c,d) and (2.5.13) into (2.5.10), results in a simpler form of solution as,

$$\bar{q}_1 = \bar{C}^{-1} \bar{T}_i \quad (2.5.14a)$$

$$\bar{q}_M = M\bar{q}_1 - \bar{C}^{-1} \bar{F} \quad \text{for } M=2, 3, \dots \quad (2.5.14b)$$

The elements of the $[N \times N]$ influence matrix $\bar{\phi}_i$ are:

$$\phi_{kji} = \phi_{kji}^{(1)} + \phi_{kji}^{(2)} \quad (2.5.15)$$

If the two bodies in contact have the same geometry and thermal properties then,

$$\phi_{kji} = 2\phi_{kji}^{(1)} = 2\phi_{kji}^{(2)} \quad (2.5.16)$$

It is helpful to display the expression for \bar{q}_M more explicitly. To illustrate, the case of perfect contact at the interface with only two elements is considered ($N=2$). In other words there are two heat flux histories, $q_1(t)$, $q_2(t)$ to be determined. For simplicity only three time steps are considered ($M=3$). At the first time step, (2.5.14a) becomes:

$$\begin{bmatrix} q_{11} \\ q_{21} \end{bmatrix} = \begin{bmatrix} C_{11} & C_{12} \\ C_{21} & C_{22} \end{bmatrix}^{-1} \begin{bmatrix} T_i \\ T_i \end{bmatrix} \quad (2.5.17)$$

where

$$C_{kj} = \phi_{kj1} \equiv \phi_{kj1}^{(1)} + \phi_{kj1}^{(2)} \quad (2.5.18)$$

Solving the above system for q_{11} and q_{21} yields

$$q_{11} = \frac{T_i(C_{22} - C_{12})}{\Delta} \quad (2.5.19a)$$

$$q_{21} = \frac{T_i(C_{11}-C_{21})}{\Delta} \quad (2.5.19b)$$

where

$$\Delta = C_{11}C_{22}-C_{12}C_{21} \quad (2.5.19c)$$

For the second time step, $M=2$, (2.5.14b) becomes:

$$\begin{bmatrix} q_{12} \\ q_{22} \end{bmatrix} = 2 \begin{bmatrix} q_{11} \\ q_{21} \end{bmatrix} - \begin{bmatrix} C_{11} & C_{12} \\ C_{21} & C_{22} \end{bmatrix}^{-1} \begin{bmatrix} F_1 \\ F_2 \end{bmatrix} \quad (2.5.20)$$

Solving (2.5.2) for q_{12} and q_{22} yields

$$\begin{aligned} q_{12} &= \frac{(2T_i-F_1)C_{22}-(2T_i-F_2)C_{12}}{\Delta} \\ &= 2q_{11} - \frac{F_1C_{22}-F_2C_{12}}{\Delta} \end{aligned} \quad (2.5.21a)$$

$$\begin{aligned} q_{22} &= \frac{(2T_i-F_2)C_{11}-(2T_i-F_1)C_{21}}{\Delta} \\ &= 2q_{21} - \frac{F_2C_{11}-F_1C_{21}}{\Delta} \end{aligned} \quad (2.5.21b)$$

where

$$F_1 = \phi_{111}q_{11} + \phi_{121}q_{21} \quad (2.5.22a)$$

$$F_2 = \phi_{211}q_{11} + \phi_{221}q_{21} \quad (2.5.22b)$$

In a similar manner, for the third time step, $M=3$, one can write

$$q_{13} = 3q_{11} - \frac{F_1 C_{22} - F_2 C_{12}}{\Delta} \quad (2.5.23a)$$

$$q_{23} = 3q_{21} - \frac{F_2 C_{11} - F_1 C_{21}}{\Delta} \quad (2.5.23b)$$

where

$$F_1 = \sum_{i=1}^2 [\phi_{11,3-i} q_{1i} + \phi_{12,3-i} q_{2i}] \quad (2.5.24a)$$

$$F_2 = \sum_{i=1}^2 [\phi_{21,3-i} q_{1i} + \phi_{22,3-i} q_{2i}] \quad (2.5.24b)$$

Notice that F_1 and F_2 are the only terms that should be evaluated at each time step.

Because of convolution behavior of the summations given in (2.5.8c) and (2.5.8d), the influence matrices, $\bar{\phi}_i$'s, need to be calculated at each time step. Consequently, most of the computation effort is in the evaluation of column matrix \bar{D} , particularly as the value of M becomes larger.

CHAPTER 3

TWO SEMI-INFINITE BODIES IN CONTACT OVER A CIRCULAR AREA

3.1 Introduction

In this chapter the transient thermal response of two semi-infinite bodies, brought suddenly into the perfect thermal contact over a small circular area is considered. The rest of the areas of the contacting planes are insulated. See Fig. 1.2a. The temperatures of the bodies are initially at uniform but different values. The SEM is employed to obtain the transient solutions for the interface heat fluxes and temperatures, and the thermal constriction resistance of the contact area. The solutions cover the entire range of dimensionless times. The results are compared with those obtained by other investigators. Two different cases are investigated; a) identical materials on both sides of the contact plane, b) different materials on the two sides of the contact plane. The former case is similar to the problem of a uniform step temperature change over a disk on the surface of a semi-infinite body and insulated elsewhere (see Fig. 3.1).

Previous Work

The steady-state problem for this geometry has been previously examined and is well known [22,23]. The transient problem for Case a has been analyzed by several authors by considering a single semi-infinite body with isothermal disk on its surface [24-29]. Normington and Blackwell [24] and later Blackwell [25] were the first to seek the solutions in oblate spheroidal coordinates, in order to eliminate the mixed boundary conditions which occur on the surface if the problem is set up in cylindrical coordinates. They developed an approximate

solution by using Laplace and Legendre transform techniques. However, the solutions were valid only for long times ($t^+ > 4$) in the first paper and for short times ($t^+ < .1$) in the second one. Keltner [26] used the same coordinates to obtain a one-dimensional approximate solution using the heat balance integral method. He has also examined a finite difference solution in cylindrical coordinates for a one-dimensional averaged model [27]. His solutions are more appropriate for early to middle times. Schneider, et al [28] have developed finite difference solutions in oblate spheroidal coordinates for the two-dimensional axisymmetric case. In a recent paper [29], Marder and Keltner examined the problem by using the method of separation of variables.

The composite Case b, where the materials on each side of the contact area are not identical, was first studied by Heasley [30] in an approximate manner. He replaced the region of contact by a perfectly conducting sphere and solved a one-dimensional problem in spherical coordinates. His solution is approximately valid for long times. Other work has been done by Schneider, Strong and Yovanovich [31], Sadhal [32], and Beck and Keltner [19]. Schneider et al [31], have employed finite difference techniques posed in oblate spheroidal coordinates to obtain the numerical solutions for the two-dimensional axisymmetric case. They have used about 200 nodes within each of the bodies. Their results as reported by Beck and Keltner [19], are too high at the early times. Sadhal [32] has solved the problem analytically by using Laplace and Legendre transform techniques. His solution is valid for large values of dimensionless time ($t^+ > 10$). Beck and Keltner [19], were the first to employ the surface element method to solve the problem. They have considered only one element across the interface and

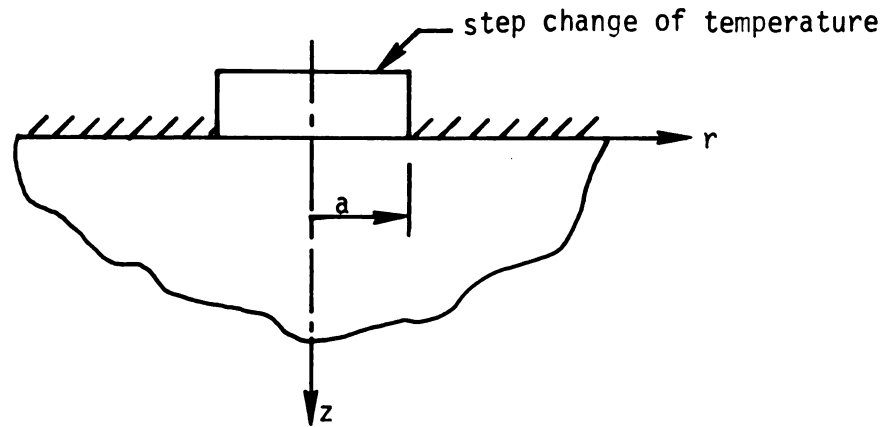


Figure 3.1 Geometry of a semi-infinite body with a step change of the surface temperature over a circular area.

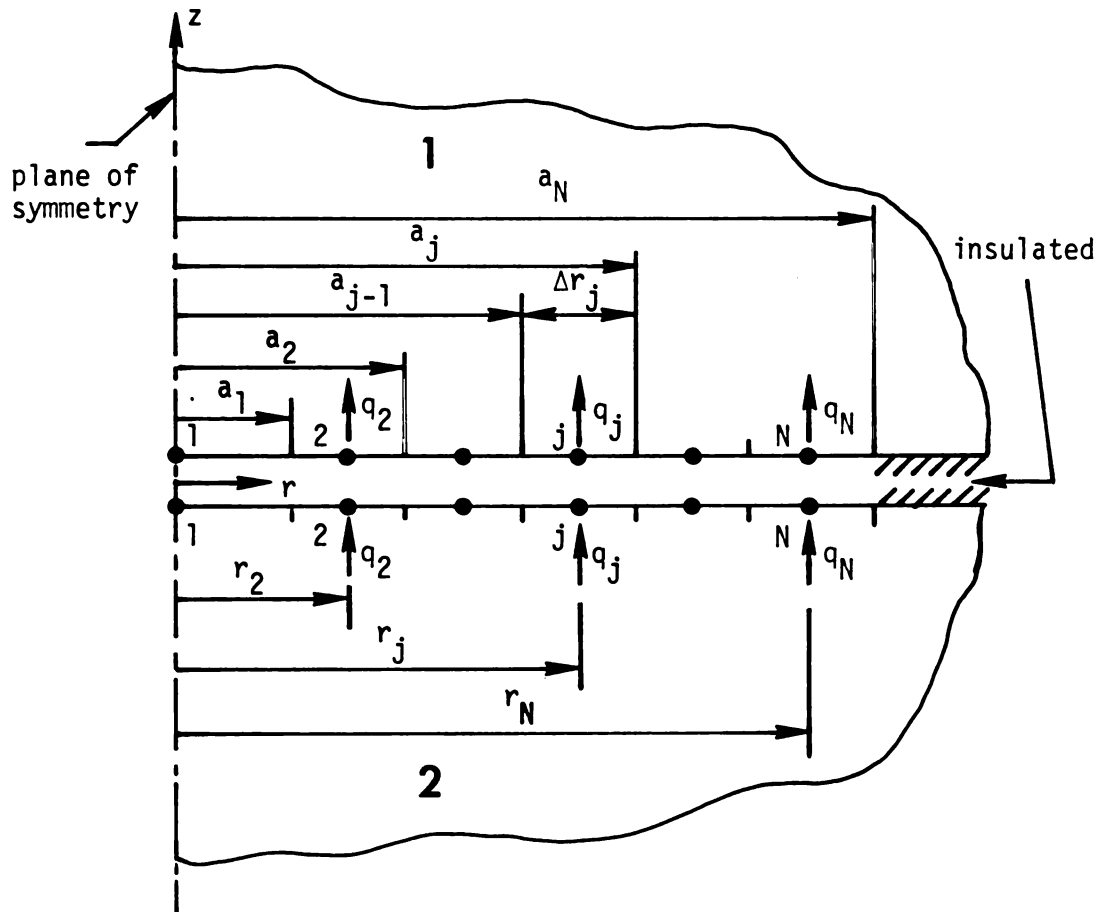


Figure 3.2 Distribution of surface elements for two semi-infinite bodies in contact over a circular area.

solved the problem analytically by utilizing Laplace transform techniques. Two expressions have been recommended. One is based on a heat flux form of Duhamel's integral (equation (22) of [19]), which is for early times and the other is based on a temperature-kernel form of the Duhamel's integral which is for late times (equation (56) of [19]).

Most of the above-mentioned solutions are restricted to either the time or the spatial validity [24-27,30,32,19]. The finite difference approaches by Schneider et. al. [28,31] also have some difficulties such as: the effort in setting up large grids, and the restricted dimensionless time step that can be used. They require a large number of nodes and consequently required considerable computer time if the accurate results are desired at early times and large times.

3.2 Statement of the Problem

Two semi-infinite bodies initially at uniform but different temperatures are brought together into perfect contact over a circular region of radius a . The rest of the surfaces of the contacting planes are assumed to be insulated. See Fig. 1.2a. The bodies can have different thermal conductivities k , and density-specific heats, ρc_p . The upper body is referred to as region 1 ($z > 0$) and the other body as region 2 ($z < 0$). The initial temperatures are denoted by T_{i1} and T_{i2} for region 1 and 2, respectively. The bodies are assumed to have temperature-independent thermal properties. The describing differential equations are

$$\frac{\partial^2 T_1}{\partial r^2} + \frac{1}{r} \frac{\partial T_1}{\partial r} + \frac{\partial^2 T_1}{\partial z^2} = \frac{1}{\alpha_1} \frac{\partial T_1}{\partial t}$$

$$\frac{\partial^2 T_2}{\partial r^2} + \frac{1}{r} \frac{\partial T_2}{\partial r} + \frac{\partial^2 T_2}{\partial z^2} = \frac{1}{\alpha_2} \frac{\partial T_2}{\partial t}$$
(3.2.1)

subject to,

$$T_1 = T_{i1} \quad \text{for } t=0, r \geq 0, z \geq 0 \quad (3.2.2a)$$

$$T_2 = T_{i2} \quad \text{for } t=0, r \geq 0, z \leq 0 \quad (3.2.2b)$$

and

$$T_1 = T_{i1} \quad \text{for } t > 0, \text{ as } r \rightarrow \infty \text{ and } z \rightarrow \infty \quad (3.2.3a)$$

$$T_2 = T_{i2} \quad \text{for } t > 0, \text{ as } r \rightarrow \infty \text{ and } z \rightarrow -\infty \quad (3.2.3b)$$

$$\frac{\partial T_1}{\partial r} = \frac{\partial T_2}{\partial r} = 0 \quad \text{at } r=0 \text{ for } t > 0 \quad (3.2.4)$$

$$T_1 = T_2 \quad \text{for } t > 0, 0 \leq r \leq a, z=0 \quad (3.2.5)$$

$$k_1 \frac{\partial T_1}{\partial z} = k_2 \frac{\partial T_2}{\partial z}$$

$$\frac{\partial T_1}{\partial z} = 0 \quad (3.2.6a)$$

for $t > 0, r > a, z = 0$

$$\frac{\partial T_2}{\partial z} = 0 \quad (3.2.6b)$$

where T_1 and T_2 denote the temperature distributions, k_1 and k_2 represent the thermal conductivities, α_1 and α_2 refer to the thermal diffusivities, r and z are the space coordinates, and t is the time.

3.3 Surface Element Solution

The surface element method which is presented in Chapter 2 is now employed to obtain the solution to the above problem.

3.3.1 Discretization of the Contact Area

Due to the axisymmetry nature of the problem, the contact area can be divided into N annular surface elements (not necessarily equal) with each of these elements having inner and outer radii denoted by a_{j-1} and a_j , respectively ($j=1, N$ and $a_0=0$). See Fig. 3.2. In general the heat flux and the temperature vary across the interface (as well as with time), but they are approximated to be constant over each surface element (and time interval) and are specified at the points;

$$\begin{aligned} r_1 &= 0 \\ r_j &= \frac{a_j - a_{j-1}}{2}; \quad j = 2, N \end{aligned} \tag{3.3.1}$$

Since the two bodies are in perfect contact ($h \rightarrow \infty$), the simplified form of solution given by (2.5.14) can be used. Using (2.5.8d) and (2.5.13) in (2.5.14) yields:

$$\bar{q}_1 = \bar{\phi}_1^{-1} \bar{T}_i \tag{3.3.2a}$$

$$\bar{q}_M = M\bar{q}_1 - \bar{\phi}_1^{-1} \left[\sum_{i=1}^{M-1} \bar{\phi}_{M+1-i} \bar{q}_i \right] \text{ for } M=2,3,\dots \tag{3.3.2b}$$

where $\bar{\phi}$ and \bar{T}_i are the influence matrix and the initial temperature vector defined by (2.5.7a) and (2.5.7d), respectively. At each time step the system (3.3.2) can be solved for unknowns q_{1M} , q_{2M} , ..., q_{NM} provided the influence functions, ϕ_{kji} 's, and \bar{T}_i are known. The ϕ_{kji} functions are given by;

$$\phi_{kji} = \sum_{m=1}^2 \phi_{kji}^m \tag{3.3.3}$$

where ϕ_{kji}^m is the temperature rise at element k due to a unit step heat flux at element j of surface m , at time $t_i = i \cdot \Delta t$. It is the building block solution and can be evaluated from the solution for the problem of a semi-infinite body heated with a constant heat flux over an annular area (see Fig. 3.3). The latter solution can be found from the known available solution for the case of semi-infinite body heated by a constant disk heat source [33]. See Fig. 3.4.

3.3.2 Evaluation of the Influence Function ϕ_{kji}^m

Consider the geometry of body m shown in Fig. 3.5. Let the temperature rise at element $k(r=r_k)$ due to unit heat flux at the disk with radius a_j and at time t_i be denoted by;

$$\theta_{kji}^m \equiv \theta^m(r_k, a_j, t_i) \quad (3.3.4)$$

By applying simple superposition one can show that:

$$\phi_{k1i}^m = \theta_{k1i}^m \quad (3.3.5a)$$

$$\phi_{kji}^m = \theta_{kji}^m - \theta_{k,j-1,i}^m \quad j=2,3,\dots,N \quad (3.3.5b)$$

which can be conveniently calculated utilizing,

$$\phi_{kji}^m = \theta_{kji}^m - \sum_{n=0}^{j-1} \phi_{kni}^m \quad \begin{array}{l} j=1,2,\dots,N \\ k=1,2,\dots,N \end{array} \quad (3.3.6)$$

3.4 Temperatures at the Surface of a Semi-Infinite Body with a Disk Heat Source

In reference [33] a solution for the local surface temperature history for a semi-infinite body exposed to a circular heat source is provided

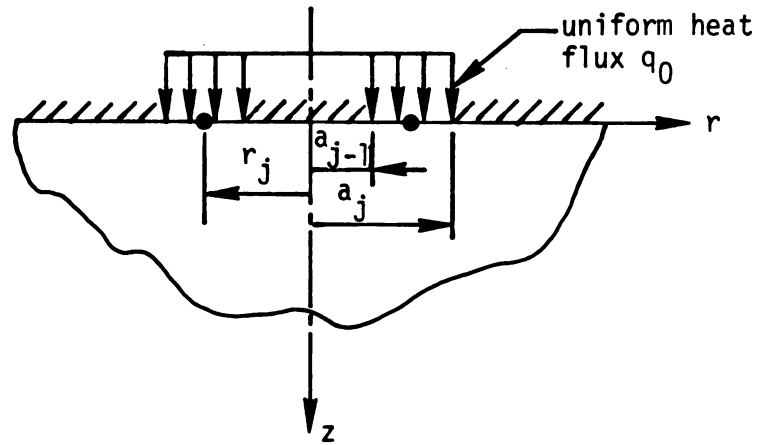


Figure 3.3 Semi-infinite body heated over an annular-shaped region $a_{j-1} < r < a_j$ and $z=0$.

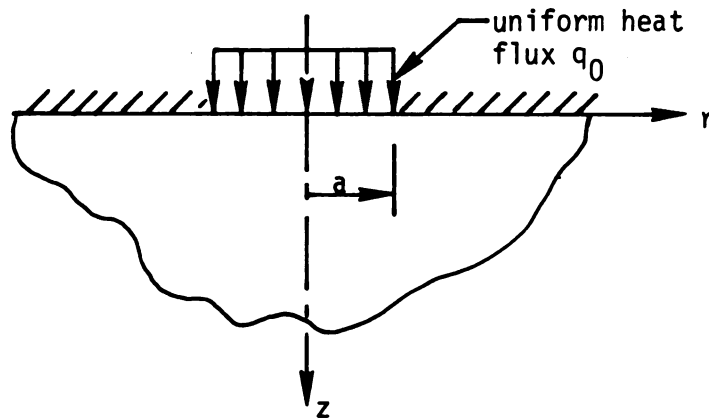


Figure 3.4 Semi-infinite body heated over a circular area $0 < r < a$ and $z=0$.

(see Fig. 3.4). This solution (termed "series solution") is given in dimensionless form and contains an infinite series that is valid for all radii and converges for all times except the earliest. The solution is,

$$\begin{aligned} T^+(r^+, 0, t^+) = & T^+(r^+, 0, \infty) - \frac{1}{2(\pi t^+)^{1/2}} \left\{ 1 - \frac{1+2r^{+2}}{24t^+} \right. \\ & + \frac{1}{480t^{+2}} (1+6r^{+2}+3r^{+4}) - \frac{1}{10752t^{+3}} \\ & \left. (1+12r^{+2}+18r^{+4}+4r^{+6}) + \dots \right\} \end{aligned} \quad (3.4.1)$$

where

$$T^+(r^+, 0, t^+) = \frac{T(r^+, 0, t^+)}{q_0 a / k}, \quad r^+ = \frac{r}{a}, \quad t^+ = \frac{\alpha t}{a^2} \quad (3.4.2a, b, c)$$

are the dimensionless surface temperature, radius, and the time, respectively. The steady state part, $T^+(r^+, 0, \infty)$, is given by,

$$T^+(r^+, 0, \infty) = \frac{2}{\pi} E(r^+) \quad \text{for } 0 < r^+ < 1 \quad (3.4.3a)$$

$$= \frac{2r^+}{\pi} [E(r^+) - (1-r^{+2})K(r^{+2})] \quad \text{for } r^+ > 1 \quad (3.4.3b)$$

$$= \frac{2}{\pi} \quad \text{for } r^+ = 1 \quad (3.4.3c)$$

The functions $K(\cdot)$ and $E(\cdot)$ are the complete elliptic integrals of the first and second kinds,

$$K(n) = \int_0^{\pi/2} [1 - n^2 \sin^2 y]^{-1/2} dy \quad (3.4.4a)$$

$$E(\eta) = \int_0^{\frac{\pi}{2}} [1 - \eta^2 \sin^2 y]^{1/2} dy \quad (3.4.4b)$$

These functions are tabulated in [34] (where the definition is slightly different) and are available in computer libraries.

Equation (3.4.1) provides a very accurate solution for large dimensionless times depending on the radial locations. It can extend down to dimensionless time $t^+ = .04$ for small r^+ 's, less than unity.

At the early times the problem of semi-infinite body heated over a disk area can be approximated by the case of a semi-infinite cylinder insulated on the sides and heated over a disk area centered at the end. See Fig. 3.6. In reference [35], the temperature solution for the surface of the semi-infinite insulated cylinder exposed to a circular heat source is provided in dimensionless form which is valid for all radii and times. The solution is,

$$T^+(r^+, 0, t^+) = \frac{2}{b^+} \left(\frac{t^+}{\pi}\right)^{1/2} - 2 \sum_{i=1}^{\infty} \frac{\operatorname{erfc}(\lambda_i^+ t^{+1/2}/b^+) J_0(\lambda_i^+ r^+/b^+) J_1(\lambda_i^+/b^+)}{[\lambda_i^+ J_0(\lambda_i^+)]^2} + I(r^+, b^+) \quad (3.4.5a)$$

where

$$I(r^+, b^+) \equiv 2 \sum_{i=1}^{\infty} \frac{J_0(\lambda_i^+ r^+/b^+) J_1(\lambda_i^+/b^+)}{[\lambda_i^+ J_0(\lambda_i^+)]^2} \quad (3.4.5b)$$

$$b^+ = b/a \quad (3.4.5c)$$

and the dimensionless eigenvalues λ_i^+ are found from;

$$J_1(\lambda_i^+) = 0 \quad (3.4.6)$$

The functions $\text{erfc}(\cdot)$, $J_0(\cdot)$, and $J_1(\cdot)$ are the complementary error function, and the Bessel functions of zero and first orders, respectively [34].

Except for extremely small dimensionless times ($t^+ < .01$) or large b^+ ($b^+ > 10$) the evaluation of (3.4.5a) does not involve a large number of terms in the summation unless one tries to evaluate the steady state part, $I(r^+, b^+)$, directly. Some simplified indirect procedures of evaluating $I(r^+, b^+)$ are provided in [35]. A new direct method is also developed by the author which evaluates this part more effectively. In this method the tail of the summation is replaced by an integral in an approximate manner. This integral can simply be integrated over the corresponding limits. (See Appendix B). The evaluation of the explicit summation (3.4.5a) requires only less than 12 terms for t^+/b^{+2} being greater than .33 and about 121 terms for extremely small values of t^+/b^{+2} ($t^+/b^{+2} \approx .0001$). This is because $\text{erfc}(\eta)$ decreases very rapidly with η and also because λ_i^+ monotonically increases with i . The solutions given by (3.4.1) and (3.4.5a) can be used to evaluate θ_{kji}^m (defined by (3.3.4)) for large and small dimensionless times, respectively. Then (3.3.6) and (3.3.3) can be employed to determine the influence functions, ϕ_{kji} 's. Once the influence functions and consequently the influence matrices, $\bar{\bar{\phi}}_i$'s, have been determined, the solutions to the heat fluxes q_{1M} , q_{2M} , \dots , q_{NM} , can be obtained by substituting the results into (3.3.2a) and (3.3.2b) for $M=1$ and $M>1$, respectively.

3.5 Thermal Constriction Resistance of the Two Solids

In reference [9] the transient thermal constriction resistance is defined as "the difference between the average temperature of the contact area and the temperature far from the contact area divided by the total instantaneous heat flow through the contact area." Based on the above definition one can write

$$R_{c1}(t) = \frac{\bar{T}_c(t) - T_{i1}}{Q_c(t)}, \quad R_{c2}(t) = \frac{T_{i2} - \bar{T}_c(t)}{Q_c(t)} \quad (3.5.1a,b)$$

where $\bar{T}_c(t)$ is the average temperature of the contact area, $Q_c(t)$ is the total heat flow through the contact area, and $R_{c1}(t)$ and $R_{c2}(t)$ are the thermal constriction resistances for body 1 and body 2, respectively. The total thermal constriction resistance for the two semi-infinite bodies can be determined by

$$R_c(t) = R_{c1}(t) + R_{c2}(t) = \frac{T_{i2} - T_{i1}}{Q_c(t)} \quad (3.5.2)$$

The average contact area temperature, \bar{T}_c , can be obtained by summing the products of the elemental temperature and the fraction of the total contact area occupied by the element.

$$\bar{T}_c(t_M) = \sum_{j=1}^N T_{jM} (A_j / A_c) \quad (3.5.3)$$

where T_{jM} is the temperature at the center of element j at time $t_M = M \cdot \Delta t$ and

$$A_c = \pi a^2, \quad A_j = \pi (a_j^2 - a_{j-1}^2) \quad (3.5.4a,b)$$

The total heat flow through the contact area, Q_c , can be determined by summing up the heat flows over all elements,

$$Q_c(t_M) = \sum_{j=1}^N q_{jM} A_j \quad (3.5.5)$$

Utilizing (3.5.3-3.5.5) into (3.5.1a,b) and (3.5.2) yields,

$$R_{c1}(t_M) = \frac{\frac{1}{A_c} \sum_{j=1}^N T_{jM} A_j - T_{i1}}{\sum_{j=1}^N q_{jM} A_j} \quad (3.5.6a)$$

$$R_{c2}(t_M) = \frac{T_{i2} - \frac{1}{A_c} \sum_{j=1}^N T_{jM} A_j}{\sum_{j=1}^N q_{jM} A_j} \quad (3.5.6b)$$

$$R_c(t_M) = \frac{T_{i2} - T_{i1}}{\sum_{j=1}^N q_{jM} A_j} \quad (3.5.6c)$$

3.6 Results and Discussions

The two cases a and b mentioned earlier in subsection 3.1 have been solved. In each case the contact area has been divided into ten variable-spaced elements with smaller elements being closer to the edge of the contact area. The exact solutions given by (3.4.5a) and (3.4.1) were used to calculate the influence functions at "early" and "late" times, respectively. The values of the influence functions for dimensionless times .001, .1, and 1000 are listed in Tables 3.1 through 3.3. These Tables also represent the influence matrices. Notice that

TABLE 3.1

Values of the influence function, ϕ_{kjM} , for semi-infinite body at dimensionless time $t_M^+ = .001$.

k/j	1	2	3	4	5	6	7	8	9	10
1	.0357	.0	.0							
2	.001	.0356	.0001	.0						
3	.0	.0012	.0332	.0014	.0					
4		.0	.0012	.0332	.0013	.0				
5			.0	.0012	.0332	.0013	.0			
6				.0	.0012	.0332	.0013	.0001		
7					.0	.0045	.0265	.0044	.0003	
8						.0003	.0042	.0265	.0044	.0003
9							.0003	.0042	.0265	.0044
10								.0003	.0042	.0265

TABLE 3.2

Values of the influence function, ϕ_{kjM} , for semi-infinite body at dimensionless time $t_M^+ = 1$.

k/j	1	2	3	4	5	6	7	8	9	10
1	.1887	.1665	.0750	.0697	.0656	.0596	.0280	.0268	.0257	.0245
2	.0600	.2312	.0909	.0791	.0710	.0643	.0299	.0285	.0272	.0259
3	.0346	.1254	.1433	.1009	.0823	.0717	.0328	.0310	.0294	.0279
4	.0260	.0880	.0830	.1447	.1003	.0809	.0361	.0338	.0318	.0299
5	.0203	.0663	.0572	.0853	.1453	.0995	.0415	.0380	.0352	.0329
6	.0162	.0519	.0431	.0595	.0866	.1454	.0530	.0456	.0408	.0373
7	.0138	.0439	.0359	.0483	.0658	.0988	.0837	.0591	.0484	.0426
8	.0124	.0394	.0320	.0426	.0567	.0789	.0558	.0836	.0589	.0482
9	.0112	.0355	.0287	.0379	.0500	.0666	.0432	.0558	.0835	.0589
10	.0102	.0321	.0258	.0339	.0439	.0576	.0360	.0433	.0558	.0834

TABLE 3.3

Values of the influence function, ϕ_{kjM} , for semi-infinite body at dimensionless time $t_{M}^{+} = 1000$.

k j	1	2	3	4	5	6	7	8	9	10
1	.1996	.1989	.0992	.0990	.0988	.0987	.0493	.0492	.0492	.0491
2	.0708	.2635	.1148	.1082	.1050	.1031	.0511	.0508	.0506	.0504
3	.0453	.1584	.1671	.1297	.1160	.1102	.0538	.0531	.0526	.0522
4	.0366	.1197	.1066	.1733	.1338	.1191	.0569	.0557	.0548	.0540
5	.0308	.0977	.0805	.1136	.1785	.1374	.0621	.0597	.0580	.0567
6	.0266	.0830	.0662	.0875	.1194	.1828	.0735	.0671	.0634	.0609
7	.0241	.0746	.0588	.0760	.0983	.1359	.1039	.0804	.0709	.0660
8	.0227	.0699	.0547	.0701	.0890	.1158	.0759	.1048	.0812	.0715
9	.0214	.0658	.0512	.0652	.0817	.1032	.0632	.0767	.1057	.0819
10	.0203	.0622	.0482	.0610	.0758	.0940	.0559	.0642	.0778	.1064

the diagonal terms of these matrices are greater than the off diagonal terms. The influence matrices were used in (3.3.2a,b) to find the unknown elemental heat fluxes. Equations (3.3.2a,b) were evaluated with three computer programs developed in the course of the project, RAN3, RAN2, and BBY9. Each used two routines called LINIV and VUMLL from the ISML Computer Library to perform the inversion and multiplication of the influence matrices. The results obtained from the surface element solution in this chapter, were compared to those given by the other investigators [24,26,29,31,32,19] on the bases of thermal constriction resistance and heat flux across the contact area.

Case a

The first problem examined is that of an isothermal disk on the surface of a semi-infinite body. With values of $k=1$, $\alpha=1$, $a=1$, and $T_i=2$, the problem was solved for elemental heat fluxes for various values of dimensionless time, from $t^+=.001$ to $t^+=10^4$. These results are tabulated in Table 3.4a, and 3.4b. Table 3.5 provides the normalized spatial variation of the surface heat flux at different times. Normalization obtained by dividing elemental values by the value of the centerline element which covers the area $0 \leq r^+ \leq .2$. It can be seen that all the elemental heat fluxes approach the steady state condition and after dimensionless time about 20, the normalized heat flux distribution remains constant. This indicates that for $t^+ \geq 20$, the heat flux across the disk can be approximated by a product of a function of t^+ and a function of r^+ . From the late time asymptotic solution given by Normington and Blackwell [24], it can be shown that the heat flux across the disk has a steady state distribution of $(1-r^{+2})^{-1/2}$. This implies that heat flux goes to infinity as

TABLE 3.4a

Results for elemental heat flux, q_j , for an isothermal disk region on the surface of a semi-infinite body ($t^+ = \alpha t/a^2$).

t^+	r^+				
	0	.3	.45	.55	.65
	El. #1	2	3	4	5
.001	18.30	18.30	18.30	18.30	18.30
.005	8.184	8.184	8.184	8.185	8.185
.01	5.787	5.788	5.789	5.789	5.791
.05	2.588	2.596	2.613	2.645	2.718
.1	1.846	1.871	1.914	1.970	2.072
.5	1.031	1.075	1.141	1.210	1.320
1.	.8979	.9395	1.003	1.067	1.170
10.	.7184	.7534	.8062	.8598	.9459
100.	.6669	.6995	.7486	.7986	.8787
1000.	.6510	.6823	.7308	.7796	.8578
10000.	.6460	.6776	.7252	.7736	.8513

TABLE 3.4b

Results for elemental heat flux, q_j , for an isothermal disk region on the surface of a semi-infinite body ($t^+ = \alpha t/a^2$).

t^+	r^+				
	.75	.824	.875	.925	.975
	El. #6	7	8	9	10
.001	18.32	18.32	18.32	18.33	25.75
.005	8.195	8.237	8.424	8.851	16.19
.01	5.830	5.966	6.270	6.864	13.51
.05	2.903	3.198	3.570	4.204	9.164
.1	2.284	2.586	2.939	3.526	7.875
.5	1.519	1.781	2.067	2.532	5.824
1.	1.354	1.595	1.856	2.281	5.269
10.	1.098	1.297	1.513	1.864	4.318
100.	1.021	1.206	1.407	1.733	4.015
1000.	.9963	1.177	1.373	1.692	3.920
10000.	.9886	1.168	1.363	1.679	3.890

TABLE 3.5

Normalized spatial variation of the surface heat flux at different times for the geometry of Case a, see Fig. 3.1. ($q^+ = q/q_{CL}$ vs $r^+ = r/a$).

t^+	r^+									
	0	.3	.45	.55	.65	.75	.825	.875	.925	.975
.001	1.	1.	1.	1.	1.	1.	1.	1.	1.	1.41
.01	1.	1.	1.	1.	1.	1.01	1.03	1.08	1.19	2.33
.1	1.	1.01	1.04	1.07	1.12	1.24	1.40	1.59	1.41	4.22
1.	1.	1.05	1.12	1.19	1.30	1.51	1.78	2.07	2.54	5.87
10.	1.	1.05	1.12	1.20	1.32	1.53	1.81	2.11	2.60	6.01
20.	1.	1.05	1.12	1.20	1.32	1.53	1.81	2.11	2.60	6.02
∞	1.	1.05	1.12	1.20	1.32	1.53	1.81	2.11	2.60	6.02
Averaged steady state values from $1/\sqrt{1-r^{+2}}$ based on the elemental area										
∞		1.05	1.12	1.20	1.32	1.52	1.77	2.08	2.67	6.35

TABLE 3.6

Normalized area averaged interface heat flux for the geometry of Case a, see Fig. 3.1. $\bar{q}^+ = \bar{q} / \bar{q}_\infty$.

t^+	TSEM	Beck & Keltner [19]		Marder & Keltner [29]	
		Eq. (56)	Eq. (22)	s = 2	s = 5
.001	15.057	12.357	14.522	13.088	8.645
.002	10.872	9.030	10.434	10.408	7.950
.005	7.169	6.079	6.792	7.063	6.485
.01	5.310	4.591	4.969	5.238	5.145
.02	3.998	3.539	3.688	3.948	3.943
.05	2.843	2.606	2.573	2.813	2.813
.1	2.268	2.136	2.038	2.248	2.248
.2	1.871	1.803	1.702	1.858	1.858
.5	1.533	1.508	1.530	1.515	1.526
1.	1.371	1.359	1.667	1.297	1.366
2.	1.259	1.254	2.334	1.104	1.257
5.	1.163	1.161		1.005	1.155
10.	1.114	1.113		1.	1.082
20.	1.080	1.080		1.	1.023
100.	1.036	1.036			1.
1000.	1.011	1.011			
10000.	1.004	1.004			
∞	1.0	1.			

r^+ goes to 1. The steady state values of the elemental heat flux given in Table 3.5 are compared with the corresponding values obtained from the asymptotic solution, $(1-r^{+2})^{-1/2}$, based on the elemental area. There is good agreement between the two solutions for all elements but the outermost element, which indicates an error of 6%. Fig. 3.7 shows the normalized flux distribution across the disk at several times. It can be seen that the region of uniform heat flux shrinks as t^+ goes to infinity, which implies that the assumption of uniform heat flux across the disk (made by Beck and Keltner [19] in their q -based solution) is only good at early times.

Fig. 3.8 and 3.9 illustrate comparisons of area averaged interface heat flux[†] calculations performed using SEM with the results obtained from the two solutions given by Equations (22) and (56) in reference [19] and the two other solutions given in reference [29] for values of $s=2$ and $s=5$. In Fig. 3.8 normalized values of averaged heat flux ($\bar{q}(t)/\bar{q}(\infty)$) is plotted versus dimensionless time t^+ . While Fig. 3.9 shows the percent of deviation in the values of the heat flux obtained by the above-mentioned alternative solution from that found by SEM solution. Values of $\bar{q}(t)/\bar{q}(\infty)$ as a function of time are also tabulated in Table 3.6 for the same five solutions.

The Eq. (22) solution [19] is based on a heat flux form of Duhamel's integral. This solution uses approximate expressions for influence functions at early dimensionless times. It closely matches the SEM solution up to time $t^+ = .005$ (less than 5% deviation, see Fig. 3.9).

[†] The area averaged interface heat flux, $\bar{q}(t)$, was obtained by summing the products of the elemental heat flux and the fraction of the total interface area occupied by the element.

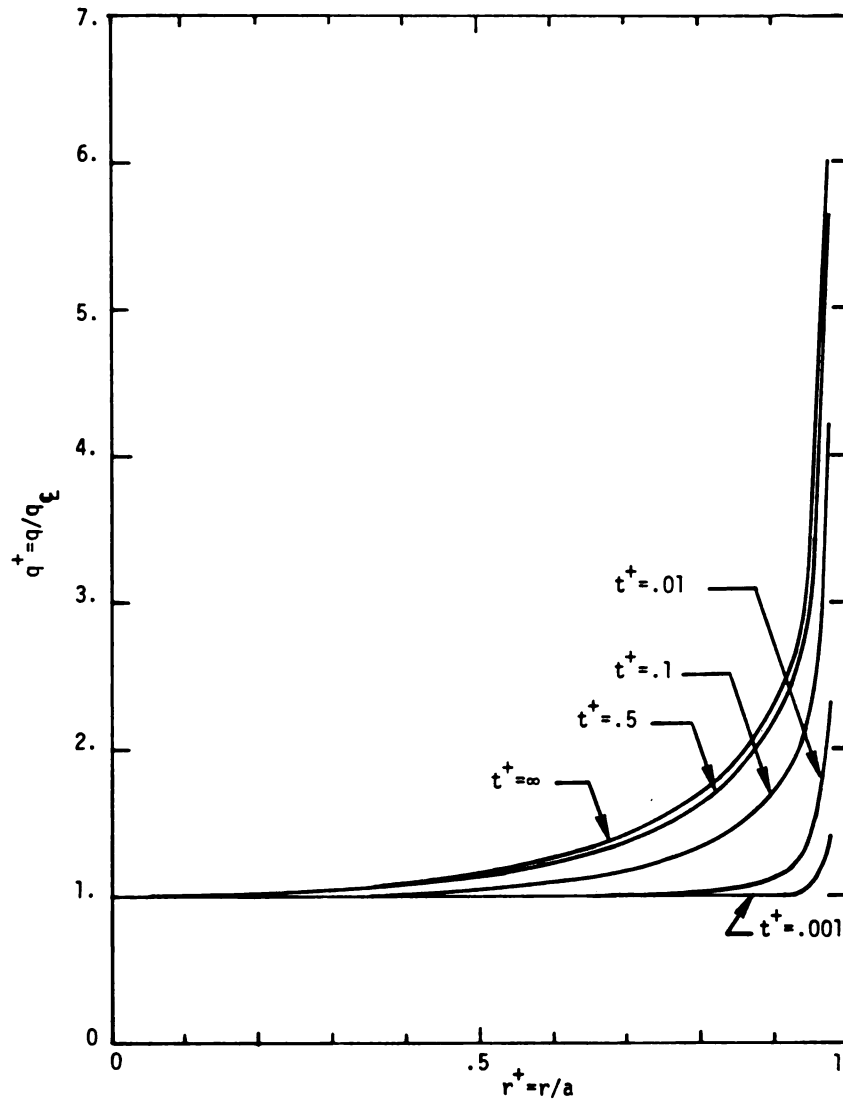


Figure 3.7 Normalized heat flux distribution across the interface at various times for the geometry of Case a, see Fig. 3.1.

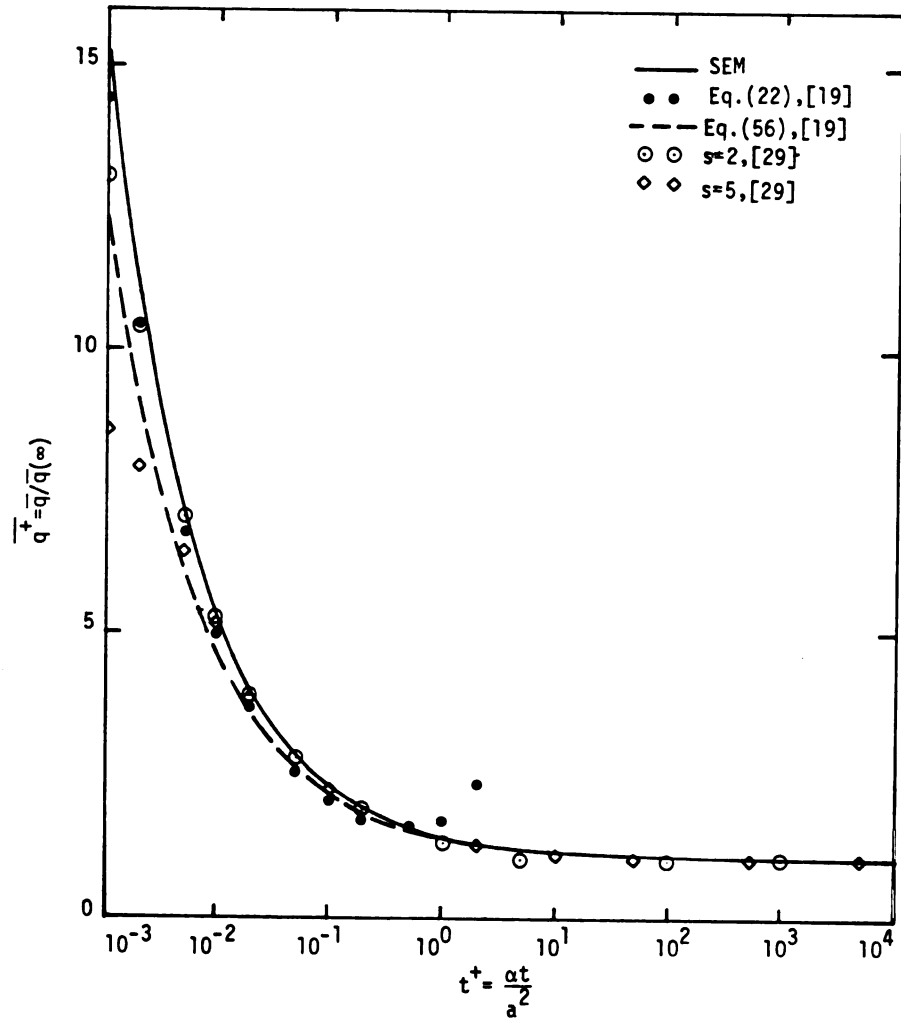


Figure 3.8 Normalized area averaged interface heat flux versus dimensionless time for the geometry of Case a, see Fig. 3.1.

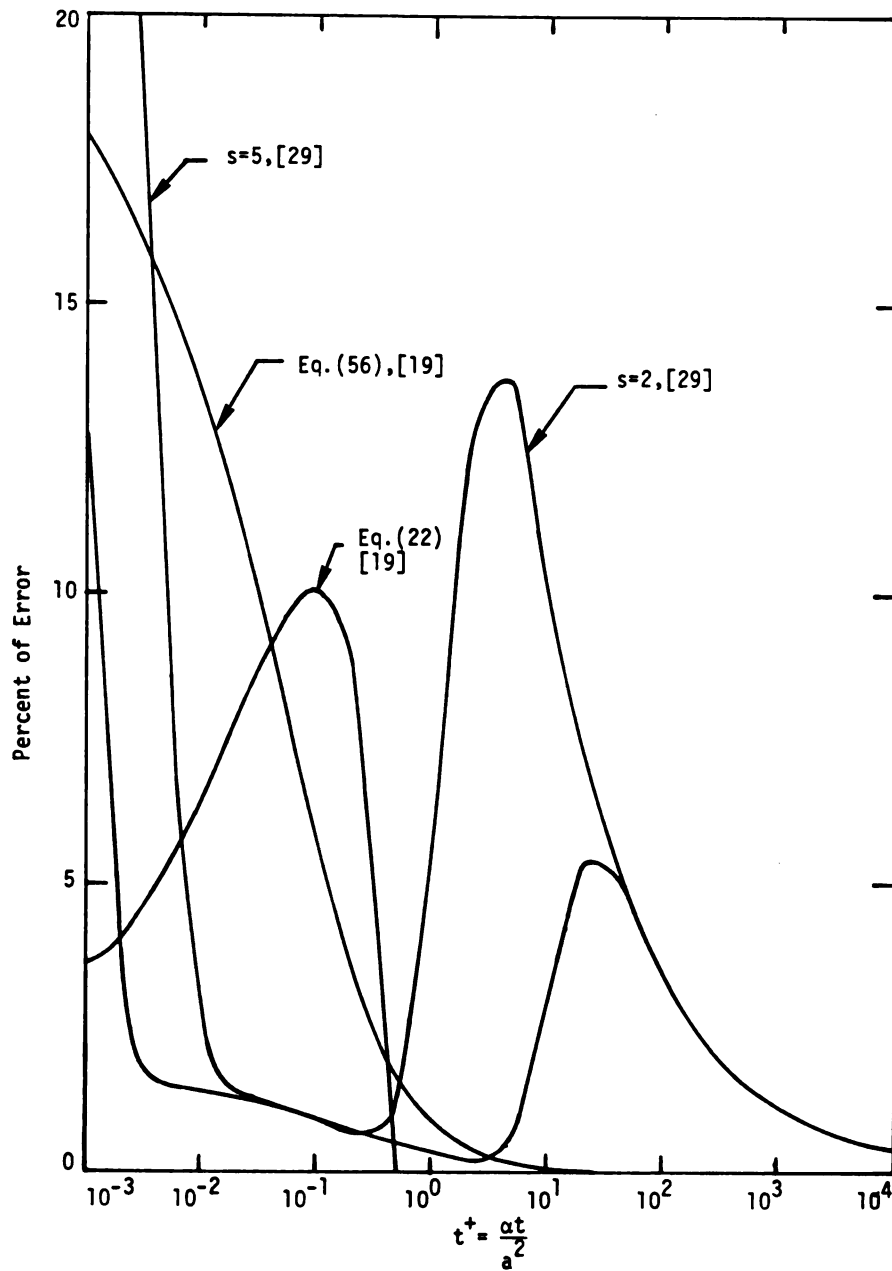


Figure 3.9 Percent of relative error in the area averaged interface heat flux with respect to SEM solution as a function of time for Case a, see Fig. 3.1.

Between $t^+ = .005$ to $t^+ = .5$ the deviation increases up to 10%, and for $t^+ > .5$ the solution ceases being useful. This solution is only appropriate for the small dimensionless times.

The Eq. (56) solution is in good agreement with SEM solution for mid-to-late times ($t^+ \geq .1$). It matches exactly the SEM solution for times greater than 20 (see Fig. 3.8). The percent of deviation in the surface heat flux starts with the maximum value of 17.9 at $t^+ = .001$ and decreases as t^+ becomes larger, it reaches a value of 5.8 at $t^+ = .1$ and approaches to zero at $t^+ \approx 20$. See Fig. 3.9.

The validity of the $s = 2$ solution is in question for very short times $t^+ \leq .001$ (13% deviation for $t^+ \approx .001$ shown in Fig. 3.9). However, it is in good agreement with the SEM solution for short and intermediate times between $t^+ \approx .002$ to $t^+ \approx 1$. The $s = 5$ solution remains good until about $t^+ \approx 10$. Even though reference [29] states that the $s = 5$ solution is very good down to nearly $t^+ = .001$, the results from Fig. 3.8, 3.9 and Table 3.6 show that it is in poor agreement with SEM solution for $t^+ < .01$ (Table 3.6 indicates a difference of 42.6% at $t^+ = .001$). Because of the effect of the finite artificial boundary location assumed in [29] (the assumption made in order to use the separation of variables technique [29]), the $s = 2$ and $s = 5$ solutions both reach the steady state value too early; at $t^+ \approx 10$ and at $t^+ \approx 100$, respectively.

Case b

The composite Case b is considered with the glass being the material of one body and copper of the other. The glass-copper combination has also been investigated in references [31,32,19]. The thermal conductivities, k 's, are 1.03 and 381 W/m-k and the thermal diffusivities,

α 's are $.06 \times 10^{-5} \text{ m}^2/\text{s}$ and $13.2 \times 10^{-5} \text{ m}^2/\text{s}$ for glass and copper, respectively. The initial temperature of glass is $T_{i1} = 0$, and that of copper is $T_{i2} = 2 \text{ K}$. With value of $a = 1 \text{ m}$, the problem was solved for the elemental surface heat fluxes and temperatures. Results for the surface heat fluxes are displayed in Table 3.7. Column one in this table contains dimensionless times, t^+ , based on the lower thermal diffusivity, $\alpha_1 < \alpha_2$, ranging between .001 and 10000.

The results for spatial variation of the surface heat flux, given in Table 3.5, for Case a, is almost the same for Case b. That means after dimensionless time about 20 the normalized heat flux distribution across the interface remains constant. In Fig. 3.10, the normalized interface temperature distribution is plotted versus dimensionless radius, r^+ , at several times. Normalization is obtained with respect to the initial temperature of body 2 (copper). It can be seen for $t^+ = .1$ that the interface temperature distribution is almost uniform. This supports the validity of the T-based solution given by Beck and Keltner for the late times. Notice that the region of uniform temperature shrinks at t^+ goes to zero which implies that the T-based solution is not appropriate for short times.

Figures 3.11 and 3.12 compare the results obtained for Case b with those found from the T-based and the q-based solutions of reference [19], based on the area averaged interface heat flux and the area averaged interface temperature[†], respectively. Again it can be seen that the q-based solution given in [19] is in good agreement at early

[†] The area averaged interface temperature, $\bar{T}(t)$, is obtained by summing the products of the elemental temperature and the fraction of the total interface area occupied by the element.

TABLE 3.7a

Results for elemental heat flux, q_j , for a disk-shaped interface of two semi-infinite bodies, one of copper and the other of glass ($t^+ = \alpha_1 t/a^2$)[†].

t^+	$r^+ = 0$.3	.45	.55	.65
	El. #1	2	3	4	5
.001	36.66	36.71	36.78	36.83	36.89
.01	11.84	11.85	11.85	11.85	11.85
.1	3.791	3.842	3.931	4.044	4.254
1.	1.844	1.929	2.059	2.191	2.403
10.	1.475	1.547	1.656	1.766	1.943
100.	1.370	1.437	1.538	1.641	1.805
1000.	1.337	1.403	1.501	1.602	1.762

[†] α_1 = Thermal diffusivity of glass (body one).

TABLE 3.7b

Results for elemental heat flux, q_j , for a disk-shaped interface of two semi-infinite bodies, one of copper and the other of glass ($t^+ = \alpha_1 t/a^2$)[†].

t^+	$r^+ = .75$.825	.876	.925	.975
	El. #6	7	8	9	10
.001	36.98	37.05	37.07	36.49	52.16
.01	11.93	12.21	12.83	14.03	27.58
.1	4.687	5.307	6.030	7.231	16.15
1.	2.780	3.274	3.811	4.684	10.82
10.	2.256	2.665	3.108	3.829	8.870
100.	2.096	2.477	2.889	3.560	8.248
1000.	2.047	2.418	2.821	3.475	8.053

[†] α_1 = Thermal diffusivity of glass (body one).

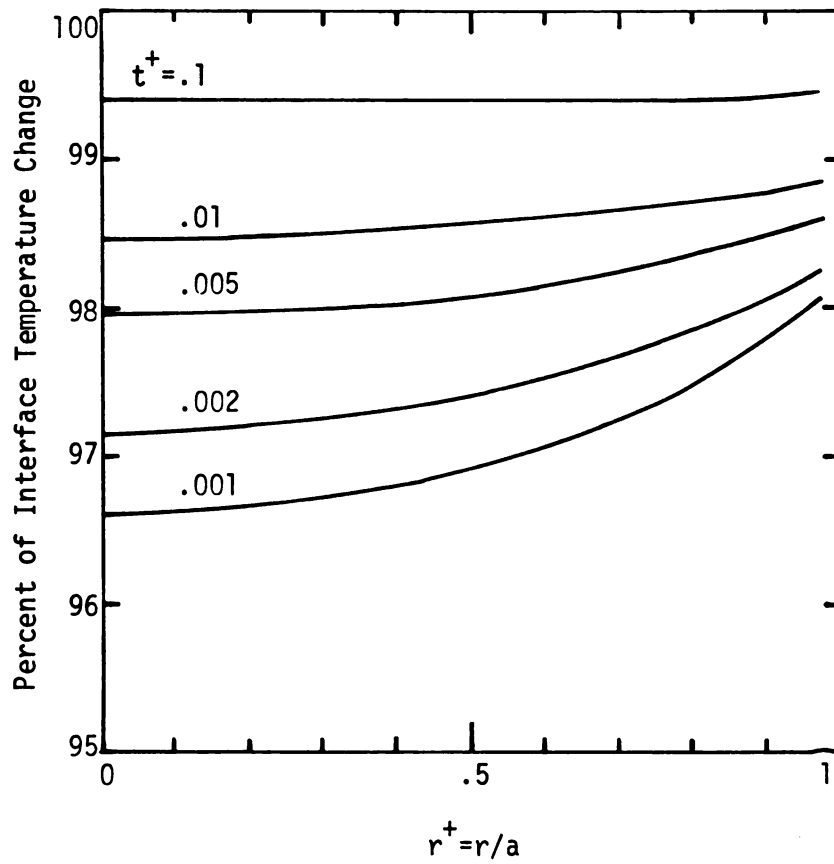


Figure 3.10 Normalized interface temperature distribution for the geometry of Case b, see Fig. 1.2a. (Normalized with respect to initial temperature of body 2, copper)

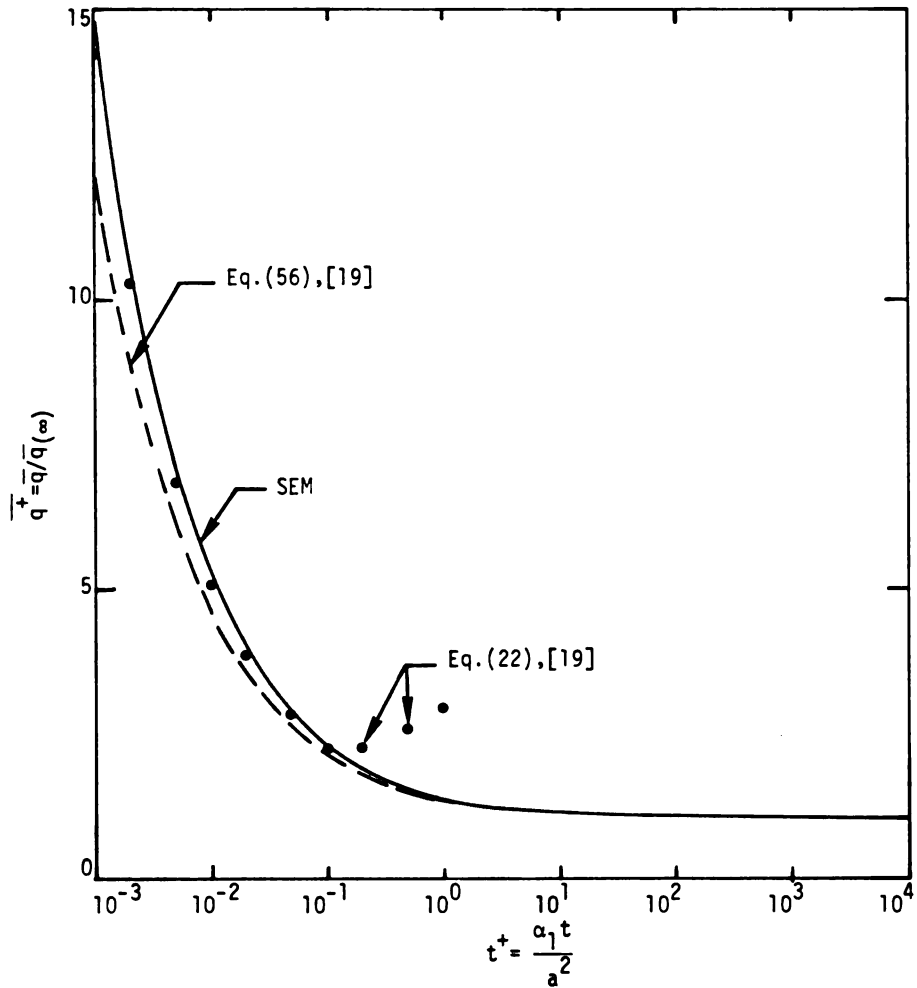


Figure 3.11 Dimensionless area averaged interface heat flux versus dimensionless time for the geometry of Case b, see Fig. 1.2a. (Normalized with respect to the steady state value of \bar{q})

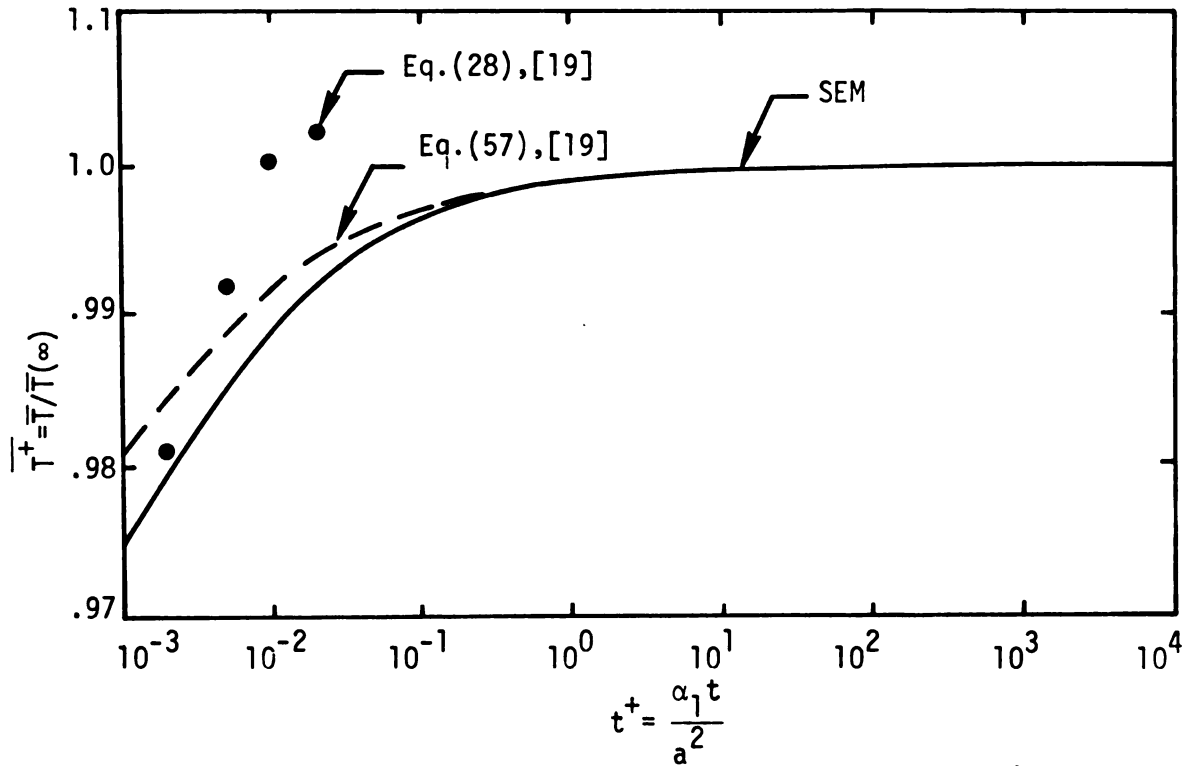


Figure 3.12 Dimensionless area averaged interface temperature versus dimensionless time for the geometry of Case b, see Fig. 1.2a. (Normalized with respect to the steady state value of \bar{T})

times while the T-based solution is suitable for mid-to-late times, $t^+ > .1$.

Comparison Based on Thermal Constriction Resistance

The SEM solution is also compared with the other available solutions on the bases of the dimensionless thermal constriction resistance across the contact area for both Cases a and b. Tables 3.8 and 3.9 provide these results. Table 3.8 is for Case a, two identical semi-infinite bodies, and Table 3.9 is for Case b, with copper being the material of one body and glass that of the other. The first column in each table is the dimensionless time, t^+ , which extends over many decades. The results from the finite difference solution of Schneider et al [31] are provided in the second columns which are least accurate at the early times and most accurate at the late times. The third columns come from the exact solution given by Sadhal [32] which is claimed to be very accurate at late times, $t^+ > 10$. The fourth columns are for the T-based solution given by Beck and Keltner [19], which is most appropriate for large times but is remarkably accurate down to $t^+ \approx .1$. Column 5 in each table is for the q-based solution [19] and is accurate at early times. The results obtained by the SEM solution are displayed in the 6th columns. The last (7th) column of Table 3.9 (for case a) was calculated from the one-dimensional approximate solution given by Keltner [26], which closely matches SEM solution at the short times and retains good accuracy for the mid-to-late times. Values of R_C^+ as a function of time are also plotted in Fig. 3.13 for the same solutions of Case b.

Fig. 3.14 shows the percent of error between the above-mentioned

TABLE 3.8

Results for dimensionless constriction resistance, for an isothermal disk region on the surface of a semi-infinite body. $R_c^+ = R_c \cdot a \cdot k$.

t^+	SSY [31]	Sadhal [32]	Beck & Keltner [19] Eq. (56) Eq. (22)		SEM	Keltner [26]
.001	.0386		.0202	.0172	.0166	.0162
.002	.0409		.0277	.0240	.0230	.0223
.005	.0463		.0411	.0368	.0349	.0340
.01	.0532		.0544	.0503	.0471	.0473
.02	.0637		.0706	.0678	.0625	.0641
.05	.0851	4.8988	.0959	.0972	.0879	.0914
.1	.1074	.2029	.1171	.1226	.1102	.1142
.2	.1336	.1685	.1386	.1468	.1336	.1382
.5	.1695	.1752	.1658	.1634	.1631	.1685
1.	.1933	.1879	.1839	.1500	.1824	.1895
2.	.2120	.2010	.1994	.1071	.1984	.2074
10.	.2368	.2247	.2245		.2242	.2347
100.	.2475	.2413	.2413		.2414	.2477
1000.	.2495	.2472	.2472		.2472	
10000.	.2499	.2491	.2491		.2491	
∞	.2500	.2500	.2500		.2500	

TABLE 3.9

Results for dimensionless constriction resistance for a disk-shaped interface of two semi-infinite bodies, one of copper and the other of glass. $R_C^+ = R_C/R_C(\infty)$.

t^+	SSY	Sadhal	Beck & Keltner [19]		SEM
	[31]	[32]	Eq. (56)	Eq. (56)	
.001	.1549		.0820	.0701	.0676
.002	.1645		.1118	.0968	.0932
.005	.1870		.1655	.1462	.1404
.01	.2158		.2187	.1961	.1890
.02	.2595		.2833	.2570	.2507
.05	.3474		.3844	.3480	.3523
.1	.4382		.4688	.4101	.4413
.2	.5442		.5552	.4418	.5349
.5	.6869		.6637	.3857	.6610
1.	.7805	.7564	.7362	.2539	.7300
10.	.9495	.8992	.8982		.8973
100.	.9903	.9654	.9654		.9654
1000.	.9982	.9888	.9888		.9889
10000.	.9997	.9964	.9964		.9964
∞	1.	1.	1.		1.

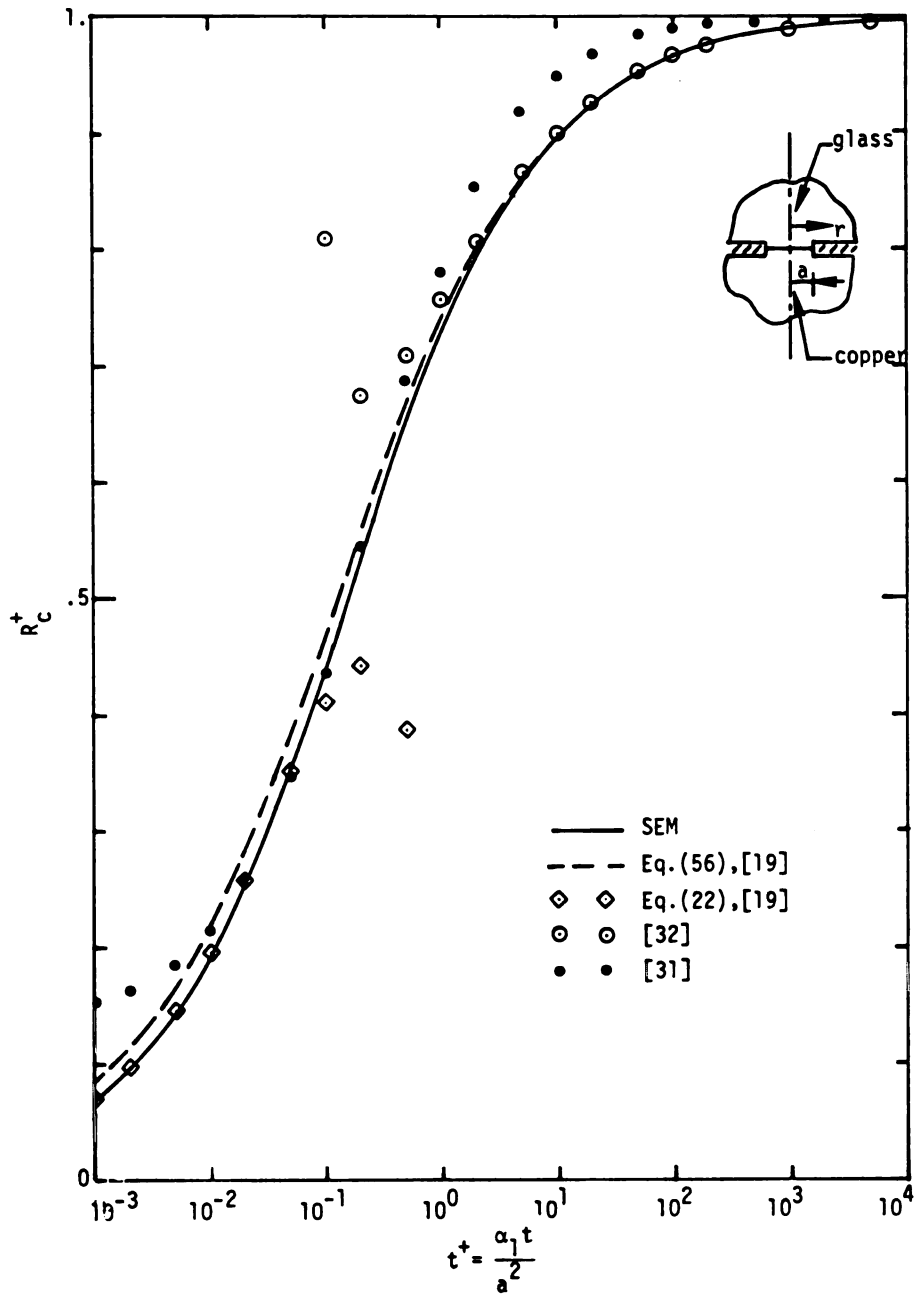


Figure 3.13 Normalized thermal constriction resistance across the interface versus time for the geometry of Case b.

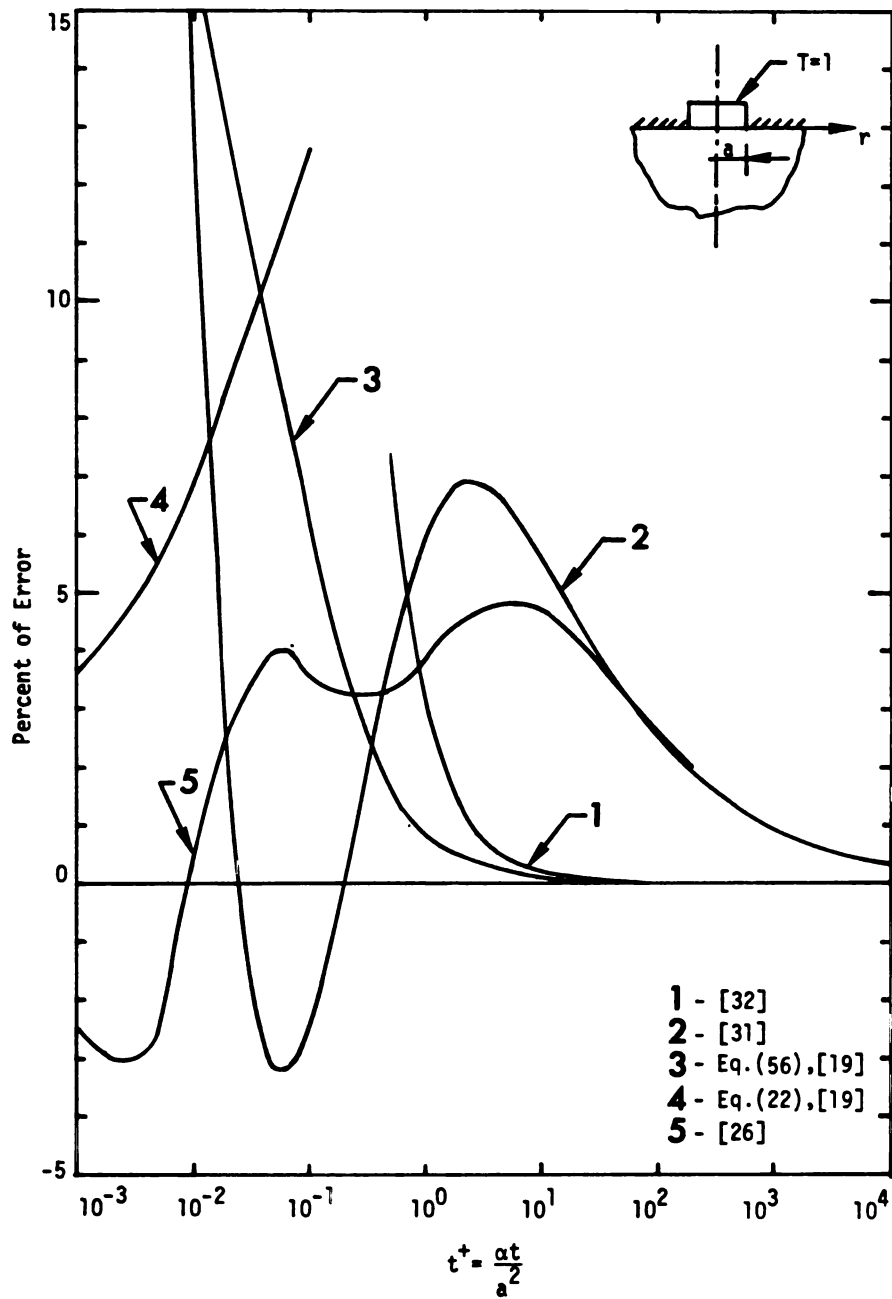


Figure 3.14 Percent of relative error in thermal constriction resistance, R_c^+ , with respect to SEM solution as function of time, Case a.

solutions [26,29,31,32,19] and the present solution for Case a. It can be seen that the solution given by Keltner [26] is in the best agreement, for the total time within approximately 5%. The two approximate solutions given by Beck and Keltner are the next closest. They provide remarkably accurate results for entire region except between $t^+ = .01$ to $t^+ = .1$ where the error is slightly high (6 to 10%). In particular the T-based solution is very accurate at the late times. It closely matches the present solution and the exact solution given by Sadhal [32] for times $t^+ > 2$ (less than .5% error). The FD solution given by Schneider et al [31], is good for mid-to-late times but is in poor agreement at early times, less than .01. It shows 13% error at $t^+ = .01$ which increases to 132.5% at $t^+ = .001$.

A study of the above results indicates that the multinode surface element solution presented here is the most accurate over the entire time region.

CHAPTER 4
INTRINSIC THERMOCOUPLE PROBLEM

4.1 Introduction

Intrinsic thermocouples are widely used for measuring rapid transient surface temperatures of conducting solids. Such measurements are important in studies of nuclear reactors, laser heating, re-entry vehicle heating, and other applications where the response of the surface temperature is of interest. An intrinsic thermocouple as defined in [27] is "one in which the material whose temperature is to be measured (called substrate) forms part of the thermocouple circuit." The most common geometry for the intrinsic thermocouple problem is a semi-infinite cylinder (called wire) attached perpendicularly to a semi-infinite solid (substrate) as shown in Fig. 1.1a.

Heat is conducted along the thermocouple wire away from the junction if the substrate's temperature increases. This heat transfer between the substrate and the wire can introduce a significant error in measurement of the interface temperature. For single step change at $t = 0$, the error is maximum at the initial moment and decreases with time.

In this chapter the transient thermal behavior of the interface between the thermocouple wire and the substrate due to a step change in the substrate temperature is analyzed. The surface element method is employed to obtain the transient solution for the interface heat fluxes and temperatures. The results are compared with those obtained by other investigators for the same problem. The wire and the substrate are considered to be in perfect contact.

Previous Work

Intrinsic thermocouple problem was first studied by Burnett [36] in 1961. He developed an approximate analytical solution for a single wire attached normally to the rear (insulated) surface of a thin slab which was exposed to a constant heat flux on its front face. The wire was infinitely long and insulated on the sides. See Fig. 4.1. The effect of the wire was simulated by a uniform disk-shaped sink. The sink strength was assumed to be equal to the flux into a semi-infinite solid which had a surface temperature equal to that of the insulated face of the slab in absence of the wire. However, this temperature was higher than that at the actual slab-wire junction and consequently, the solution provided a conservative estimate for the error in the temperature measurements. Larson [37], and Larson and Nelson [38] improved Burnett's solution by applying a correction factor which provides a more accurate value for the strength of the sink. Their solution, like the Burnett solution, is only valid for the dimensionless times (with respect to the substrate) greater than one.

In 1967, Henning and Parker [39] studied the transient thermal response of an intrinsic thermocouple due to a step change in the substrate temperature. They modeled the system as a semi-infinite cylinder attached normal to the surface of a semi-infinite body (called the idealized model). See Fig. 4.2. Perfect thermal contact was assumed between the wire and the substrate and all thermal properties were considered temperature independent and constant (linear). Also it was assumed that the heat loss from the wire to the surrounding was negligible. To simplify the analysis, they introduced a hemispherical region shown in Fig. 4.2, between $r = R$ and $x = 0$, with infinity thermal

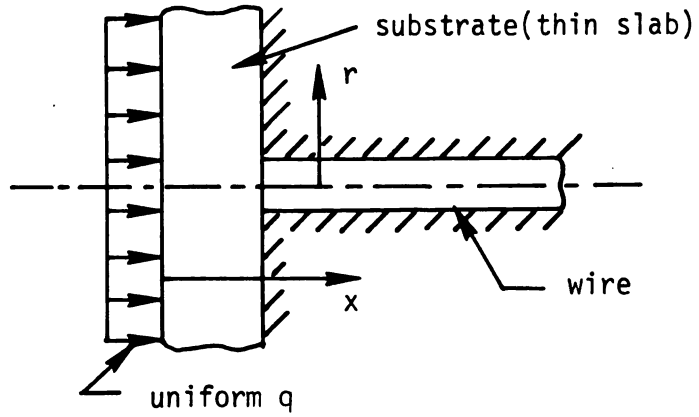


Figure 4.1 The geometry for Burnett's problem.

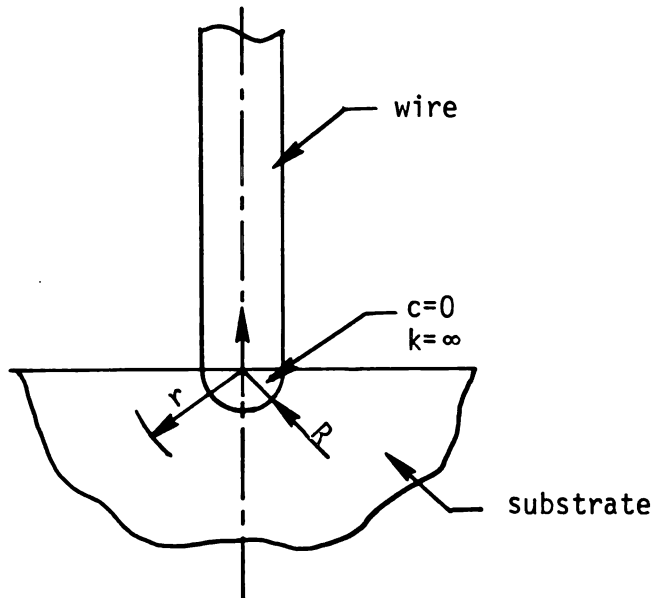


Figure 4.2 Henning and Parker's idealized geometry for an intrinsic thermocouple problem.

conductivity and no heat capacity. This assumption resulted in the temperature distributions in both the wire and the substrate being functions of only one space dimension (axial in the wire and radial in the substrate) and time. Utilizing the above assumptions they derived analytical solutions for transient temperature distributions in the semi-infinite substrate and the semi-infinite wire by using the method of separation of variables.

To investigate the validity of the analysis, they further performed a series of experiments by means of the capacitor pulse-heating method [39,40]. The experimental data were compared with the analytical results based on the response-time[†] of the thermocouples. In order to improve agreement between analytical and experimental results, Henning and Parker introduced an empirical correction factor, "G", which is related to the shape of the isotherms in the substrate. This modification improved the analytical solution for the late times. However, (as stated by other authors too [27,41]) errors up to 20% were still observed for early-to-mid times ($t^+ < 4$). Giedt and Nunn [42], further improved Henning and Parker's solution by applying a modification which provided a more accurate value for the early time response of a thermocouple. They stated that the early time solution of an intrinsic thermocouple can be approximated by using the solution for two semi-infinite bodies (initially at different temperatures) that are suddenly brought together.

[†] The response-time of an intrinsic thermocouple is the time that the junction temperature reaches 95% of the initial step change in the substrate temperature [27,39].

In 1971, Bickle [43] and Bickle and Keltner [44] examined the problem by using a combined experimental-numerical method. They employed the "deconvolution" technique developed in [43,44] to predict the thermocouple response due to an arbitrary substrate temperature variation.

In 1973, Keltner [27] studied the response of a single wire intrinsic thermocouple for the case where the substrate undergoes a step temperature change utilizing finite difference and quasi-coupling methods. He was first to employ the finite-difference procedure to solve the problem for both one-dimensional and two-dimensional models. He examined four finite difference models. In his first model (Two-D), Keltner used spherical coordinates in the substrate and cylindrical coordinates in the wire. Because of an unexpected inflection point which occurred in the interface temperature and heat flux distributions, he dropped this model in favor of the next two models which used cylindrical coordinates in both the wire and the substrate [29]. Models II and III were both axisymmetric and two-dimensional as shown in Figures 4.3 and 4.4. Model III is essentially the same as model II except in the node size and the total number of nodes. Because of the finer node structure, model III provided better results than model II, specially for the region near the outer radius of the interface between the substrate and the wire. However, it was found that the model III finite difference grid is still not fine enough to precisely model the corner region near $r^+ = 1$ [27]. The fourth FD model was one dimensional in oblate spheroidal coordinates for the substrate and in cartesian coordinates for the wire.

Because of the deficiencies involved in the finite difference solution such as; the effort in setting up large grids, large computer

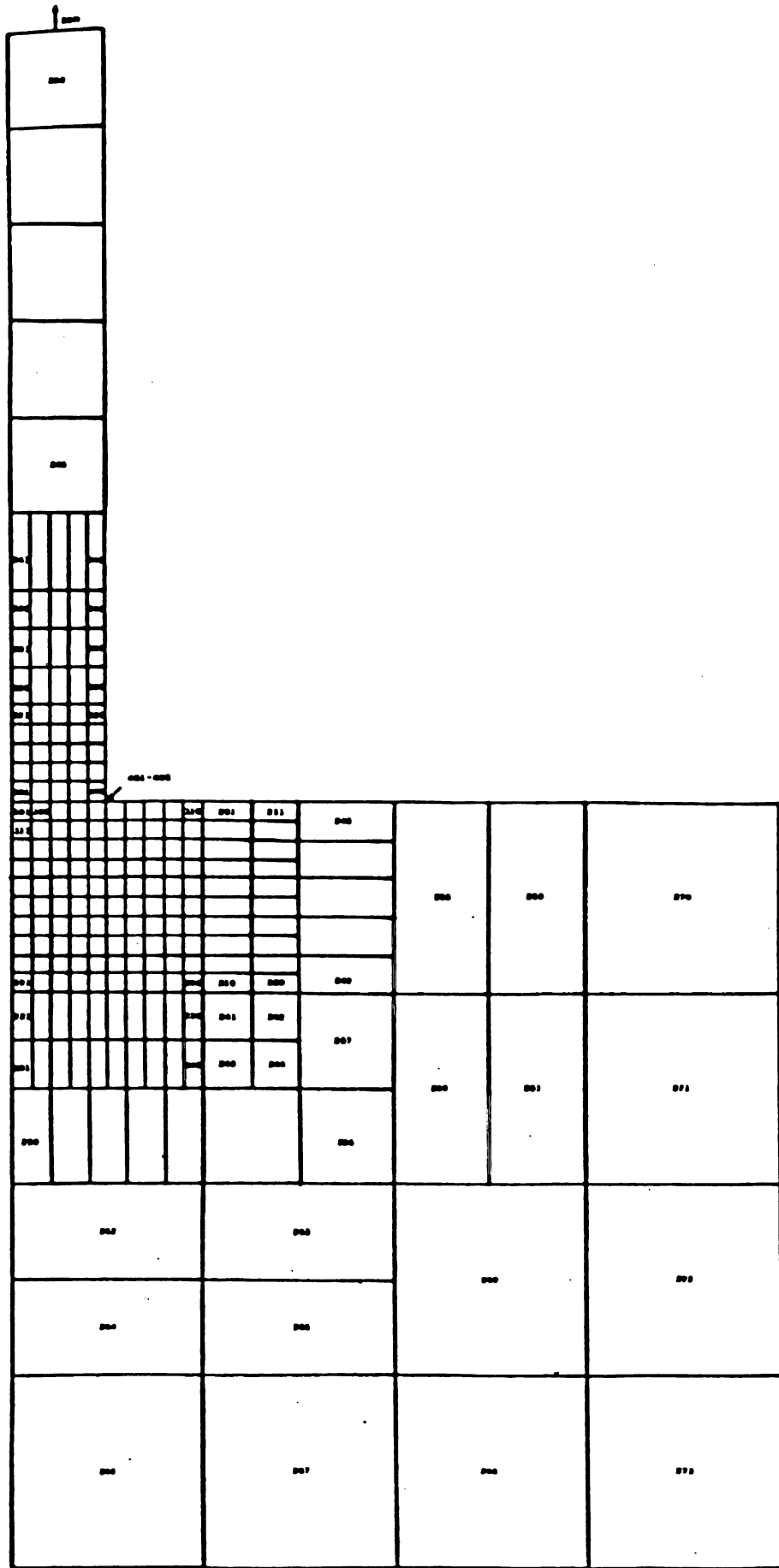


Figure 4.3 Finite difference mesh for Model II considered in reference [27]

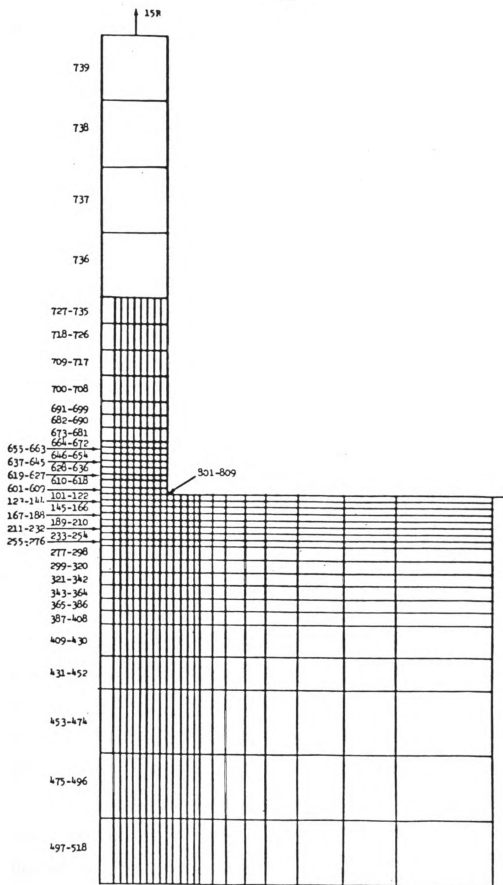


Figure 4.4 Finite difference mesh for Model III considered in reference [27]

expense and restricted dimensionless time that could be covered, Keltner developed an alternative method that he called "quasi-coupling". In this procedure, he assumed one-dimensional temperature distributions in both the substrate and the wire. To provide a uniform heat flux into the end of the cylinder (wire), a disk-shaped infinitesimally thin region having zero heat capacity and infinite thermal conductivity was inserted between the substrate and the wire. (In other words, the interface temperatures were assumed to be only a function of time; the interface temperature could be considered to be the average across the interface.) Utilizing this method Keltner obtained remarkably good agreement with his finite difference solutions. The quasi-coupled solutions unlike his finite difference solutions were simple and inexpensive to obtain.

In 1976, Shewen [41] examined the problem by utilizing a two-dimensional finite difference model in oblate spheroidal coordinates for the substrate and in cylindrical coordinates for the wire. The two dimensionality of his solution allowed a more detailed study of the temperature variations along the interface, and, consequently, provided more accurate results particularly at the early times. Keltner and Beck [18] were the first to employ the surface element method to solve the problem. They have considered only one element across the interface and solved the problem analytically by utilizing Laplace transform techniques. Some approximate solutions based on the heat flux and temperature kernel forms of Duhamel's integral were presented for early and late times.

All of the above-mentioned solution methods (except the two-dimensional finite difference solutions given by Keltner and Shewen) ignored the two-dimensionality of the problem which is especially important at early times. Even though the two-dimensional finite

difference solutions of Keltner and Shewen provided more accurate results, they are not entirely satisfactory. They have some difficulties due to the necessity of setting up extremely fine grids near the interface and many large grids further from the interface. This in turn increases the number of numerical calculations and computer time.

4.2 Statement of the Problem

The idealized geometry for the intrinsic thermocouple problem is shown in Fig. 1.1a. The semi-infinite cylinder referred to as region 1 and the semi-infinite substrate as region 2. At zero time the entire substrate undergoes a step change of temperature to T_{i2} while the wire is at its initial temperature of T_{i1} . The describing differential equations, initial and boundary conditions are the same as those for two semi-infinite bodies attached over a circular area given in Section 3.2 of Chapter 3, except for the initial and some boundary conditions of region 1, given by (3.2.2a), and (3.2.3a) and (3.2.6a), respectively. These conditions for the wire (insulated cylinder) are changed to,

$$T_1 = T_{i1} \quad \text{for } t = 0, 0 \leq r \leq a, z \geq 0 \quad (4.2.1)$$

and

$$T_1 = T_{i1} \quad \text{for } t > 0, 0 \leq r \leq a \quad \text{as } z \rightarrow \infty \quad (4.2.2)$$

$$\frac{\partial T_1}{\partial r} = 0 \quad \text{for } t > 0, r = a, z \geq 0 \quad (4.2.3)$$

4.3 Solution

The solution to the intrinsic thermocouple problem can be found using the surface element method in the same manner as presented in

Chapter 3. The contact area between the wire and the substrate is divided into ten annular variable-spaced elements with smaller elements being closer to the corner region. See Fig. 4.5. The temperature and the heat flux are assumed uniform over each element. Equations given in Sections 3.3 and 3.4 are valid and can be used for the intrinsic thermocouple problem. The only exception is that in Chapter 3 both bodies were semi-infinite and thus the required influence functions were both evaluated from the solution of a semi-infinite geometry heated by a constant heat flux over an annular region on its surface. In the intrinsic thermocouple problem only one of the bodies has semi-infinite geometry (substrate); the other one is a semi-infinite cylinder (wire),

$$\phi_{kji}^1 \neq \phi_{kji}^2 \quad (4.3.1)$$

To evaluate the influence function for the wire the exact solution for the case of a semi-infinite insulated cylinder heated by a constant heat flux over a disk area centered at the end, given by (3.4.5a), can be utilized in conjunction with (3.3.5).

The problem is analyzed for a chromel substrate and an alumel wire. The chromel and alumel combination has also been investigated in references [18,27,41]. The thermal conductivities, k 's, are 19.21 and 29.76 w/m-K, and the thermal diffusivities, α 's, are $.492 \times 10^{-5}$ and $.663 \times 10^{-5}$ m²/s for chromel and alumel, respectively. The initial temperature between the substrate and the wire is, $T_{i2} - T_{i1} = 1K$. The problem is solved for the elemental surface temperatures and heat fluxes for various values of dimensionless time, ranging between $t^+ = .001$ to $t^+ = 10^4$. The dimensionless time is based on the thermal diffusivity of the substrate (body 2),

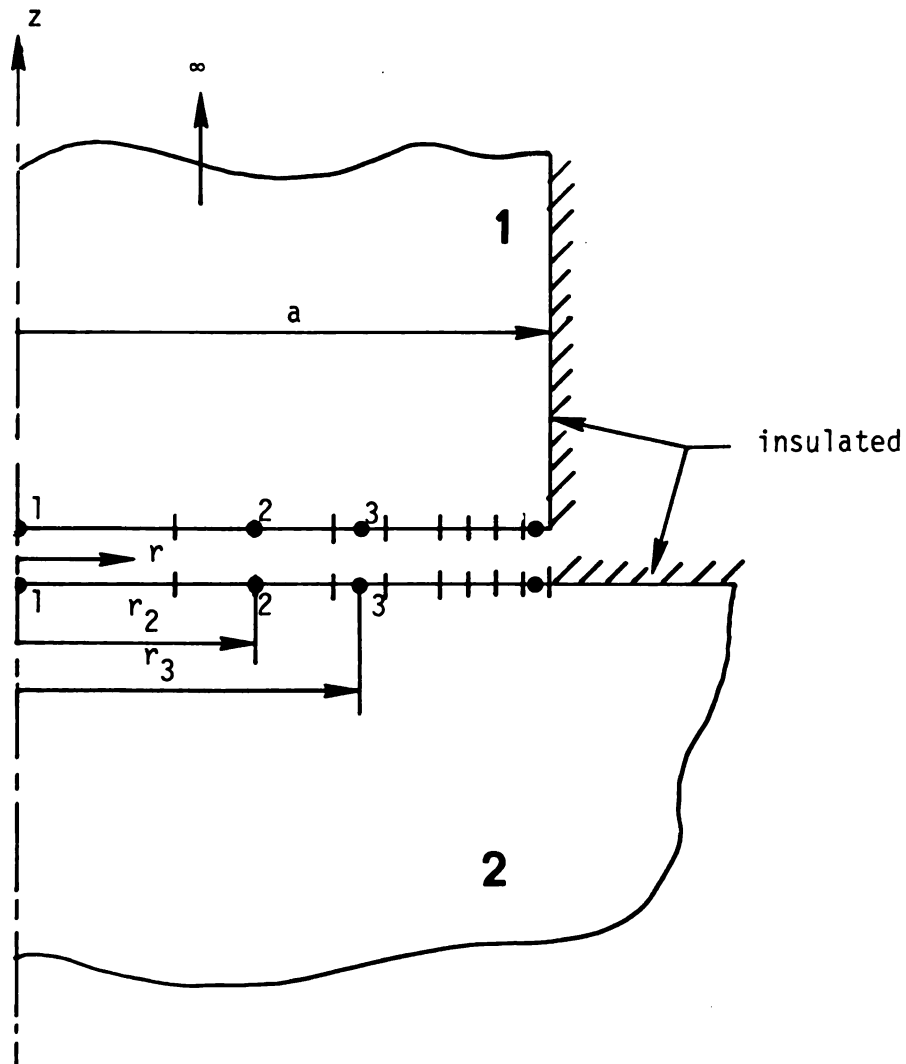


Figure 4.5 Discretization of the interface between the semi-infinite thermocouple wire and the semi-infinite substrate.

$$t^+ = \frac{\alpha_2 t}{a^2} \quad (4.3.2)$$

The results are compared with those obtained from the Henning and Parker's solution [39], Keltner's model III finite difference solution [27], Shewen's finite difference solution [41], and Keltner and Beck's single node surface element solution [18] on the bases of the area averaged interface temperature.

4.4 Results and Discussion

The results of the surface element solution are presented in terms of the temperature and heat flux distributions across the interface, and the area averaged interface temperature and heat flux as functions of time. Fig. 4.6 shows the normalized spatial variation of the interface temperature at different dimensionless times. These results are also provided in Table 4.1. Normalization is obtained by subtracting T_{i1} from elemental values, T_j , and dividing the results by $T_{i2} - T_{i1}$. It can be seen from Fig. 4.6 that the temperature gradient in the region near the corner of the interface is very large at early time and approaches to zero as t^+ goes to infinity. This justifies the two dimensionality of the problem and also indicates that more accurate studies are required in this region, especially at the early times.

Keltner in his model III finite difference solution used more than 400 nodes in the semi-infinite body to represent the corner region effectively. He found that even his fine grid structure introduces some errors. Employing oblate spheroidal coordinates Shewen [41] obtained approximately the same results with a smaller number of nodes (120) and consequently less computational effort than that used by

TABLE 4.1
 Normalized values of elemental interface temperature, T_j^+ , as a function of dimensionless time $t^+ = \alpha_2 t/a^2$.

t^+	r^+	.0	.3	.45	.55	.65	.75	.825	.875	.925	.975
	El. #1	2	3	4	5	6	7	8	9	10	
.001	.4285	.4285	.4285	.4285	.4286	.4286	.4286	.4286	.4288	.4336	.4743
.002	.4285	.4285	.4285	.4285	.4286	.4286	.4286	.4289	.4312	.4436	.4925
.005	.4285	.4285	.4285	.4285	.4286	.4293	.4336	.4336	.4430	.4654	.5157
.01	.4285	.4285	.4285	.4287	.4295	.4338	.4445	.4445	.4593	.4851	.5320
.02	.4285	.4286	.4291	.4305	.4347	.4455	.4620	.4620	.4796	.5056	.5472
.05	.4294	.4317	.4366	.4437	.4542	.4718	.4916	.4916	.5093	.5327	.5669
.1	.4383	.4449	.4547	.4647	.4787	.4979	.5172	.5172	.5334	.5538	.5826
.2	.4669	.4754	.4867	.4975	.5114	.5293	.5465	.5465	.5604	.5977	.6015
.5	.5331	.5402	.5495	.5582	.5692	.5833	.5966	.5966	.6073	.6205	.6385
1.	.5955	.6011	.6084	.6152	.6239	.6350	.6455	.6455	.6539	.6643	.6785
5.	.7503	.7532	.7571	.7606	.7652	.7711	.7766	.7766	.7811	.7867	.7943
10.	.8091	.8113	.8141	.8167	.8201	.8244	.8285	.8285	.8319	.8360	.8416
100.	.9332	.9340	.9349	.9358	.9369	.9384	.9397	.9397	.9409	.9422	.9441
1000.	.9786	.9788	.9791	.9794	.9797	.9802	.9806	.9806	.9810	.9814	.9820
10000.	.9932	.9933	.9934	.9935	.9936	.9937	.9939	.9939	.9940	.9941	.9943
10 ⁷	.9998	.9998	.9998	.9998	.9998	.9998	.9998	.9998	.9998	.9998	.9998

$$T_j^+ = \frac{T_j - T_{i1}}{T_{i2} - T_{i1}}$$

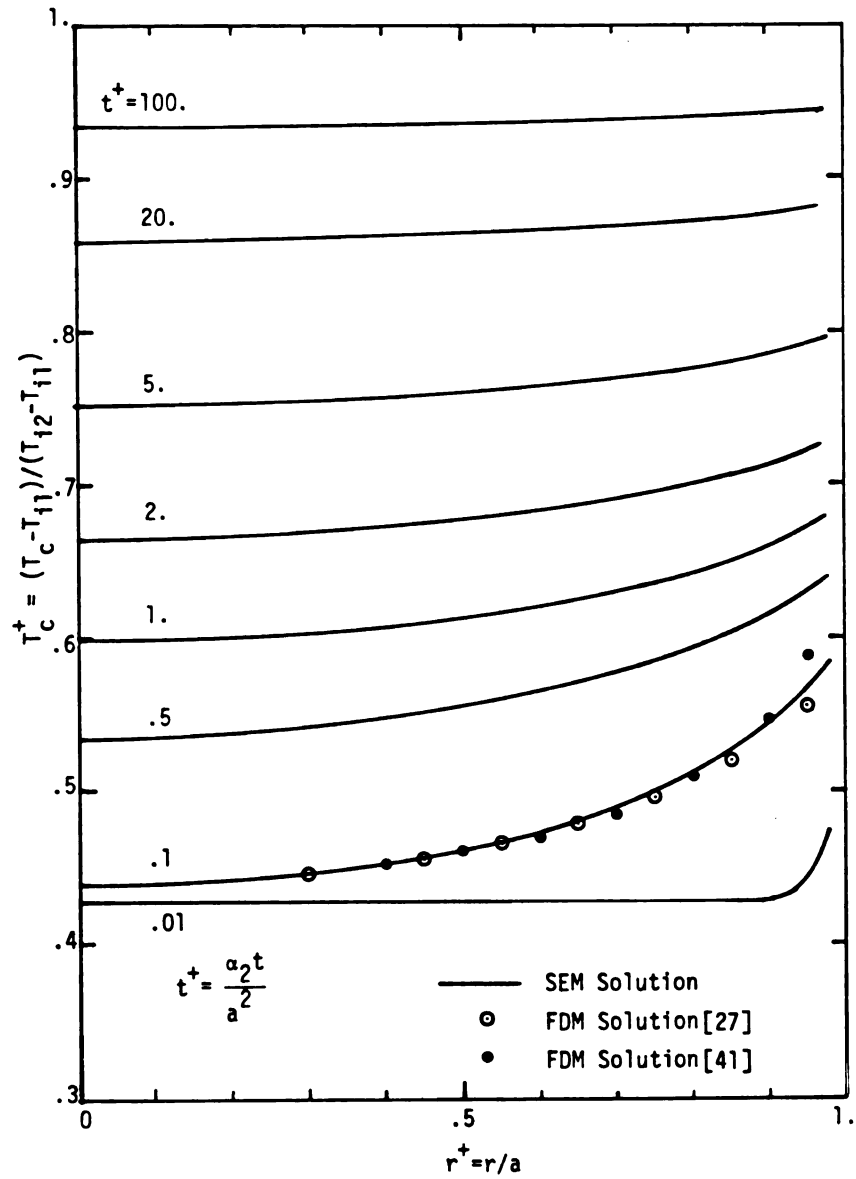


Figure 4.6 Normalized interface temperature distribution for intrinsic thermocouple with chromel half-space and alumel wire.

Keltner. Their results are also shown in Fig. 4.6 for time $t^+ = .1$. It can be seen that the agreement between the above finite difference solutions and the present surface element solution is very good. Notice that the number of nodes used in the SEM solution is only ten, 12 times less than that used by Shewen, and about 40 times less than that used by Keltner.

When the substrate initially undergoes a step change of temperature, there is an instantaneous change to a common interface temperature which depends upon the thermal properties of the substrate and the wire[†]. The normalized value of this initial interface temperature^{††} is given by [18],

$$T_{ic}^+ = \frac{T_{ic} - T_{i1}}{T_{i2} - T_{i1}} = (1+\beta)^{-1} \quad (4.4.1)$$

where

$$\beta = [k_1 \rho_1 c_1 / k_2 \rho_2 c_2]^{1/2} \quad (4.4.2)$$

For a chromel substrate and an alumel wire the value of T_{ic}^+ is equal to .4285. After the initial moment the effect of the edge starts to penetrate toward the center of the contact area. This is evident from the results given in Table 4.1. It can be seen that at $t^+ = .001$, the interface temperature is almost at its initial value (.4285) for

[†] Notice that at the initial moment there is no spatial variation in the interface temperature.

^{††} This temperature corresponds to the surface temperature of two semi-infinite bodies initially at different temperatures suddenly brought into the perfect contact.

$r^+ \leq .825$. The only part of the contact area which is disturbed by the edge effect is between $r^+ = .825$ and $r^+ = 1$. The edge effect penetrates further toward the center as t^+ becomes larger, reaching $r^+ = .45$ at $t^+ = .01$ and covering the entire area for $t^+ > .02$. The difference between the centerline and the outermost element temperatures is about 10.7% at time $t^+ = .001$ and decreases as t^+ becomes larger. For $t^+ > 20$ the interface temperature distribution becomes almost uniform which indicates that the one-dimensional approximate solution given by Henning and Parker and the T-based solution of Keltner and Beck [18] are appropriate for the late times.

Fig. 4.7 shows the normalized flux distribution across the interface, $q^+(t)$, at several times. It can be seen that the region of uniform heat flux shrinks as t^+ increases. After dimensionless time about 20 the q^+ distribution remains constant and a universal curve is obtained.

Fig. 4.8 shows the normalized area averaged interface temperature versus the dimensionless time. Results for the model III finite difference solution of reference [27], and the finite difference solution of reference [41] as well as the SEM solution are presented. Table 4.2 provides the results of the above-mentioned three solutions along with the results from the approximate analytical solution of reference [39], and the T-based and the q-based solutions of [18]. The first column in this table is the dimensionless time which extends from $t^+ = .001$ to $t^+ = 500$. The results of the finite difference solutions of references [27] and [41] are given in the second and the third columns, respectively. The fourth column is evaluated from equation (22) given by Henning and Parker, which is only good for the late time, $t^+ > 20$. The early and the late times results of the T-based solution and the

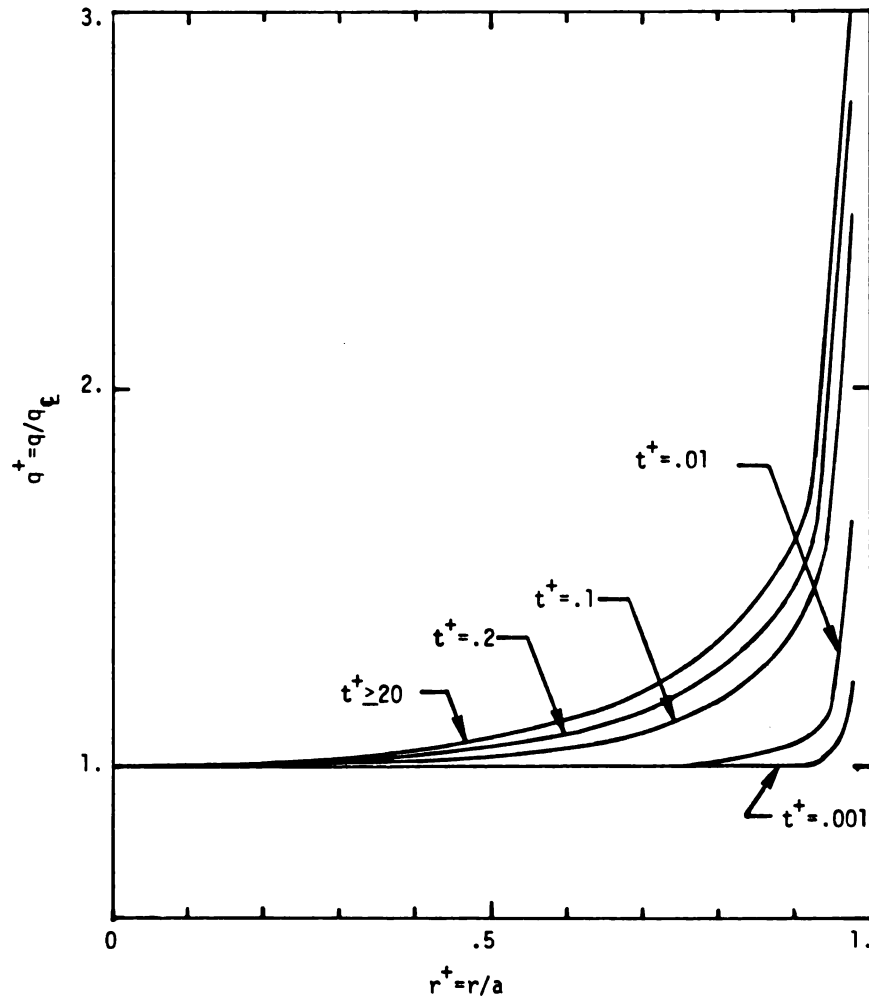


Figure 4.7 Normalized heat flux distribution across the interface at various values of time for intrinsic thermocouple.

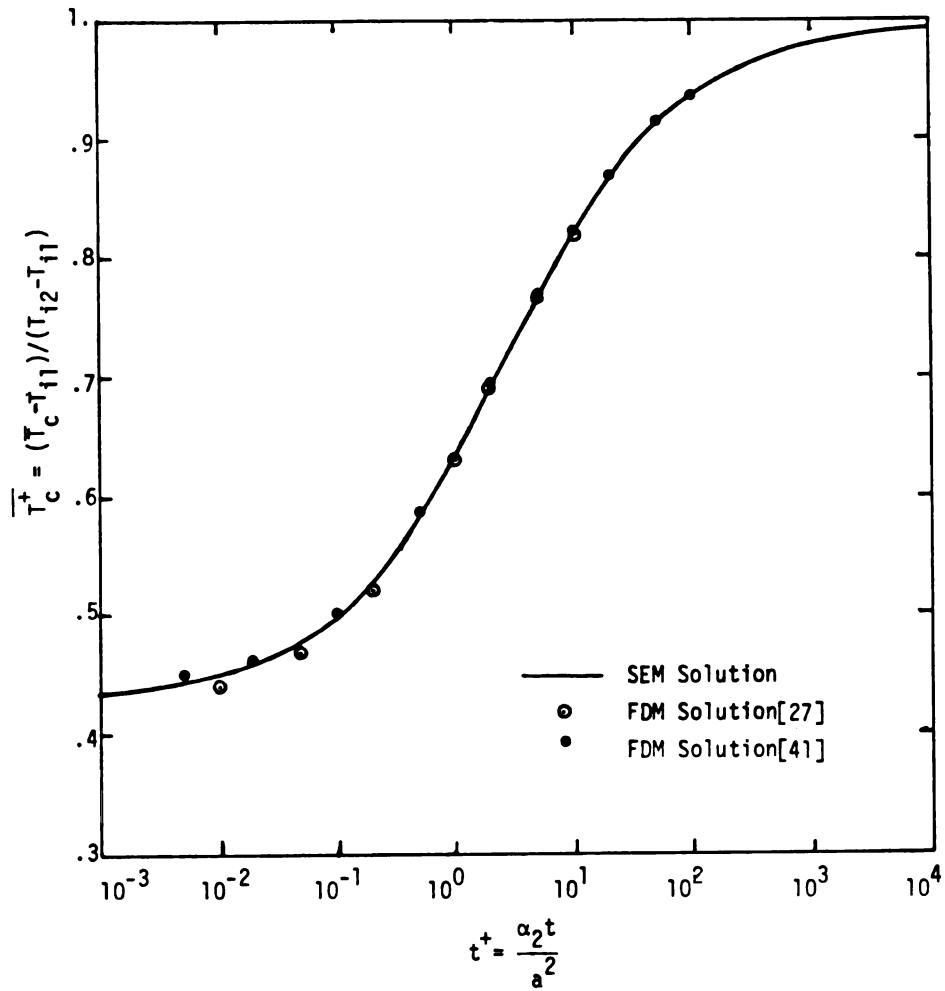


Figure 4.8 Normalized area averaged interface temperature histories for intrinsic thermocouple problem.

q-based solution of Keltner and Beck, are displayed in the next four columns. The last column represents the present SEM solution. As can be seen from Fig. 4.8 and Table 4.2, there is very good agreement between the finite difference solutions and the present solution for the time range covered. For a given time between $t^+ = .01$ and 10, the SEM values are between the two finite difference solutions. The FD solution of reference [41] is more accurate at early times than that of reference [27]. This is because of that the oblate spheroidal coordinates used in the former model describes the geometry more closely than the cylindrical coordinates used in the latter model. As mentioned earlier, however, both solutions have difficulties regarding the computational effort and cost, particularly for the early times, $t^+ < .01$.

The T-based and the q-based single node surface element solutions given by Keltner and Beck [18] are convenient in that the mathematics is not difficult and the expressions are simple to evaluate. Each solution provides two expressions; one for early times and the other for late times. The q-based solution is more appropriate for the early times. It approaches the exact solution (.4285) as $t^+ \rightarrow 0$, and closely matches the SEM solution up to dimensionless time $t^+ = .1$. It also provides relatively good results for the late times $t^+ > 10$. The T-based solution does not approach the exact solution as $t^+ \rightarrow 0$, and consequently it is less accurate than the q-based solution for the early times. Because of the constant interface temperature assumption, however, it yields very good results for the late times of $t^+ > .1$. It should be noted that neither the T-based solution nor the q-based solution is solely suitable for the complete time domain. However, a combination of the early-time q-based solution (equation (41a) of [18]) and the late-time T-based solution (equation (33a) of [18]) provides

TABLE 4.2

Normalized area averaged interface temperature histories for chromel substrate and alumel wire.

t^+	FD Solutions		Henning and Parker [39]	T-based Solution [18]		q-based Solution		SEM
	[27]	[41]		early time	late time	early time	late time	
.001			.6084	.4489		.4342		.4335
.002		.4421	.6118	.4500		.4366		.4364
.005		.4480	.6185	.4521		.4413		.4422
.01	.4402	.4510	.6257	.4545		.4467		.4488
.02	.4505	.4599	.6356			.4546		.4581
.05	.4700	.4782	.6540			.4709		.4765
.1	.4916	.4991	.6731		.4907	.4904		.4973
.2	.5215	.5283	.6972		.5280			.5263
.5	.5770	.5826	.7373		.5910			.5805
1.	.6302	.6338	.7729		.6452			.6328
2.	.6896	.6921	.8109		.7042			.6915
5.	.7688	.7714	.8602		.7810			.7700
10.	.8202	.8246	.8933		.8327		.8091	.8236
20.		.8694	.9207		.8757		.8614	.8687
50.		.9139	.9482		.9186		.9108	.9137
100.		.9382	.9629		.9417		.9365	.9381
200.			.9735		.9585		.9550	.9559
500.			.9832		.9737		.9715	.9719

very good results over the entire time range. These two solutions match very closely at dimensionless time $t^+ = .1$. Fig. 4.9 shows the percent of error between the above-mentioned solutions [27,41,39,18], and the present solution. It can be seen that the finite difference solution given by Shewen [41] is in the best agreement for $t^+ > .002$ within approximately 1%. The model III finite difference solution of Keltner has a deviation about 2% at $t^+ = .01$ which decreases to less than 1% at late times. The solution given by Henning and Parker is good for late times but is in poor agreement for early-to-mid times less than 20. It shows 6% error at $t^+ = 20$ which increases to 40.3% at $t^+ = .001$. All approximate solutions presented by Keltner and Beck lie within 2% of the present solution over their range of validity except the early-time T-based solution which shows an error of about 4.2% at time zero. This solution can be modified by letting the factor of 1.90484 (given in equation (34) of [18]) be replaced by $\pi^{1/2}$. The modified solution provides better results for the early times ($t^+ < .005$) and approaches the exact solution as $t^+ \rightarrow 0$. See Fig. 4.9. In Fig. 4.10 normalized values of averaged interface heat flux, $\overline{q^+}$, is plotted versus dimensionless time. Normalization is obtained by dividing the heat flux values by $k_2 \cdot a \cdot (T_{i2} - T_{i1})$.

A study of the above results shows that the multinode surface element solution provides an accurate representation of the idealized intrinsic thermocouple. It is superior to other available solutions in terms of accuracy and ability to treat the complete time domain. The method is most suitable for calculating the interface temperature and heat flux, particularly at early times when the two-dimensionality of the problem is significant.

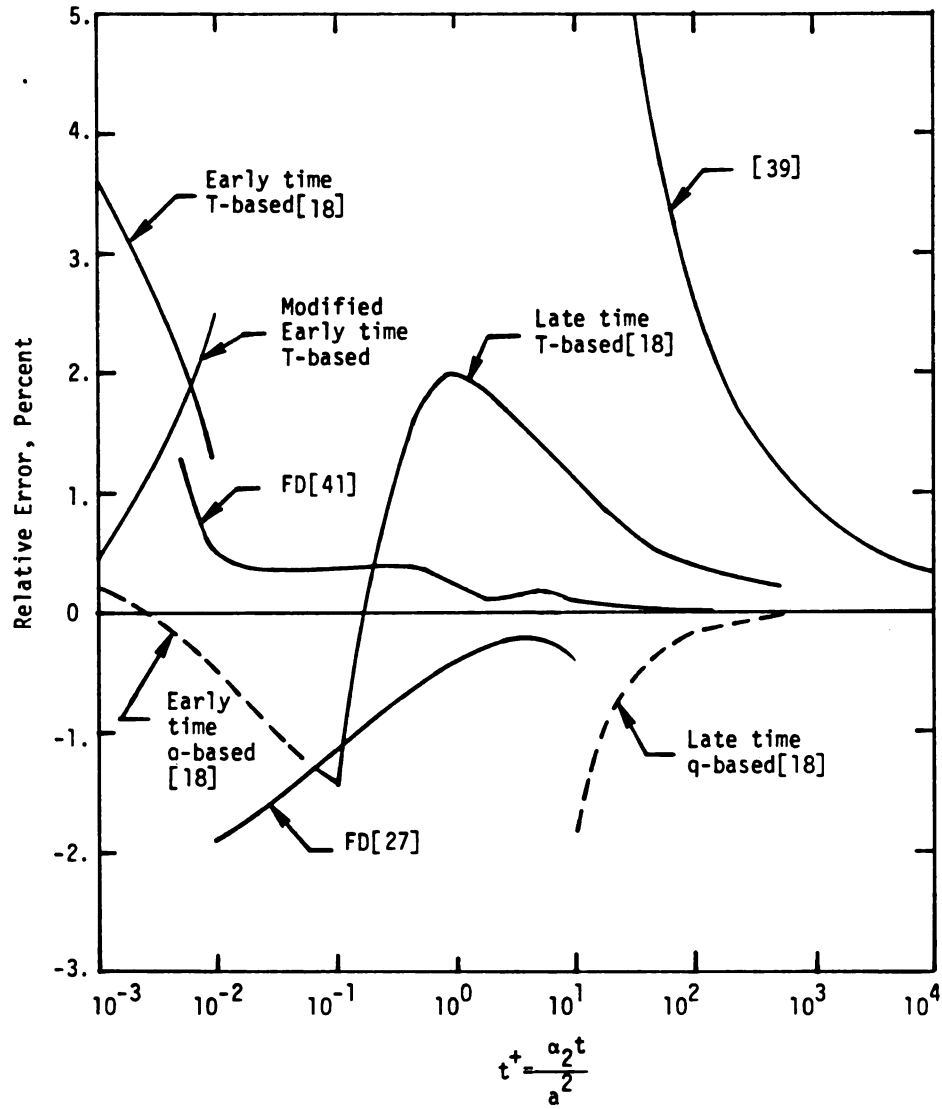


Figure 4.9 Percent of relative error (with respect to SEM solution) in interface temperature as function of time for intrinsic thermocouple problem.

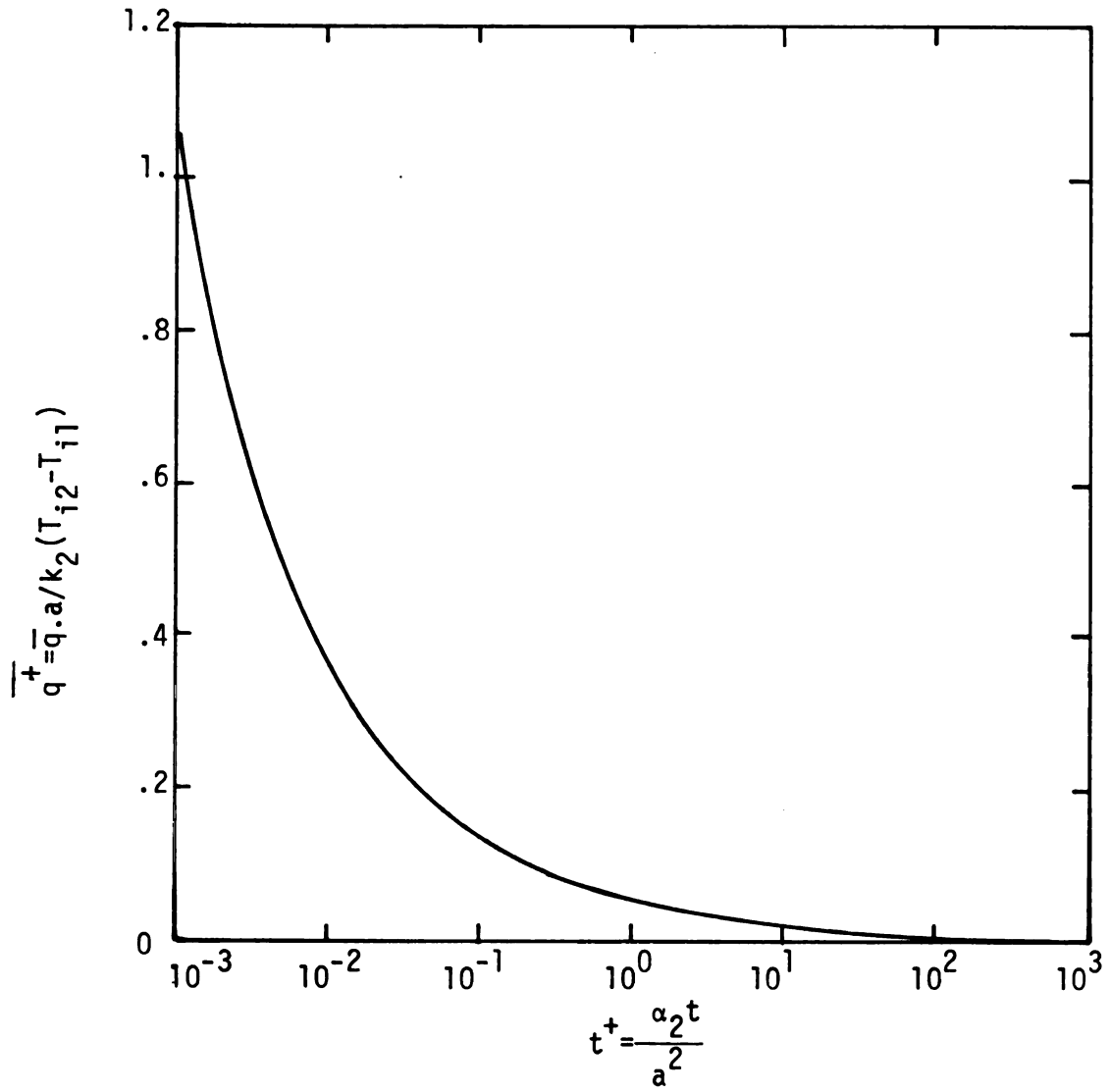


Figure 4.10 Normalized area averaged interface heat flux histories for intrinsic thermocouple problem.

CHAPTER 5

SEMI-INFINITE BODY WITH MIXED BOUNDARY CONDITIONS

5.1 Introduction

In this chapter the transient thermal response of a semi-infinite body with the mixed boundary conditions of a step change of the surface temperature over an infinite strip and insulated elsewhere is considered. See Fig. 1.3a. This problem is similar to the problem of two semi-infinite bodies with identical properties having different initial temperatures brought suddenly into the perfect thermal contact over an infinite strip and insulated over the rest of the contacting planes. The surface element method is employed to obtain the transient solutions for the interface heat fluxes and the thermal constriction resistance of the contact area.

The solution has applications in the problems involving electronic cooling, strip welding, fins, and thermal contact conductance. To the author's knowledge there is no solution available for the above problem in the open literatures. Sadhal [45] has examined the related problem of two semi-infinite bodies having perfect contact over a series of equally-spaced infinite strips. The regions between these strips were insulated. By considering the planes of symmetry between the strips (see Fig. 5.1) he solved the problem for large times by utilizing the Laplace tranform technique. However, his solution is not valid for the situations in which there is a small fraction of the interface in contact ($c \leq \ell$), and consequently cannot be applied to the problem of two semi-infinite bodies with a single strip contact.

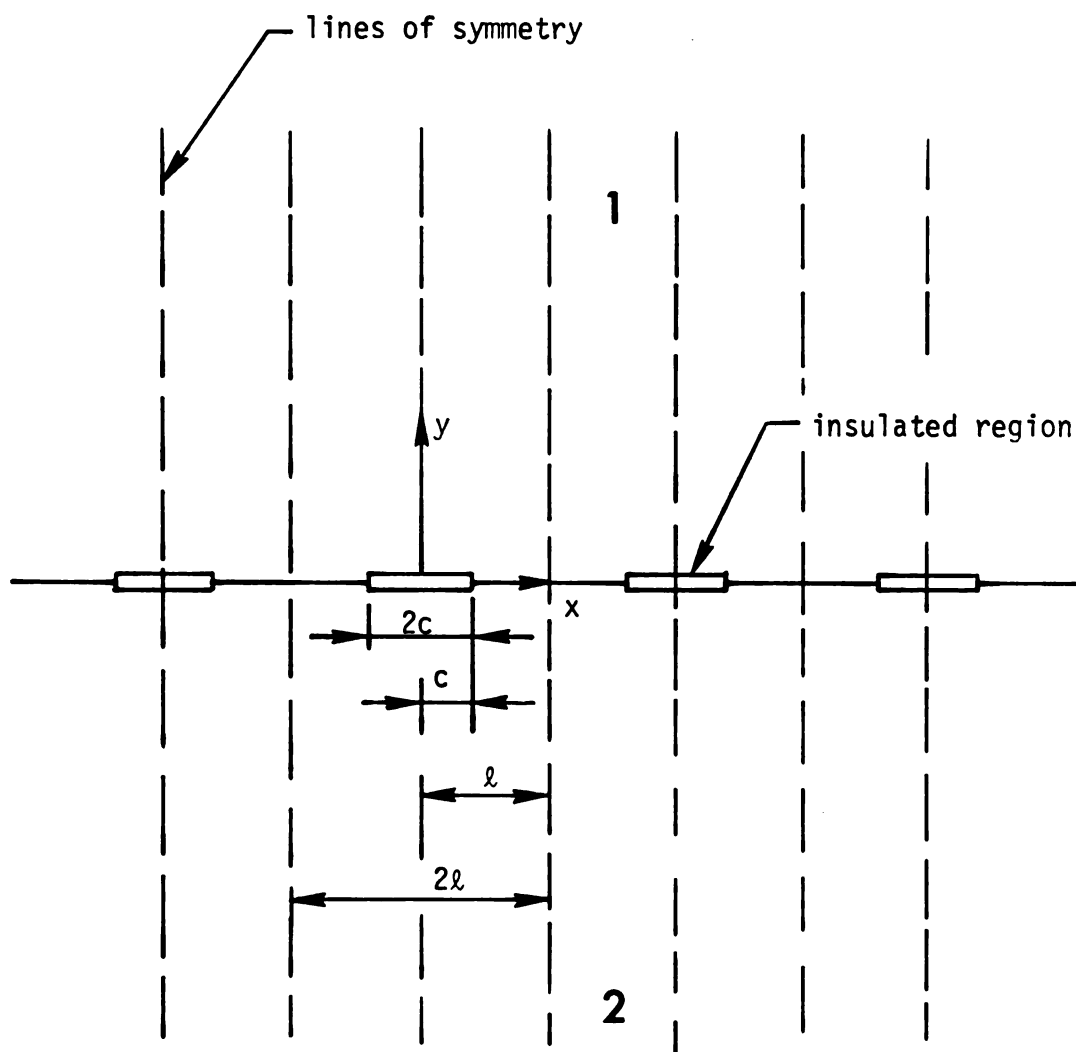


Figure 5.1 Geometry for Sadhal's problem.

5.2 Statement of the Problem

The geometry being considered is shown in Fig. 1.3a. A semi-infinite body is subjected to a uniform step temperature change, T_c , over an infinite strip with width $2a$, on its surface. The rest of the surface is insulated. The body is initially at the uniform temperature of T_0 , and the thermal properties are assumed to be independent of temperature. The describing equations are:

$$\frac{\partial^2 T}{\partial x^2} + \frac{\partial^2 T}{\partial z^2} = \frac{1}{\alpha} \frac{\partial T}{\partial t} \quad (5.2.1)$$

$$T = T_0 \quad \text{for } t = 0; |x| \geq 0; z \geq 0 \quad (5.2.2)$$

$$T = T_c \quad \text{for } t > 0; -a \leq x \leq a; z = 0 \quad (5.2.3a)$$

$$\frac{\partial T}{\partial z} = 0 \quad \text{for } t > 0; |x| > a; z = 0 \quad (5.2.3b)$$

$$T = T_0 \quad \text{for } t > 0 \text{ as } x \rightarrow \pm \infty \text{ and } z \rightarrow \infty \quad (5.2.4)$$

where T denotes the temperature distribution, α represents the thermal diffusivity, x and z are space coordinates, and t is time.

5.3 Solution

By considering the problem symmetry about the x axis, the solution is required only for the region $x \geq 0$, and consequently only half of the contact area need to be discretized. To apply the surface element method, the surface region between $x = 0$ to $x = a$ is divided into ten elements (each being an infinite strip) over each of which the heat flux is uniform and at the center of which the prescribed temperature is T_c . See Fig. 5.2. Equations (3.3.2a) and (3.3.2b) given in Chapter

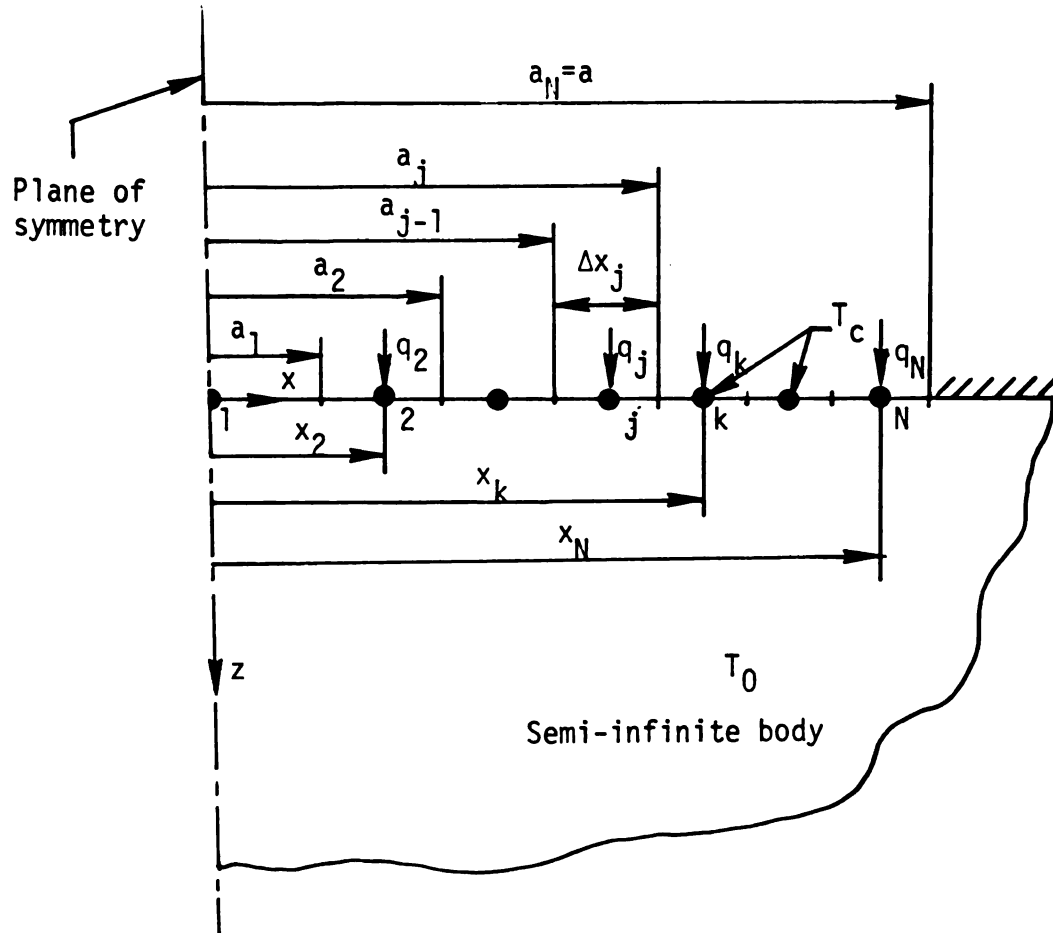


Figure 5.2 Possible distribution of surface elements for the problem of semi-infinite body with constant surface temperature, T_c , over an infinite strip.

3 can be used to determine the elemental heat fluxes at various values of time. It should be noted that for this case where only a single body exists, the elements of the initial temperature vector, \bar{T}_i , are the same and equal to $T_c - T_0$.

The influence functions for the geometry shown in Fig. 5.2 can be evaluated from the exact solution for the problem of a semi-infinite body heated with a constant heat flux over an infinite strip by applying simple superposition. The procedure is the same as that presented in Section 3.3.2. It should be noted, however, that for the geometry of Fig. 5.2, the function θ_{kji} represents the temperature rise at element k due to a unit heat flux over the elements 1 through j ($x = 0$ to $x = a_j$) at time t_i , while the influence function ϕ_{kji} denotes the temperature rise at element k due to a unit heat flux at only element j at the same time.

The solutions for the local and the spatial average surface temperature histories for a semi-infinite body exposed to a constant heat flux over an infinite strip are provided in Chapter 6. The solutions are given by (6.4.3) and (6.4.4a), respectively. In the SEM solution presented here, both local and average values of the influence function are used and the results are compared.

Averaged Interface Heat Flux

The spatial average of the interface heat flux can be obtained by summing the products of the elemental heat flux and the fraction of the total contact area occupied by the element,

$$\bar{q}(t_M) = \sum_{j=1}^N q_{jM} (A_j/A_c) \quad (5.3.1)$$

where q_{jM} is the heat flux at element j at time $t_M = M \cdot \Delta t$, A_j is the area of element j , A_c is the total contact area, and N is the number of elements. For the case where all elements are semi-infinite strips, (5.3.1) can be written as

$$\bar{q}(t_M) = \sum_{j=1}^N q_{jM} \cdot [(a_j - a_{j-1})/a] \quad (5.3.2)$$

where a_j , a_{j-1} , and a are shown in Fig. 5.2. If further the elements are equally-spaced, the average heat flux can be given by,

$$\bar{q}(t_M) = \frac{1}{N} \sum_{j=1}^N q_{jM} \quad (5.3.3)$$

Thermal Constriction Resistance

Based on the definition given in Section 3.5, the thermal constriction resistance (per unit length of the strip) for the above problem can be written as,

$$R_c(t_M) = \frac{T_c - T_0}{2a \bar{q}(t_M)} \quad (5.3.4)$$

which is related to dimensionless heat flux by,

$$R_c(t_M) = \frac{1}{2k \bar{q}^+(t_M)} \quad (5.3.5)$$

where

$$\bar{q}^+ = \frac{\bar{q} \cdot a}{k(T_c - T_0)} \quad (5.3.6)$$

Equation (5.3.5) can be written in dimensionless form as,

$$R_c^+ (t_M) = \frac{1}{2 \bar{q}^+ (t_M)}, \quad R_c^+ \equiv R_c \cdot k \quad (5.3.7a,b)$$

Analytical Solution for the Average Interface Heat Flux

By considering only one element along the interface an approximate analytical solution for the average interface heat flux can be obtained by utilizing the Laplace transform technique. This method was first used by Keltner and Beck [18] for the intrinsic thermocouple problem. Their solution was discussed in Chapter 4. Starting with Duhamel's integral for the average interface temperature one can write,

$$T_c - T_0 = \frac{\partial}{\partial t} \int_0^t \bar{q}(\lambda) \bar{\phi}(0, t-\lambda) d\lambda \quad (5.3.8)$$

where the influence function $\bar{\phi}(0, t)$ is the spatial average temperature rise over the element ($z=0$) for a unit heat flux. Taking the Laplace transform of (5.3.8) gives

$$[T_c - T_0] = s \mathcal{L} \left[\int_0^t \bar{q}(\lambda) \bar{\phi}(0, t-\lambda) d\lambda \right] \quad (5.3.9)$$

or

$$\frac{1}{s} [T_c - T_0] = s \hat{q}(s) \cdot \hat{\phi}(s) \quad (5.3.10)$$

where the functions $\hat{q}(s)$ and $\hat{\phi}(s)$ are the transforms of $\bar{q}(t)$ and $\bar{\phi}(t)$, respectively. Solving for $\hat{q}(s)$ provides

$$\hat{q}(s) = \frac{T_c - T_0}{s^2 \cdot \hat{\phi}(s)} \quad (5.3.11)$$

This equation can be written in dimensionless form as

$$\frac{\hat{q}^+}{(s^+)^2} = \frac{1}{\overline{\phi}^+(s^+)} \quad (5.3.12)$$

where

$$t^+ = \frac{\alpha t}{a^2}, \quad \overline{\phi}^+ = \frac{k \cdot \overline{\phi}}{a}, \quad s^+ = \frac{sa^2}{\alpha} \quad (5.3.13a,b,c)$$

and \overline{q}^+ is given by (5.3.6).

Early Time Solution

For small dimensionless times, the average influence function $\overline{\phi}^+$ is given by (6.4.4c) as

$$\overline{\phi}^+ \approx 2 (t^+/\pi)^{1/2} - \frac{t^+}{\pi} + \frac{1}{2} (t^+)^3 e^{-1/t^+} (1 - \frac{9}{2} t^+) \quad (5.3.14)$$

For an error less than .033% the exponential term can be dropped for $t^+ < .3$, and thus

$$\overline{\phi}^+ \approx 2 (t^+/\pi)^{1/2} - \frac{t^+}{\pi} \quad (5.3.15)$$

Taking the Laplace transform of (5.3.15) yields

$$\frac{\hat{\phi}^+}{(s^+)^2} = (s^+)^{-3/2} - \frac{1}{\pi (s^+)^2} \quad (5.3.16)$$

substituting (5.3.16) into (5.3.12) and taking the inverse transform

gives

$$\overline{q^+}(t^+) = (\pi t^+)^{-1/2} + \frac{1}{\pi} e^{t^+/\pi^2} \operatorname{erfc}(-t^{+1/2}/\pi) \quad (5.3.17)$$

This equation can be further simplified to

$$\overline{q^+}(t^+) = (\pi t^+)^{-1/2} + \frac{1}{\pi} \quad (5.3.18)$$

which provides less than 3% error for $t^+ < .01$.

Late Time Solution

For late dimensionless times, the function $\overline{\phi^+}$ is given by (6.4.4b). For an error less .2% the second term on the right hand side of this expression ($\frac{4}{3\pi t^+}$) can be dropped for $t^+ > 100$, and one can write

$$\overline{\phi^+} = \frac{1}{\pi} [\ln t^+ + 3 - \gamma], \quad (\gamma = 5772\dots) \quad (5.3.19)$$

Taking the Laplace transform of (5.3.18) gives

$$\frac{\hat{\phi^+}}{\pi s} = \frac{1}{\pi s} (3 - 2\gamma - \ln s^+) \quad (5.3.20)$$

substituting (5.3.19) into (5.3.12) and taking the inverse transform by utilizing the approximate method (which is accurate for $f(s)$ functions that vary slowly with $\ln s$) given in [46] yields

$$\overline{q^+}(t^+) = \pi(\ln 2t^+ + 3 - 2\gamma)^{-1} \quad (5.3.21)$$

which shows that the average surface heat flux increases as the inverse of the logarithm of time for large times.

5.4 Solution to the Interior Region

Once the elemental heat flux histories have been determined, the solution to the interior temperature history, $T(x,z,t)$, can be obtained by superimposing the total effect of all these heat fluxes. That is

$$T(x,z,t_M) = T_0 + \sum_{j=1}^N \sum_{i=1}^M q_{ji} \Delta \phi_{j,M-i}(x,z) \quad (5.4.1)$$

where

$$\Delta \phi_{j,M-i}(x,z) = \phi_{j,M+1-i}(x,z) - \phi_{j,M-i}(x,z) \quad (5.4.2)$$

and the influence function, $\phi_{jM}(x,z)$, is the temperature rise at point (x,z) due to a unit heat flux at element j at time $t_M = M \cdot \Delta t$. Equation (5.4.2) can be written in a more convenient form as,

$$T_M(x,z) = M T_0 - \sum_{k=1}^{M-1} T_k(x,z) + \sum_{j=1}^N \sum_{i=1}^M q_{ji} \phi_{j,M+1-i}(x,z) \quad (5.4.3)$$

The solution for the influence function, $\phi_{jM}(x,z)$, can be obtained from (6.3.18) given in Chapter 6.

5.5 Results and Discussion

Two cases of equally-spaced elements and variable-spaced elements are examined. The first case is utilized to learn how the accuracy varies with the size of element, while the second case is used to obtain accurate results in the corner region near $x = \pm a$. For both cases, elemental surface heat fluxes are determined for various values

of dimensionless time, ranging between $t^+ = .01$ to 1000. At each time, the elemental heat fluxes are evaluated in twenty time steps. This means that for larger times, larger time steps are considered. For instance, to determine, $q_j(t^+)$'s, at dimensionless times of $t^+ = .01$, 1, and 1000, the time steps of $\Delta t^+ = .0005$, $.05$, and 50 are used, respectively.

$$\text{No. of Time Steps (NTS)} = \frac{.01}{.0005} = \frac{1}{.05} = \frac{1000}{50} = 20 \quad (5.5.1)$$

This substantially reduces the computational effort and provides more uniform accuracies for results (with respect to NTS) than the case where a small constant time step is used for the entire time range.

To show how accuracies of results change with NTS, the case of equally-spaced elements is also examined with values of NTS being equal to 10, 5, and 2. In Fig. 5.3, the normalized area averaged interface heat flux is plotted versus $1/\text{NTS}$, for different values of dimensionless times. Study of this figure leads to the following observations:

1. The accuracy of the heat flux histories vary linearly with $\frac{1}{\text{NTS}}$, and become more accurate as NTS increases. (The most accurate values can be obtained at $\frac{1}{\text{NTS}} = 0$ by employing linear interpolation). For $\text{NTS} = 2$, however, slight deviation (from a straight line) can be seen at early times, $t^+ < .1$. The deviation is less than 2% at $t^+ = .01$, and approaches zero as t^+ becomes larger.
2. The slope of the straight lines shown in the figure are large at early times and become smaller for late times. This implies that, in order to have good accuracy at early times, NTS should be large, while the same accuracy can be obtained with smaller values of NTS, at later times. For instance, the required NTS for less than 3% errors in heat

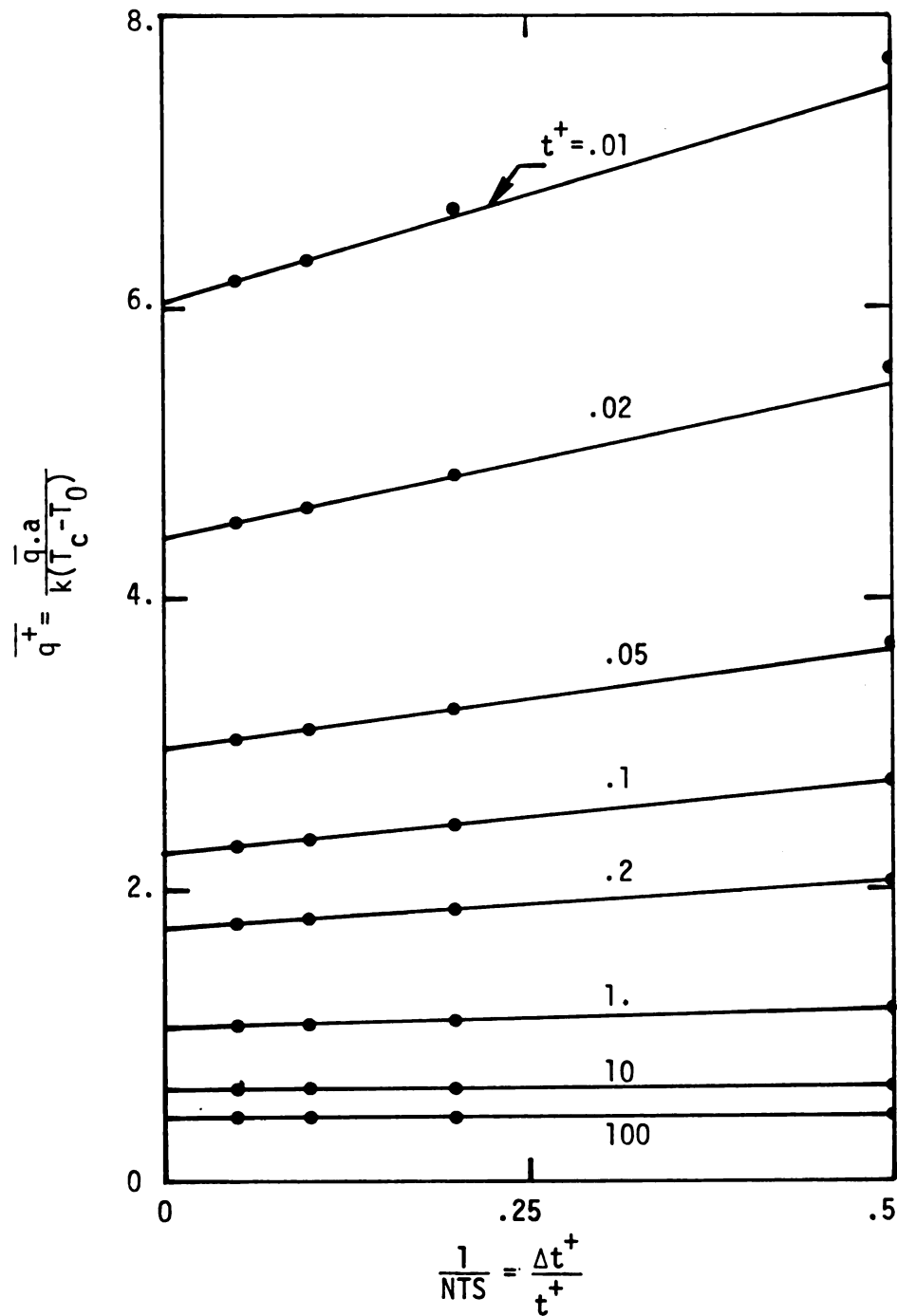


Figure 5.3 Variation of the normalized area averaged interface heat flux with number of time steps used in the calculations.

flux histories are; 20, 10, and 5 for dimensionless times of $t^+ = .01$, 1, and 10, respectively.

To show how accuracy changes with the size of elements, the case of equally-spaced elements is considered with different number of elements along the interface ($N = 1, 2, 5, 10$). The number of time steps (NTS) used was fixed and equal to 20. The results are shown in Figures 5.4 and 5.5. Fig. 5.4 shows the normalized interface heat flux, $\overline{q^+}$, versus $\Delta x^+ = \Delta x/a$ for various values of t^+ , while in Fig. 5.5, $\overline{q^+}$ is plotted versus t^+ for different cases of $N = 1, 2, 5$ and 10. A similar behavior to that of Fig. 5.3 is observed in Fig. 5.4. It can be seen that $\overline{q^+}$ varies linearly with Δx^+ , and becomes more accurate as Δx^+ approaches zero, especially for early times. The slopes of the lines decrease as t^+ goes to infinity. This indicates that even few elements along the interface can produce good accuracy for large times. (This can also be observed in Fig. 5.5.)

In order to show precisely the heat flux distribution across the strip, especially in the corner region near $x = \pm a$, ten variable-spaced elements were used with NTS = 20. The elements near the corner were smaller (about 1/4) than those close to the center line. Fig. 5.6 shows the normalized spatial variation of the heat flux across the strip at several times. Normalization is obtained by dividing elemental values by the value of the center line element which covers the region $0 \leq x^+ \leq .2$. It can be seen that the region of uniform heat flux shrinks as t^+ increases. At a dimensionless time about 30, the normalized heat flux distribution remains constant, which indicates for large times that the heat flux across the strip can be approximated by a product of a function of t^+ and a function of x^+ . This behavior was

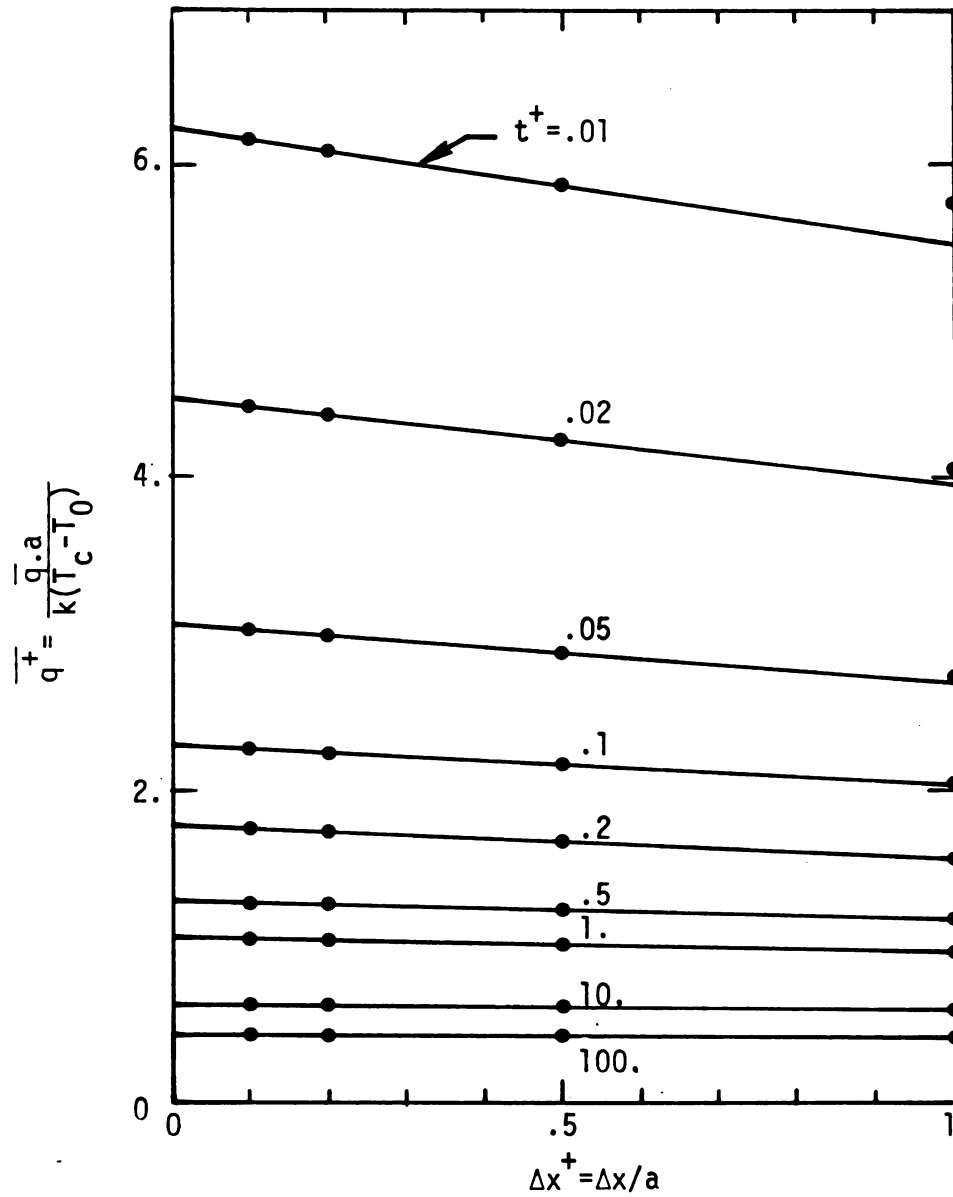


Figure 5.4 Variation of the normalized area averaged interface heat flux with the size of elements.

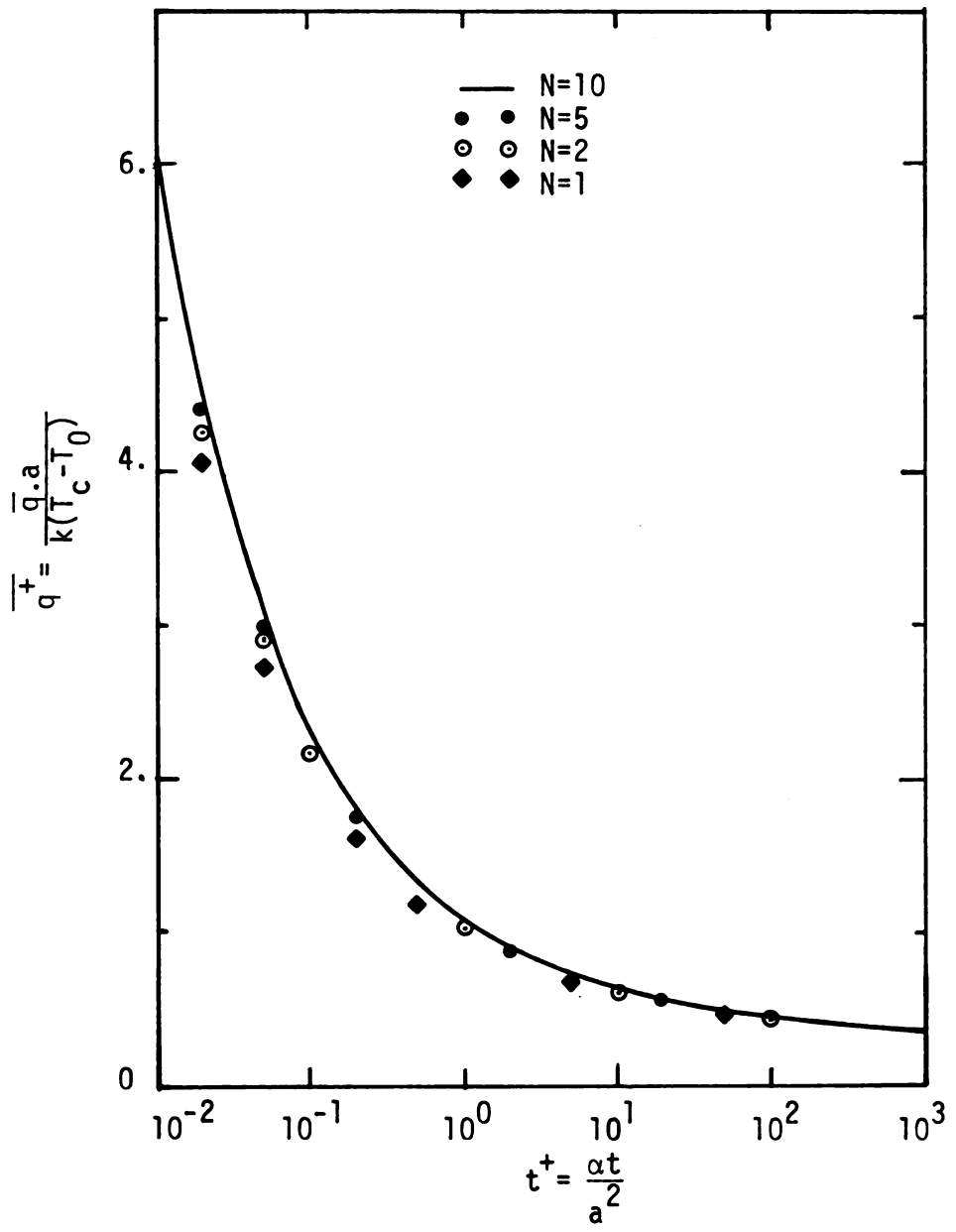


Figure 5.5 Results of average interface heat flux using different number of elements along the interface(local ϕ 's used).

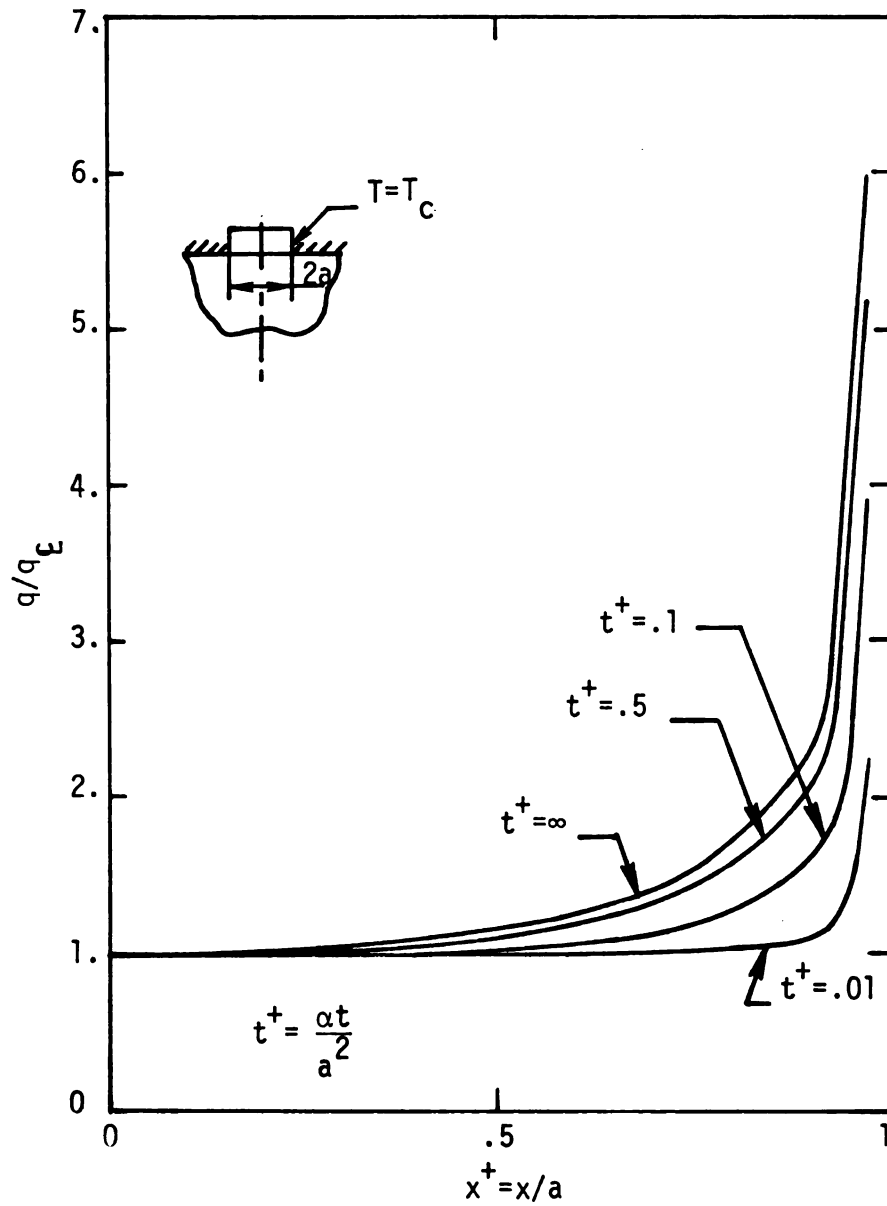


Figure 5.6 Normalized heat flux distribution across the strip at various values of time.

also observed in the problems considered in Chapters 3 and 4.

As mentioned earlier, both local and average values of the influence functions are examined in this problem. Table 5.1 shows the results obtained from the local- ϕ solution and those found from the average- ϕ solution. Both solutions use ten equally-spaced element with $NTS = 20$. The first column is the dimensionless time ranging between .01 to 100. The next two columns show the normalized values of the area averaged interface heat flux resulting from the local- ϕ and the average- ϕ solutions, respectively. The last column provides the corrected values of the average heat flux for the case where $N \rightarrow \infty$ (corresponding to the values of $\overline{q^+}$ at $\Delta x^+ = 0$, in Fig. 5.4). Comparison of the results from the second and third columns with the corrected values in the last column indicates that the average- ϕ solution gives more accurate results than the local- ϕ solution. The errors associated with the average- ϕ solution are about 2/3 of those related to the local- ϕ solution, which implies that the former solution is more appropriate than the latter one, particularly when the number of elements is small.

In Fig. 5.7 the results obtained from the multinode surface element solution (with 10 equally-spaced elements and $NTS = 20$) are compared with those evaluated from the early time analytical solution and the late time analytical solution given by (5.3.17) and (5.3.21), respectively. As it can be seen the multinode SEM solution is in very good agreement with the early time solution up to dimensionless time about 1., and matches closely the late time solution for times greater than 5. Notice that the early and late times analytical solutions match surprisingly well near a dimensionless time of 1.

TABLE 5.1

Comparison between the results obtained from the local- ϕ solution and the average- ϕ solution.

$$\bar{q}^+ = \frac{\bar{q} \cdot a}{k(T_c - T_0)}$$

t^+	local- ϕ solution	Av.- ϕ solution	Corrected Solution N = (∞)
.01	6.1886	6.2228	6.2710
.05	3.0424	3.0578	3.0856
.1	2.2750	2.2858	2.3058
.5	1.3028	1.3076	1.3172
1.	1.0582	1.0616	1.0684
10.	.6340	.6354	.6380
100.	.4416	.4428	.4436

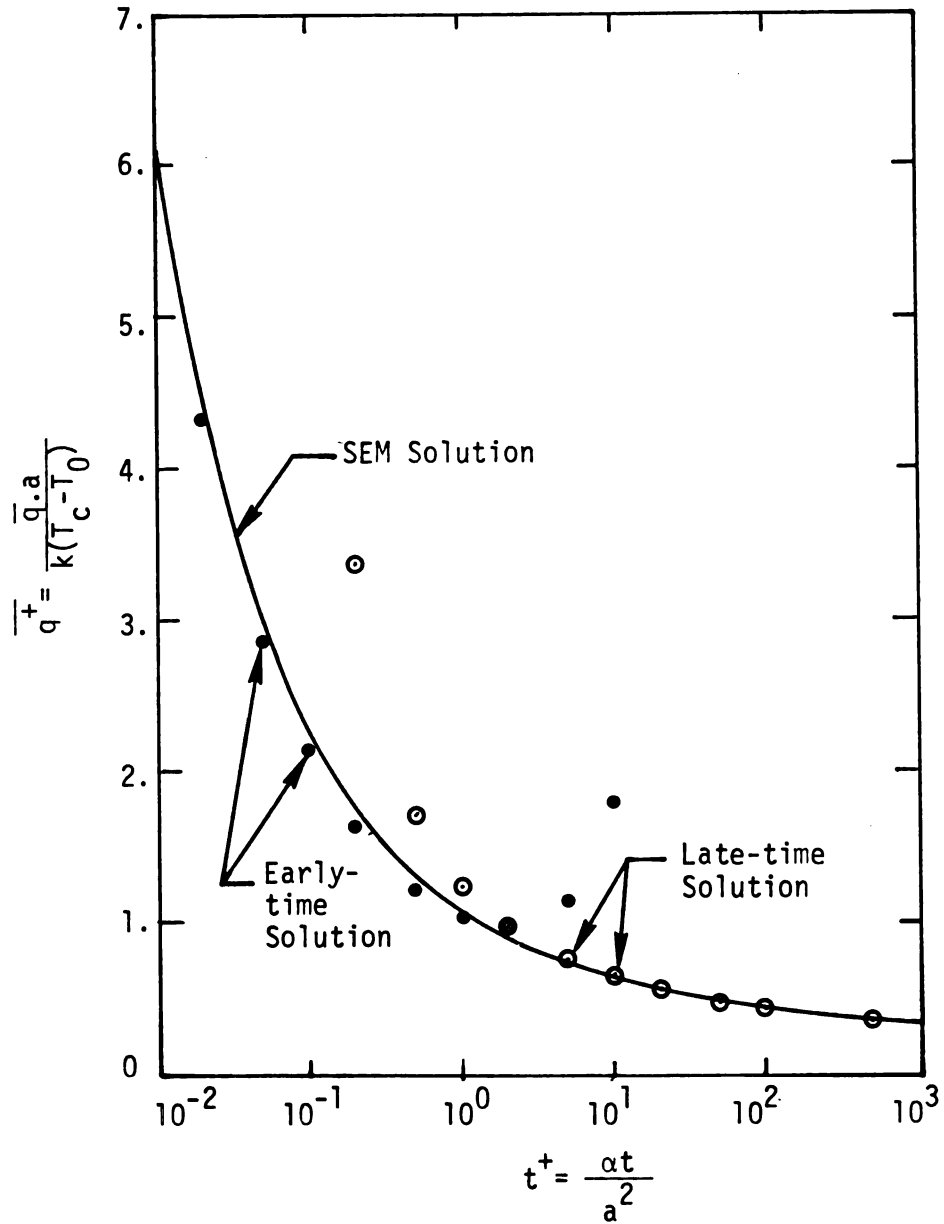


Figure 5.7 Comparison of the multinode surface element solution and the approximate analytical single node solutions for the early and the late times.

CHAPTER 6
TEMPERATURES IN SEMI-INFINITE BODY HEATED BY
CONSTANT HEAT FLUX q_0 OVER HALF SURFACE

6.1 Introduction

This chapter presents the analytical solution for the transient temperature distribution in a semi-infinite body that is heated by a constant flux over half the surface and is insulated over the other half. The solution is a basic one in heat conduction and has a number of direct applications. It is important for the problems involving electronic cooling, contact conductance, fins and oil and gas wells. However, the prime motivating force behind the development of this solution is its application as a basic kernel for the surface element technique.

The solution for the surface temperature is given in Carslaw and Jaeger [22]. See also [47]. Grimado, [48], considered the temperature distribution in a composite semi-infinite body subject to constant heat fluxes at the surface. His solution is expressed in terms of integrals of the form given by (6.3.11) which were solved numerically. Interior temperatures are more difficult to obtain than for the surface and are not given in a convenient closed form in the literature.

The general solution presented here is valid for all times and any location in the entire region. It is given in terms of an integral which is shown to be conveniently and efficiently evaluated by two series expressions.

6.2 Mathematical Description

The describing differential equation, initial and boundary conditions for an isotropic, homogeneous, semi-infinite body that is heated by a constant heat flux over half its surface are (see Fig. 6.1)

$$\frac{\partial^2 T}{\partial x^2} + \frac{\partial^2 T}{\partial z^2} = \frac{1}{\alpha} \frac{\partial T}{\partial t} \quad (6.2.1)$$

$$T(x, z, 0) = T_i \quad (6.2.2)$$

$$-k \left. \frac{\partial T}{\partial z} \right|_{z=0} = q_0 \quad x < 0 \quad (6.2.3a)$$

$$= 0 \quad x > 0 \quad (6.2.3b)$$

$$T(x, z, t) = T_i \quad t > 0 \quad (6.2.4)$$

$$\text{as } z \text{ and } x \rightarrow \infty$$

There is no heat generation inside the body and the thermal properties are independent of temperature.

6.3 Derivation of the Solution

The exact transient temperature solution for the problem described by equations (6.2.1) through (6.2.4), can be obtained starting with the equation (1) given on page 258 of Carslaw and Jaeger [22], which gives the temperature rise for an instantaneous line source parallel to the y axis and passing through the point (x', z') for an infinite region. By considering the semi-infinite geometry of (z > 0) and integrating the effect of line sources at z=z' for the range of negative x (-∞ < x < 0), the solution for the above problem is

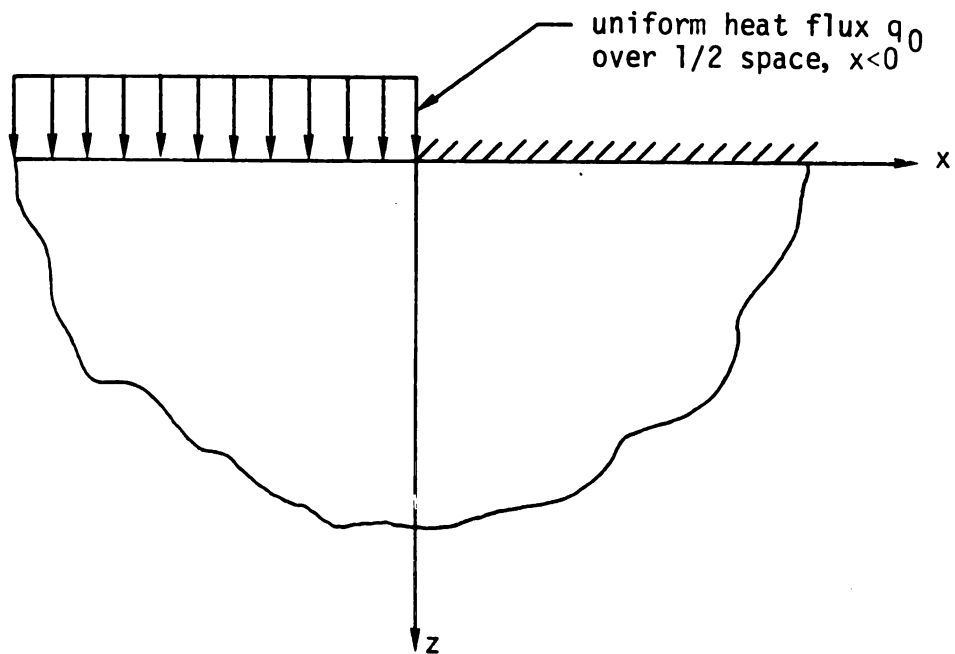


Figure 6.1 Geometry of a semi-infinite region heated by a uniform heat flux, q_0 , over half space $-\infty < x < 0$ and $z=0$.

$$\hat{T} = \frac{Q}{2\pi kt} \int_{-\infty}^0 e^{-\{(x-x')^2 + (z-z')^2\}/4\alpha t} dx' \quad (6.3.1)$$

Equation (6.3.1) gives the temperature rise for an instantaneous plane source of strength Q (J/m^2) at time $t=0$; the source is parallel to the plane $z=0$, passes through the point z' and is over negative x 's, that is, $-\infty < x < 0$. (The caret on T denotes the instantaneous pulse case). Integrating (6.3.1) yields

$$\hat{T} = \frac{Q}{2\rho c_p (\alpha t)^{1/2}} e^{-(z-z')^2/4\alpha t} \text{erfc}\left(\frac{x}{2(\alpha t)^{1/2}}\right) \quad (6.3.2)$$

If the source is at the plane $z' = 0$, then (6.3.2) reduces to

$$\hat{T} = \frac{Q}{2\rho c_p (\alpha t)^{1/2}} e^{-z^2/4\alpha t} \text{erfc}\left(\frac{x}{2(\alpha t)^{1/2}}\right) \quad (6.3.3)$$

Continuous heat flux

For a time variable heat flux $q(t)$ at the surface, the temperature at any time t can be obtained using Duhamel's integral,

$$T(x,z,t) - T_i = \int_0^t q(\lambda) \hat{\phi}(x,z,t-\lambda) d\lambda \quad (6.3.4)$$

where $\hat{\phi}$ is \hat{T} for a unit Q at the surface. Then from (6.3.4) for the constant heat flux, q_0 , over the negative x surface, the solution for the temperature rise is

$$T(x,z,t)-T_i = \frac{q_0(\alpha/\pi)^{1/2}}{2k} \int_0^t \frac{d\lambda}{(t-\lambda)^{1/2}} e^{-z^2/4\alpha(t-\lambda)} \operatorname{erfc}\left(\frac{x}{2[\alpha(t-\lambda)]^{1/2}}\right) d\lambda \quad (6.3.5)$$

This expression is valid for all x values less than, equal to, and greater than zero, and all z values equal to and greater than zero.

Special cases

a) For the special case of $z=0$, the solution is

$$T(x,0,t)-T_i = \frac{q_0}{k} \left(\frac{\alpha t}{\pi}\right)^{1/2} \left[\operatorname{erfc}\left(\frac{x}{2(\alpha t)^{1/2}}\right) - \frac{x}{2(\pi\alpha t)^{1/2}} E_1\left(\frac{x^2}{4\alpha t}\right) \right] \quad (6.3.6)$$

which is also given for zero initial temperature in Carslaw and Jaeger [22], equation (1), page 246.

b) For the special case of $x=0$, temperature at the center line, the solution from (6.3.5) is

$$T(0,z,t)-T_i = \frac{q_0}{k} (\alpha t)^{1/2} \operatorname{ierfc}\left(\frac{z}{2\sqrt{\alpha t}}\right) \quad (6.3.7)$$

which is exactly one half of the solution for the body heated over the entire $z=0$ surface.

General case

The general case of $z > 0$ is not available in the literature.

Introducing u as

$$u = \frac{z}{2[\alpha(t-\lambda)]^{1/2}} \quad (6.3.8)$$

into (6.3.5), the general solution becomes

$$T(x,z,t) - T_i = \frac{q_0 z}{2k\pi^{1/2}} \int_{z/2(\alpha t)^{1/2}}^{\infty} \frac{du}{u^2} e^{-u^2} \operatorname{erfc}\left(\frac{xu}{z}\right) \quad (6.3.9)$$

To better describe the results, define the dimensionless groups as follows

$$X = \frac{x}{2(\alpha t)^{1/2}}, \quad Z = \frac{z}{2(\alpha t)^{1/2}} \quad (6.3.10a,b)$$

$$p = \frac{z}{x} = \frac{Z}{X}, \quad T = \frac{T - T_i}{(q_0/k)(\alpha t/\pi)^{1/2}} \quad (6.3.10c,d)$$

Notice that p is independent of time. Using these definitions (6.3.9) can be written in dimensionless form as

$$T(p,Z) = Z \int_Z^{\infty} \frac{1}{u^2} e^{-u^2} \operatorname{erfc}\left(\frac{u}{p}\right) du \quad (6.3.11)$$

The number of independent variables in (6.3.9) has been reduced from three, (x,z,t) , to two dimensionless variables, (Z,p) , in (6.3.11). It can be shown that the integration of (6.3.11) by parts yields

$$\begin{aligned} T(X,Z) = & (\pi)^{1/2} \operatorname{ierfc}(Z) - e^{-Z^2} \operatorname{erf}(X) \\ & - \frac{X}{(\pi)^{1/2}} E_1(X^2 + Z^2) + 2pZ \int_X^{\infty} e^{-p^2 y^2} \operatorname{erf}(y) dy \end{aligned} \quad (6.3.12)$$

(For details see Appendix C.)

The functions $\text{erf}(\cdot)$, $\text{erfc}(\cdot)$, $\text{ierfc}(\cdot)$, and $E_1(\cdot)$ which appear in the equations (6.3.2) through (6.3.12) are the error function, the complementary error function, the integrated error function, and the exponential function, respectively defined by,

$$\text{erf}(\eta) = \frac{2}{\pi^{1/2}} \int_0^\eta e^{-y^2} dy \quad (6.3.13)$$

$$\text{erfc}(\eta) = 1 - \text{erf}(\eta) = \frac{2}{\pi^{1/2}} \int_\eta^\infty e^{-y^2} dy \quad (6.3.14)$$

$$\text{ierfc}(\eta) = \frac{2}{\pi^{1/2}} \int_\eta^\infty \text{erfc}(Y) dy \quad (6.3.15)$$

$$E_1(\eta) = \int_\eta^\infty \frac{e^{-y}}{y} dy \quad (6.3.16)$$

These functions are tabulated in [34], and are also available in computer libraries.

The integral in the last term in (6.3.12) can be represented by a function H defined as

$$H(X,p) = \frac{2p}{(\pi)^{1/2}} \int_X^\infty e^{-p^2 y^2} \text{erf}(y) dy = H(X,Z/X) \quad (6.3.17)$$

(See [49] for related integrals). Then the general temperature solution for a constant heat flux and $Z \geq 0$ can be written as

$$\begin{aligned} T(X,Z) = & (\pi)^{1/2} \text{ierfc}(Z) - e^{-Z^2} \text{erf}(X) - \\ & \frac{X}{(\pi)^{1/2}} E_1(X^2+Z^2) + (\pi)^{1/2} Z H(X,Z/X) \end{aligned} \quad (6.3.18)$$

This expression is skew-symmetric with respect to x-axis and it can be shown that,

$$T_{-}(X,Z) = Z \pi^{1/2} \operatorname{ierfc}(Z) - T_{+}(X,Z) \quad (6.3.19)$$

where the plus and minus subscripts indicate that the solution is for positive and negative values of X, respectively. The first term on the right hand side of (6.3.19) is the solution to the same problem if the entire surface was heated by a constant heat flux.

The function, $H(X,p)$, can be represented in series form for the three different regions indicated in Fig. 6.2.

a) For the Region $|p| > 1$

$$H(X,p) = \frac{2}{\pi} \sum_{n=0}^{\infty} \frac{(-1)^n e_n(p^2 X^2)}{p^{2n+1} (2n+1) e^{p^2 X^2}} \quad (6.3.20a)$$

or

$$= \frac{2}{\pi} \sum_{n=0}^{\infty} \frac{(-1)^n \Gamma(n+1, p^2 X^2)}{p^{2n+1} (2n+1) n!} \quad (6.3.20b)$$

where the functions $e_n(\cdot)$ and $\Gamma(n, \cdot)$ are the truncated exponential function and the incomplete gamma function, respectively, and are defined in [34] by

$$e_n(\eta) = \sum_{m=0}^n \frac{\eta^m}{m!} = \frac{\Gamma(n+1, \eta)}{n!} e^{\eta} \quad (6.3.21)$$

$$\Gamma(n, \eta) = \int_{\eta}^{\infty} e^{-y} y^{n-1} dy \quad (6.3.22)$$

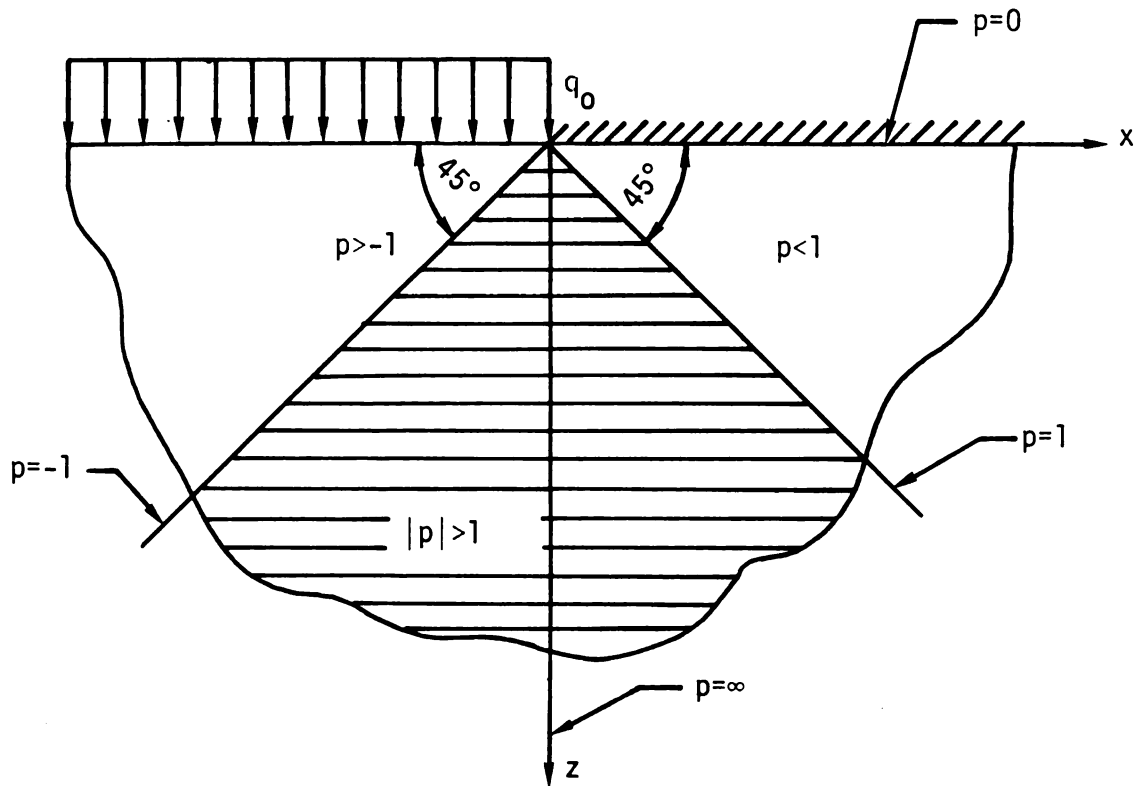


Fig. 6.2 Geometry showing various regions of $|p| < 1$, $|p| \leq 1$, and $|p| > 1$.

b) For the Region $|p| < 1$

Equation (6.3.20a) cannot be used for the case for which $|p| < 1$ since p appearing in the denominator of (6.3.20a) causes the summation to diverge. For this case of $|p| < 1$ the following expression is provided,

$$H(X,p)=1-\operatorname{erf}(X)\operatorname{erf}(pX)-\frac{2}{\pi}\sum_{n=0}^{\infty}\frac{(-1)^n p^{2n+1} e_n(X^2)}{(2n+1) e^{X^2}} \quad (6.3.23a)$$

or

$$H(X,p)=1-\operatorname{erf}(X)\operatorname{erf}(pX)-\frac{2}{\pi}\sum_{n=0}^{\infty}\frac{(-1)^n p^{2n+1} \Gamma(n+1, X^2)}{(2n+1)n!} \quad (6.3.23b)$$

c) For the lines $|p| = 1$

It can be shown for $p=1$ that $H(X,p)$ is given by

$$H(X,1) = -H(X,-1) = 1/2[1-\operatorname{erf}^2(X)] \quad (6.3.24a)$$

which results in

$$\begin{aligned} T_+(X=Z,Z) &= \frac{\operatorname{erfc}(Z)}{2} [e^{-Z^2} + \pi^{1/2} i \operatorname{erfc}(Z)] \\ &\quad - \frac{Z}{\pi^{1/2}} E_1(2Z^2) \end{aligned} \quad (6.3.24b)$$

The general solution given by equation (6.3.18), is valid for all times and any location in the entire region. Even though this expression is valid for both positive and negative values of X , it is recommended only for $X>0$. For $X<0$ the complementary expression given by (6.3.19) can be employed. In the next section the behavior and

evaluation of the function $H(X,p)$, is discussed.

6.3.1 Evaluation of the Function $H(X,p)$

The evaluation of the function $H(X,p)$ can be accomplished using (6.3.20a) and (6.3.23a) for the regions $|p| > 1$ and $|p| < 1$, respectively.

Efficient subroutines can be provided by utilizing several recursive relations. The summations in these equations are well-behaved for all values of X and p (within the appropriate p range). Table 6.1 provides values for $H(X,p)$ for various X and p values. In Fig. 6.3, the function $H(X,p)$ is plotted versus X for various values of p . There are several interesting points regarding the behavior of $H(X,p)$ which can be seen from (6.3.17), Table 6.1 and Fig. 6.3; some of these are:

- a) Regardless of values of p , $H(X,p) \rightarrow 0$ as $X \rightarrow \infty$.
- b) For large values of p compared to unity, $H(X,p)$ goes to zero even for small values of X .
- c) For finite X , $H(X,p) \rightarrow 1$, as $p \rightarrow 0$.
- d) From (6.3.17) one can write,

$$1) \quad H(X,-p) = -H(X,p) \quad (6.3.25a)$$

$$2) \quad H(-X,p) = H(X,p) \quad (6.3.25b)$$

e) The series expressions given by (6.3.20), and (6.3.23) for $H(X,p)$ are valid only for positive values of $p(X>0)$. For negative values of $p(X<0)$, (6.3.25a) can be used.

- f) For X equal to zero, one can show that

TABLE 6.1

Values of function $H(X,p)$

X	p=0.1	p=0.4	p=0.8	p=1	p=1.5	p=2	p=4
.001	.936549	.757762	.570446	.499999	.374333	.295166	.155956
.010	.936543	.757737	.570396	.499936	.374239	.295040	.155704
.050	.936390	.757126	.569175	.498411	.371954	.292001	.149720
.100	.935913	.755222	.565378	.493676	.364907	.282707	.132464
.200	.934020	.747676	.550466	.475202	.338043	.248406	.081170
.400	.926634	.718571	.494960	.408240	.249144	.148182	.011453
.600	.914951	.673616	.415510	.317679	.150202	.062803	.000439
1.000	.881962	.554237	.241324	.144928	.030329	.004109	.000000
1.200	.862366	.488908	.168218	.085664	.010251	.000640	.000000
1.400	.841662	.424669	.111029	.046577	.002883	.000072	.000000
1.600	.820358	.363883	.069597	.023372	.000677	.000006	.000000
2.000	.777192	.257694	.023607	.004667	.000022	.000000	.000000
2.200	.755665	.213246	.012800	.001861	.000003	.000000	.000000
2.400	.734287	.174557	.006620	.000688	.000000	.000000	.000000
2.600	.713096	.141345	.003265	.000236	.000000	.000000	.000000
3.000	.671373	.089686	.000689	.000022	.000000	.000000	.000000

TABLE 6.2

Values of the functions $H(X,p)$ and $ERFC(pX)$ for various X values

X	p=0.1		p=0.4		p=0.8	
	H(X,p)	ERFC(pX)	H(X,p)	ERFC(pX)	H(X,p)	ERFC(pX)
1.00	.881962	.887537	.554237	.571608	.241324	.257899
1.20	.862366	.865242	.488908	.497250	.168218	.174576
1.40	.841662	.843053	.424669	.428384	.111029	.113212
1.60	.820358	.820988	.363883	.365414	.069597	.070266
2.00	.777192	.777297	.257694	.257899	.023607	.023652
2.60	.713096	.713100	.141345	.141350	.003265	.003266
3.00	.671373	.671373	.089686	.089686	.000689	.000689

TABLE 6.3

Number of terms in series of function $H(X,p)$ given by equations (6.3.20a) and (6.3.23a) to obtain 8 decimal places accuracy

X	p=0.6	p=0.8	p=0.98	p=1.02	p=1.2	p=1.5
0.01	1	1	1	1	1	1
0.1	2	3	3	3	3	3
1.	7	8	10	10	10	9
2.	10	14	18	18	17	15
3.	13	20	27	28	25	19

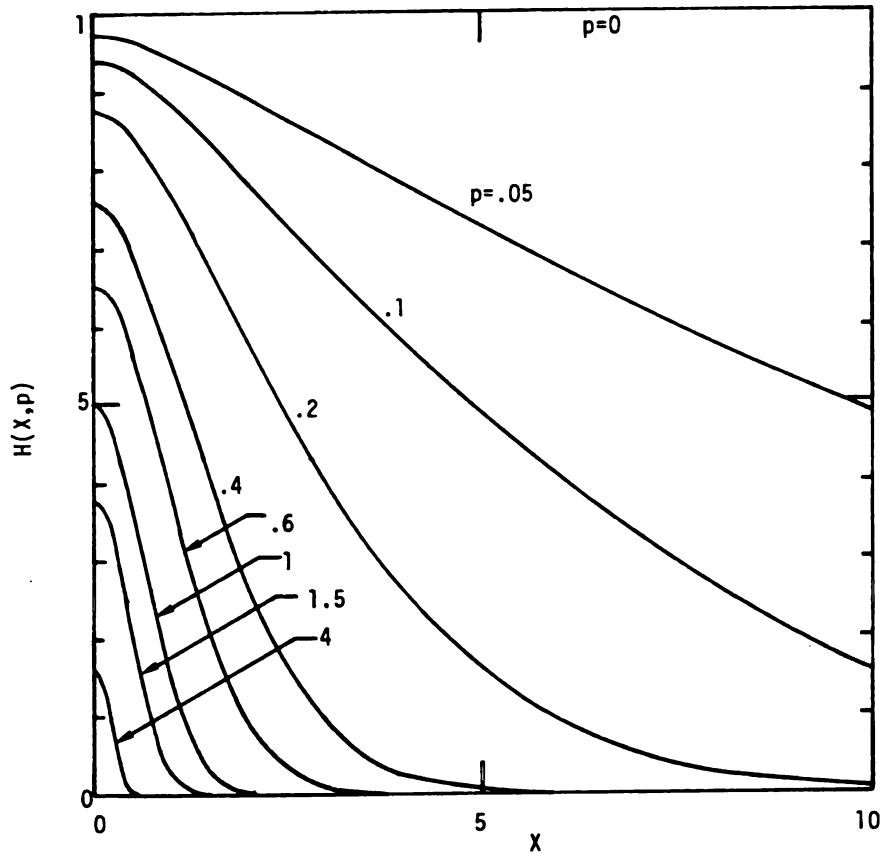


Figure 6.3 Function $H(X,p)$ versus X for different values of p .

$$\frac{2}{\pi} \arctan \left(\frac{1}{p} \right) \quad \text{for } |p| > 1 \quad (6.3.26a)$$

$$H(0,p) =$$

$$1 - \frac{2}{\pi} \arctan (p) \quad \text{for } |p| < 1 \quad (6.3.26b)$$

g) For large values of X , say $X > 3$, function $H(X,p)$ can be approximated by the complementary error function of pX ,

$$H(X,p) \approx \frac{2p}{(\pi)^{1/2}} \int_X^\infty e^{-p^2 y^2} dy = \operatorname{erfc}(pX) \quad (6.3.27)$$

In the next section this result is utilized to obtain a simplified expression for the solution of $T(X,Z)$. In Table 6.2, the values of $H(X,p)$ and $\operatorname{erfc}(pX)$ (with 6 significant digit accuracy) are compared for various X and p values.

The number of terms required to obtain 8 decimal places accuracy, in the series expression for $H(X,p)$ is shown in Table 6.3. It can be seen that the number of terms increases as X increases, and also as $|p-1|$ decreases (p close to one). The number of the terms increases rapidly as X becomes greater than 10. But fortunately, the evaluation of the series is needed only for $X < 3$. (For values of X greater than 3, the H function can be approximated by (6.3.27)). Hence, no more than 30 terms are required to obtain 8 decimal places accuracy for evaluation of the series in the H function for the large range of any X and $|p-1| > .02$.

h) For small values of $p^2 X^2$, H can be approximated by

$$H(X,p) \approx \frac{2}{\pi} \left[\arctan\left(\frac{1}{p}\right) - pX^2 \right] \quad \text{for } p > 1 \quad (6.3.28a)$$

and

$$H(X,p) \approx 1 - \operatorname{erf}(pX)\operatorname{erf}(X) - \frac{2}{\pi} [\arctan(p) - pX^2] \quad \text{for } p < 1 \quad (6.3.28b)$$

6.3.2 Simplified Relations for $|X| > 3$

For $|X| > 3$, the general solution for the dimensionless temperature given by (6.3.18) can be reduced to a simpler form. By introducing (6.3.27) into (6.3.18) and noticing that $pX = Z$ one can write

$$T_+(X,Z) = e^{-Z^2} \operatorname{erfc}(X) - \frac{X}{(\pi)^{1/2}} E_1(X^2+Z^2) \quad \text{for } X > 3 \quad (6.3.29a)$$

Equation (6.3.29a) is very accurate (to 6 decimal places), for $X > 3$. It also gives good accuracy down to $X > 2$ (to 3 decimal places). This accuracy (for $2 < X < 3$) can be further improved to 5 decimal places, by subtracting an additional term, $\frac{p}{\pi} E_1(X^2+Z^2)$, from the right hand side of the (6.3.27), which results in (6.3.29a) becoming:

$$T_+(X,Z) = e^{-Z^2} \operatorname{erfc}(X) - \frac{X(1+p^2)}{(\pi)^{1/2}} E_1(X^2+Z^2) \quad (6.3.29b)$$

Furthermore, due to the nature of the terms $\exp(-Z^2) \operatorname{erfc}(X)$ and $X(\pi)^{-1/2} E_1(X^2+Z^2)$ in equation (6.3.29a), there are negligible contributions of these terms for $X > 4$. It can be shown that for $X > 4$ the first term is less than 1.6×10^{-8} and the second term is less than 1.5×10^{-8} . Hence, for say 8 decimal places accuracy, these terms can be dropped and the equation becomes independent of X . Then one can write

$$T_+(X,Z) = 0.0 \quad \text{for } X > 4 \quad (6.3.30a)$$

$$T_-(X,Z) = 2\text{ierfc}(Z) \quad \text{for } X < -4 \quad (6.3.30b)$$

These equations also give excellent accuracy down to $|X| > 3$.

6.3.3 Evaluation of $T(X,Z)$ and Discussion of the Results

The evaluation of $T(X,Z)$ given by equation (6.3.18) is not difficult if a computer is employed. The first three terms in the equation can be directly calculated using a computer library for the error and the exponential functions. The evaluation of the last term ($H(X,p)$) also can be easily obtained as discussed in the previous section. For the special cases of $Z=0$, $X=0$, $p=1$, $X > 3$, and $|X| > 4$ the simplified equations (6.3.6), (6.3.7), (6.3.24b), (6.3.29a), and (6.3.30) are provided, respectively. Table 6.4 provides values of the dimensionless temperature $T(X,Z)$, for various values of the dimensionless X and Z . In Fig. 6.4, $T(X,Z)$ is plotted versus X for various Z values. It can be seen that the solution is skew-symmetric with respect to X -axis. The solution is well-behaved for all times and any location over the entire region. Fig. 6.5 shows the lines of the dimensionless isotherms in the X and Z coordinates. It can be seen that for $|X| > 1.5$ the solution is almost independent of X .

6.4 Other Cases of Boundary Conditions

The exact solution given herein is important because it is a basic geometry in heat conduction. There are many other possible cases that can be obtained using this solution. It can be utilized as a building block for a number of other boundary conditions for both semi-finite

TABLE 6.4

Values of dimensionless temperature for solution given by equation (6.3.18), for different values of X and Z

X	Z=0.0	Z=0.2	Z=0.6	Z=1.0	Z=1.2	Z=2.0
-4.000	2.000000	1.370489	.552776	.178148	.092341	.003467
-3.000	1.999999	1.370488	.552776	.178147	.092341	.003467
-2.000	1.999587	1.370095	.552506	.178019	.092264	.003463
-1.000	1.966475	1.338908	.532887	.169798	.087610	.003249
-.600	1.866022	1.246380	.481679	.151056	.077569	.002849
-.200	1.525251	.959476	.360987	.113288	.058273	.002153
-.100	1.340279	.832317	.319722	.101382	.052313	.001946
-.050	1.209176	.760328	.298190	.095254	.049253	.001840
-.010	1.059991	.700368	.280757	.090312	.046788	.001755
0.000	1.000000	.685245	.276388	.089074	.046171	.001734
.010	.940009	.670122	.272019	.087836	.045553	.001712
.050	.790824	.610162	.254587	.082894	.043088	.001627
.100	.659721	.538172	.233054	.076765	.040029	.001521
.200	.474749	.411013	.191790	.064860	.034068	.001314
.600	.133978	.124109	.071098	.027092	.014773	.000618
1.000	.033525	.031582	.019889	.008350	.004731	.000218
2.000	.000413	.000394	.000270	.000129	.000078	.000004
3.000	.000001	.000001	.000001	.000000	.000000	.000000
4.000	.000000	.000000	.000000	.000000	.000000	.000000

TABLE 6.5

Values of dimensionless temperature, $\tau(x^+, q^+, t^+)$, for various values of x^+ and z^+ due to a strip source, at time $t^+ = .25$.

x^+	$z^+=0.0$	$z^+=0.2$	$z^+=0.6$	$z^+=1.0$	$z^+=1.2$	$z^+=2.0$
.000	1.932950	1.307326	.512998	.161448	.082878	.003031
.010	1.932908	1.307287	.512977	.161440	.082874	.003031
.100	1.928771	1.303467	.510862	.160683	.082475	.003016
.200	1.915898	1.291610	.504375	.158384	.081265	.002970
.600	1.743545	1.137423	.429491	.133704	.068534	.002508
.800	1.524128	.958406	.360259	.112948	.058070	.002142
1.000	.999587	.684851	.276118	.088945	.046093	.001729
1.200	.474607	.410877	.191696	.064814	.034040	.001312
1.600	.133964	.124096	.071088	.027087	.014770	.000617
2.000	.033524	.031581	.019888	.008350	.004731	.000218
3.000	.000413	.000394	.000270	.000129	.000078	.000004
4.000	.000001	.000001	.000001	.000000	.000000	.000000

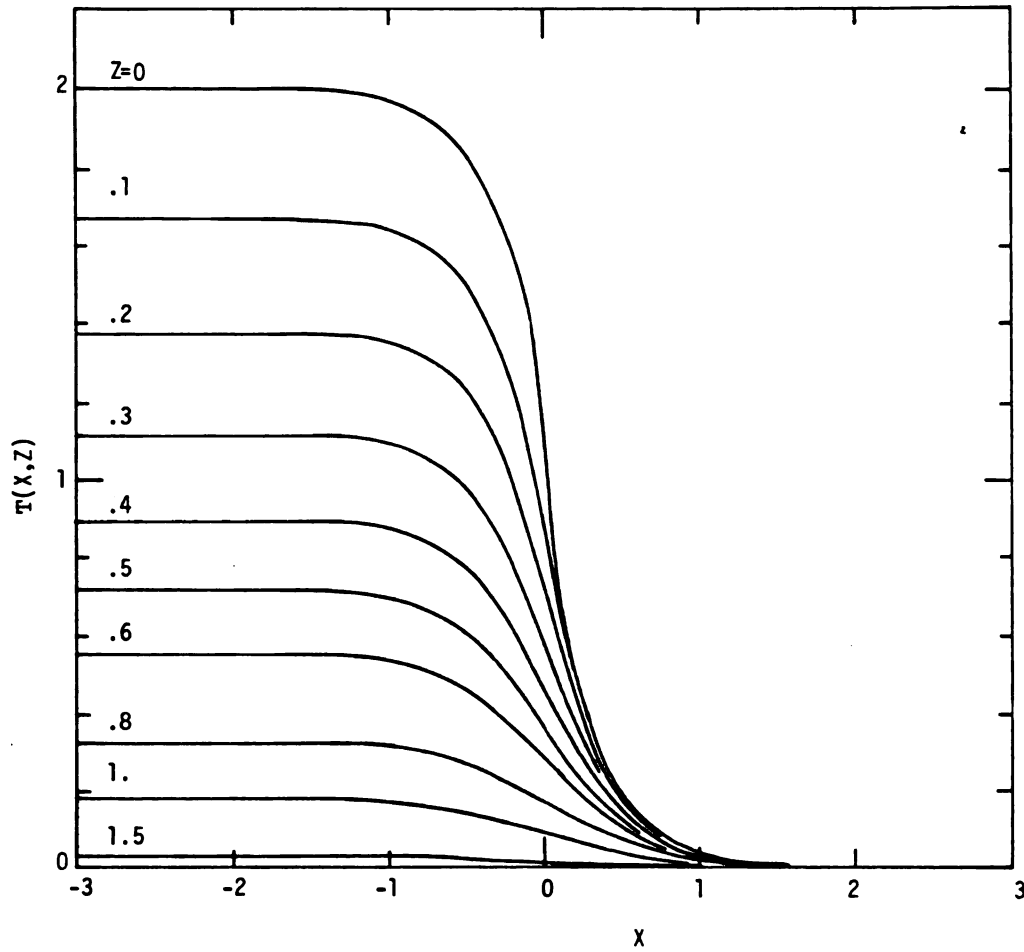


Fig. 6.4 Dimensionless temperature $T(X,Z)$ versus X for different values of Z in semi-infinite body heated by a uniform heat flux over half space $x < 0$, $z = 0$.

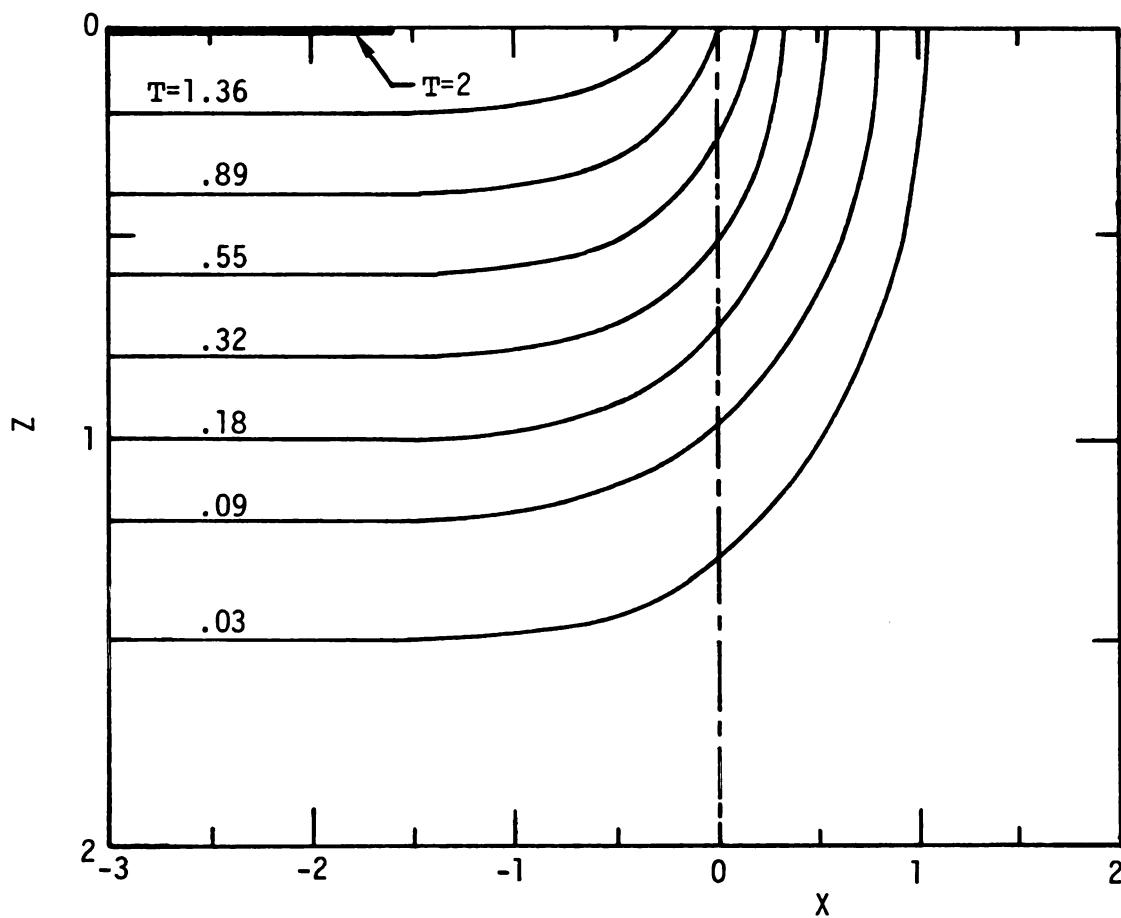


Figure 6.5 Lines of dimensionless isotherms in semi-infinite body heated by a uniform heat flux over half space $x < 0$.

and finite geometries. Fig. 6.6 is given to illustrate some of these, for both semi-infinite and finite geometries. For most semi-infinite cases the solution can be obtained by simple superposition. For example, the solution for Fig. 6.6b, is the solution for a semi-infinite body that is uniformly heated minus the solution for the semi-infinite body heated across an infinite strip with the same heat flux. For the finite cases the solutions can be found by using the method of images. In this method, a number of sources and sinks are distributed inside the body such that the corresponding boundary conditions are satisfied (see [22] and [50] for more details).

6.4.1 Application to Strip Heat Source

As suggested by the foregoing there are other boundary conditions that can be obtained using the above results. One case of particular interest is for the semi-infinite geometry heated by a constant heat flux over an infinite strip with the width $2a$ and insulated elsewhere. See Fig. 6.7. The solution to this case is needed in Chapter 5 in order to find the required influence functions. This solution can be found from the solution given by equation (6.3.18) by applying simple superposition to get:

$$\begin{aligned}
 T(x^+, z^+, t^+) = & e^{-z^{+2}/4t^+} \left[-\operatorname{erf} \left(\frac{x^+-1}{2(t^+)^{1/2}} \right) + \operatorname{erf} \left(\frac{x^++1}{2(t^+)^{1/2}} \right) \right] \\
 & - \frac{x^+-1}{2(\pi t^+)^{1/2}} E_1 \left[\frac{(x^+-1)^2+z^{+2}}{4t^+} \right] + \frac{x^++1}{2(\pi t^+)^{1/2}} E_1 \left[\frac{(x^++1)^2+z^{+2}}{4t^+} \right] \\
 & + \frac{\pi^{1/2} z^+}{2(t^+)^{1/2}} \left[H \left(\frac{x^+-1}{2(t^+)^{1/2}}, p \right) - H \left(\frac{x^++1}{2(t^+)^{1/2}}, p \right) \right] \quad (6.4.1)
 \end{aligned}$$

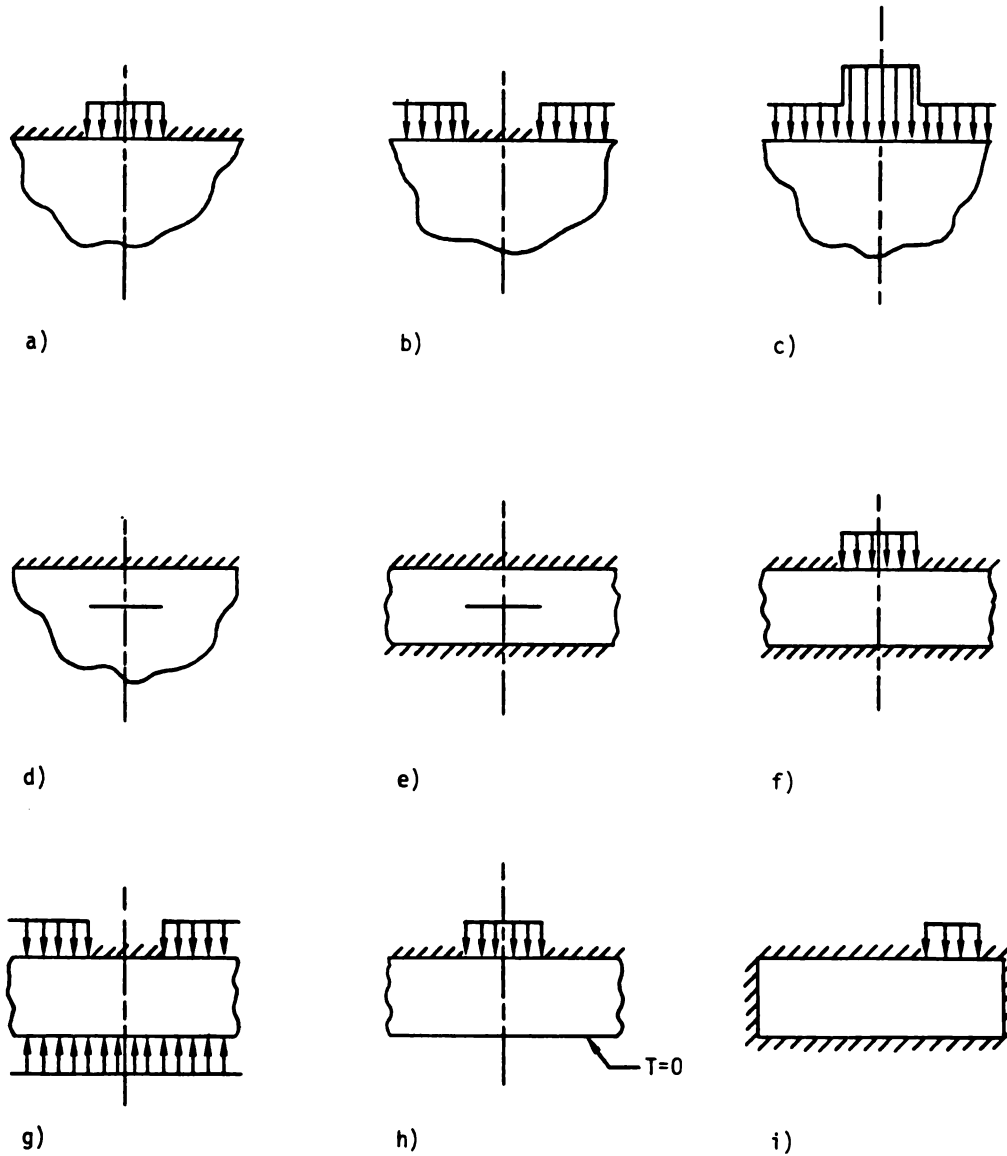


Figure 6.6 Various possible cases that can be treated using the solution given for figure 6.1 as a building block.

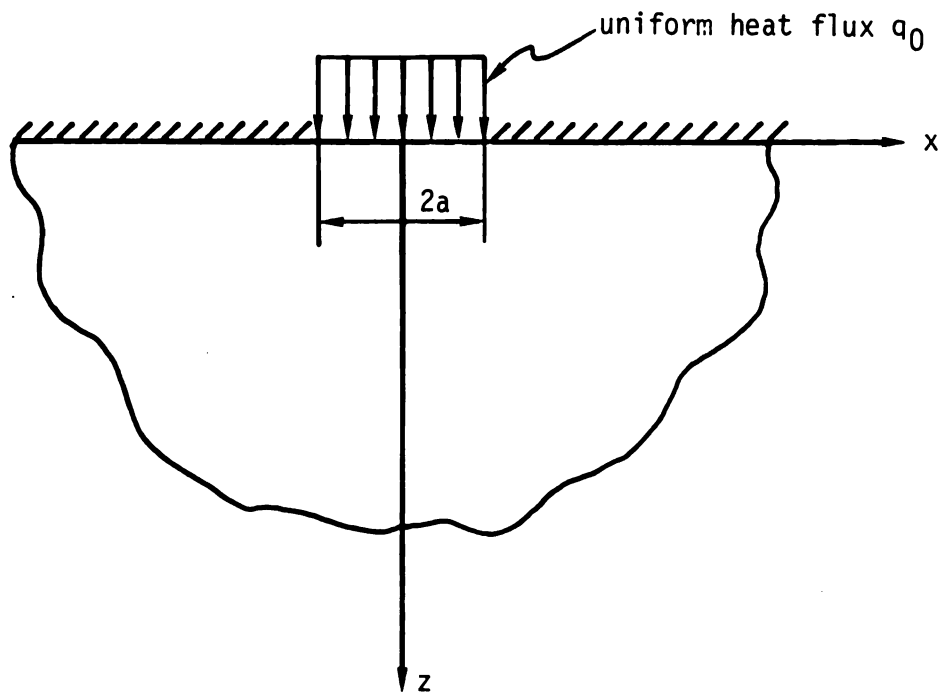


Figure 6.7 Geometry of a semi infinite body heated by a uniform heat flux, q_0 , over an infinite strip with width $2a$.

where

$$x^+ \equiv x/a, \quad z^+ \equiv z/a, \quad (6.4.2a,b)$$

$$t^+ \equiv \alpha t/a^2, \quad p \equiv z/x = z^+/x^+ \quad (6.4.2c,d)$$

and T is defined by equation (6.3.10d).

For the special case of $z^+ = 0$, the solution becomes:

$$\begin{aligned} T(x^+, 0, t^+) = & \operatorname{erf} \frac{x^++1}{2(t^+)^{1/2}} - \operatorname{erf} \frac{x^+-1}{2(t^+)^{1/2}} \\ & + \frac{x^++1}{2(\pi t^+)^{1/2}} E_1 \left[\frac{(x^++1)^2}{4t^+} \right] - \frac{x^+-1}{2(\pi t^+)^{1/2}} E_1 \left[\frac{(x^+-1)^2}{4t^+} \right] \end{aligned} \quad (6.4.3)$$

which is also given in [22], equation (3), page 264.

Equation (6.4.1) is valid for all times and any location in the entire region. Table 6.5 provides values of the dimensionless temperature $T(x^+, z^+, t^+)$, for various values of x^+ and z^+ at time $t^+ = .25$. Results are also shown in Fig. 6.8. It can be seen that for large values of z^+ (deep in the body), the temperature distributions become flatter as expected. In Fig. 6.9, some values of dimensionless surface temperature $T(x^+, 0, t^+)$ are plotted versus x^+ for various values of t^+ . Another way of illustrating the results is provided in Fig. 6.10, which shows the isotherms in the x^+ and z^+ coordinates for time $t^+ = 1$.

In the application of the surface element method the solution for the spatial average temperature over the heated region is sometimes utilized. At the heated surface this average temperature is

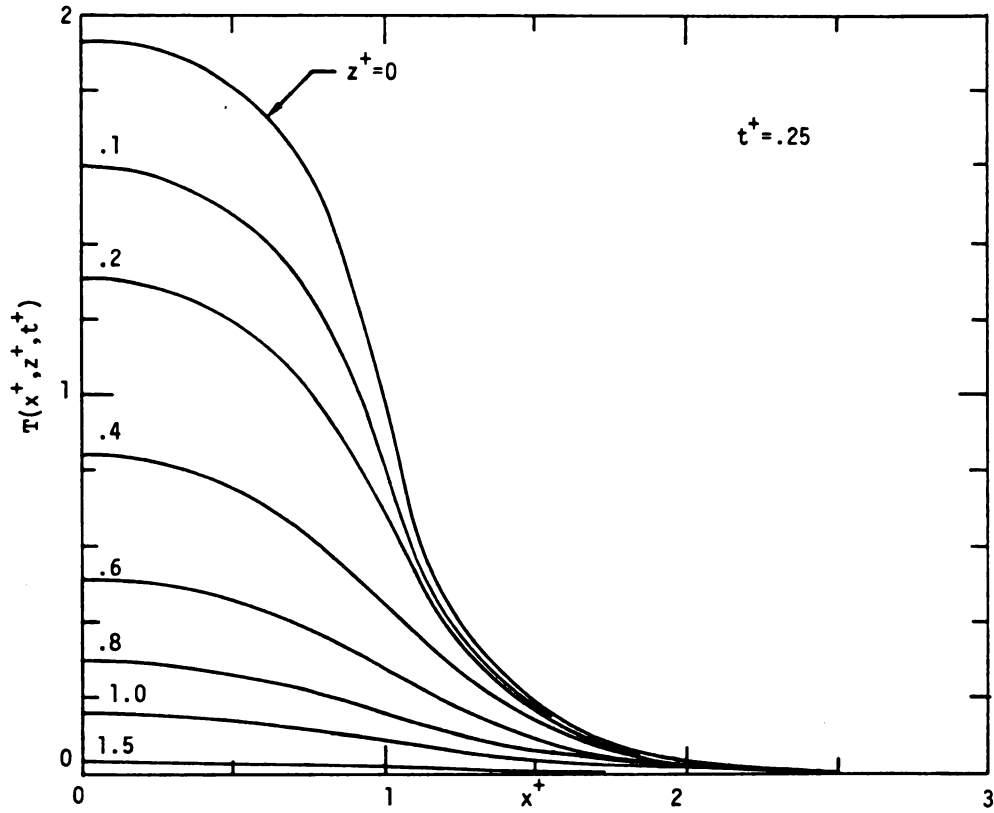


Figure 6.8 Dimensionless temperatures $T(x^+, z^+, t^+)$ versus x^+ , for various values of z^+ at $t^+ = .25$.

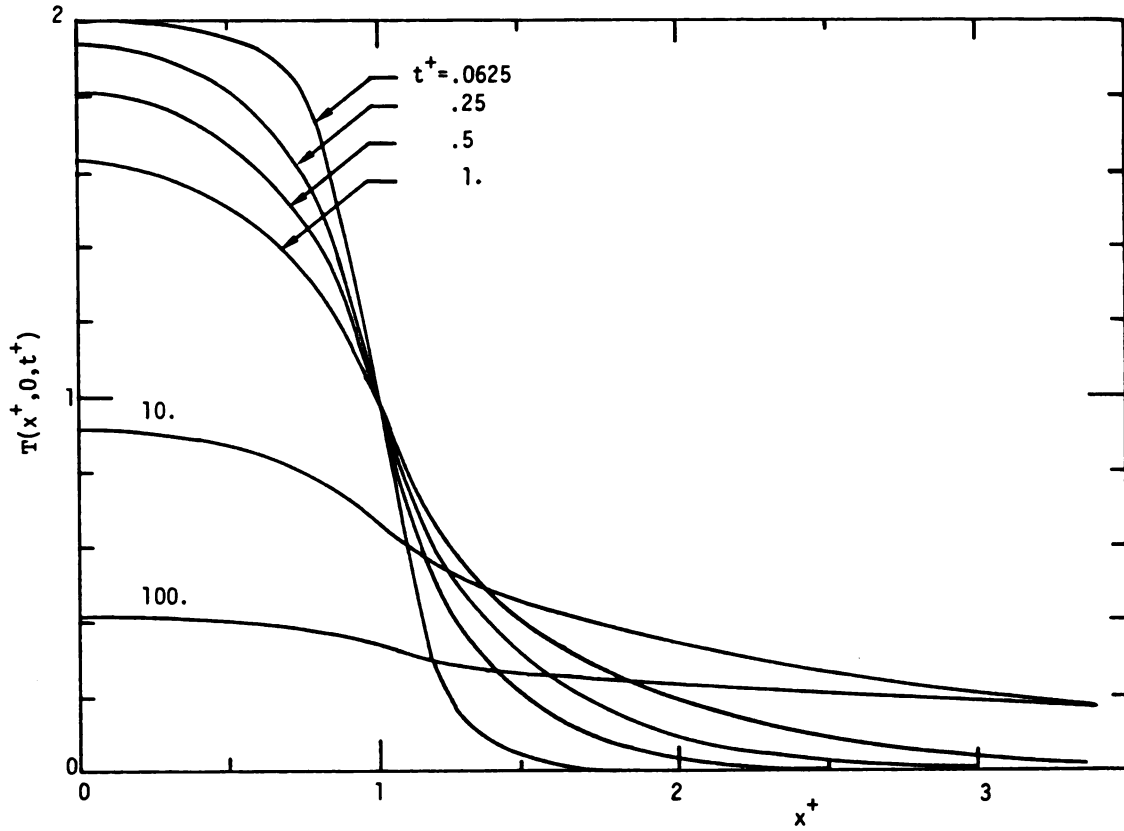


Fig.6.9 Dimensionless surface temperature $T(x^+, 0, t^+)$ versus dimensionless x^+ , for various values of dimensionless times.

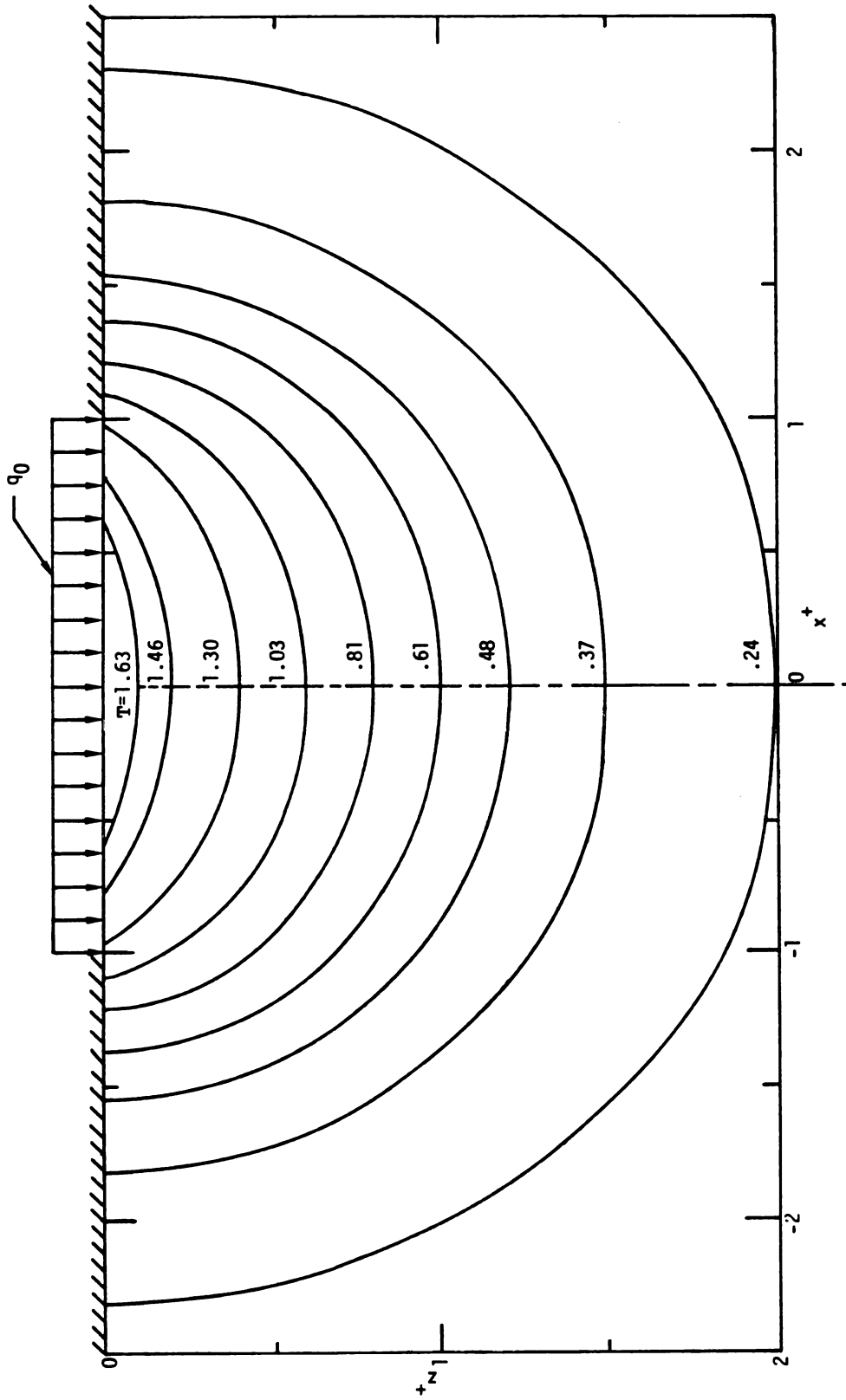


Figure 6.10 Dimensionless isotherms in semi-infinite body heated by a uniform heat flux over an infinite strip at $z^+ = 0$, for $t^+ = 1$.

$$\begin{aligned} \bar{T}(0, t^+) = & 2+(t^+)^{1/2}\{2\text{ierfc}(t^+)^{-1/2} \\ & -\pi^{-1/2}[1+E_2(1/t^+)]\} \end{aligned} \quad (6.4.4a)$$

For large times the average temperature is found from (6.4.4a) to be

$$\begin{aligned} \frac{\bar{T}(0, t^+) - T_i}{q_0 a/k} \approx & \frac{1}{\pi} \left[\ln t^+ - \frac{4}{3} \frac{1}{t^+} + 3 - \gamma \right], \\ & (\gamma = .5772\dots) \end{aligned} \quad (6.4.4b)$$

which shows that the temperatures near the heated surface increases as the logarithm of time for large times. For an error less than .2% the second term in (6.4.4b) can be dropped for $t^+ > 100$. For small times (6.4.4a) can be approximated by

$$\frac{\bar{T}(0, t^+) - T_i}{q_0 a/k} \approx 2(t^+/\pi)^{1/2} - \frac{t^+}{\pi} + \frac{1}{2}(t^+)^3 e^{-1/t^+} \left(1 - \frac{9}{2}t^+\right) \quad (6.4.4c)$$

For an error less than .033%, the exponential term can be dropped for $t^+ < 0.3$.

CHAPTER 7

SUMMARY AND CONCLUSIONS

A transient multinode surface element method for solution of two and three dimensional heat conduction problems with linear boundary conditions has been presented. The method uses Duhamel's integral and involves the inversion of a set of Volterra integral equations, one for each surface element. The use of Duhamel's integral requires that the describing differential equations be linear.

In Chapter 1, Duhamel's theorem was introduced and integral equations with temperature-based kernel and heat flux-based kernel were presented and discussed. Though both types of kernels can be employed in the SEM, only heat flux-based kernels were used in the examples given in this dissertation.

The method is applicable to homogeneous and composite geometries with perfect or imperfect contact. In Chapter 2, the multinode surface element method formulations for two arbitrary geometries in perfect (or imperfect) contact over part of their boundaries were developed and discussed. Through the use of piecewise uniform approximations of time and space variables, it was demonstrated how the integral equations presented in Chapter 1 can be transformed to a set of algebraic equations.

To show the flexibility and applicability of the method to two-dimensional homogeneous and composite bodies, the multinode surface element formulations developed in Chapter 2, were applied to three different problems given in Chapters 3, 4 and 5.

In Chapter 3, the SEM was employed to solve the problem of two semi-infinite bodies (initially at two different temperatures) that are suddenly brought together over a small circular region and insulated

elsewhere. The intrinsic thermocouple problem was investigated in Chapter 4. Values for the thermal constriction resistance of the contact area (in Chapter 3), and the interface heat fluxes and temperatures (in Chapters 3 and 4) were presented for complete range of dimensionless time. The results obtained from the SEM solutions had excellent agreement with existing analytical and numerical solutions. In Chapter 5, the method was further applied to the problem of a semi-infinite body with mixed boundary conditions of a step change of surface temperature over an infinite strip and insulated elsewhere, for which analytical solutions do not currently exist. It was found that the accuracy of results varies linearly with the size of element and the size of the time step used in the numerical computations.

For each of these problems the multinode surface element method performed very well. It was found that the heat flux and temperature at any point along the interface can be readily obtained utilizing this method. The method is most suitable for calculating interface temperatures and heat fluxes for the geometries connected over relatively small portion of their surface boundaries. The results obtained in Chapters 3, 4 and 5 showed that very high accuracy is attainable with a relatively small number of surface elements. This feature makes the surface element method superior to the alternative numerical methods such as FDM, FEM, or BIEM for the type of problems considered. In the SEM only the interface between the two geometries requires discretization as opposed to the discretization of the whole domain needed in the finite difference and finite element methods or discretization of the whole boundaries in the BIEM. This in turn reduces the size of the numerical calculations and computer time.

The advantage of considering only interface nodes requires,

however, that the "building blocks" (or kernels, or the "influence functions"), ϕ 's be known for the geometries under consideration. For many geometries the kernels are known or can be obtained by well-known analytical or numerical procedures.

The influence functions required for the geometries of Chapters 3 and 4 were obtained from the known solutions given in [33,35], while those needed in Chapter 5 were found from the exact solution for the problem of a semi-infinite body heated by a constant heat flux over half the surface which was presented in Chapter 6.

Three computer programs were written in the course of this research, RAN3, RAN4, and BBY9. (Documentation is available from the author.) Both uniform and nonuniform nodes can be employed in the programs. The programs have the capability of treating up to twenty interface nodes and can be applied to both symmetrical and nonsymmetrical geometries. They also can be adapted to be used for a number of different cases with different geometries, providing the proper influence functions, ϕ 's, are used. Because of the convolution behavior of the integral equations, the influence functions need to be calculated at each time step and stored for later use. This can result in a large computational effort, particularly if the number of the time steps (NTS) is large. However, it was found that (see Chapter 5) in most cases (except for very early times, $t^+ < .001$) a value of NTS between twenty to forty can produce very accurate results. It was further shown that for large times ($t^+ > 10$), even a few time steps (≈ 5) can provide good accuracy.

Further improvement in terms of capability, accuracy and computer time is needed in the multinode surface element method. The following recommendations are given for future work:

1. Though the method has been applied to the problems with linear

boundary conditions it can be used for nonlinear boundary conditions. In particular, the radiative boundary condition can be investigated.

2. The assumption of constant temperature and heat flux over each element and time interval as was done in this dissertation is not necessary and higher order interpolation functions (linear, quadratic, etc.) can be introduced to improve the accuracy.
3. Work is needed to explore new methods for reducing the computer time. One possibility is to use the Laplace transform technique to avoid the convolution behavior of the numerical computations.
4. New influence functions for more basic geometries (such as semi-infinite body heated by a constant heat flux over a rectangular area or infinite cylinder heated over a portion of its circumferential area) need to be derived.
5. The basic theory that is given in this dissertation is also applicable to three-dimensional problems and the problems with multiple interfaces. Some of these cases should be investigated.
6. Finally, the method can be extended to include some specific problems of convection heat transfer and fluid flow problems. This in turn will make the method more competitive with already existing numerical procedures.

APPENDICES

APPENDIX A

DERIVATION OF EQUATIONS (2.5.11a) AND (2.5.11b)

Equation (2.5.11a) can readily be obtained by considering for the first time step ($M = 1$), the vectors \bar{E} and \bar{F} (given by (2.5.8c) and (2.5.8d), respectively) are zero.

$$\bar{E} = \bar{F} = 0 \quad \text{for } M = 1 \quad (A1)$$

Substituting (A1) into (2.5.8b) and then its result in (2.5.10) yields

$$\bar{q}_1 = \bar{C}^{-1} \bar{T}_i \quad (A2)$$

which is the same as (2.5.11a).

To show how (2.5.11b) is derived, equation (2.5.9) is expanded for different values of M . By introducing (2.5.8b,c,d) into (2.5.9), for $M = 1, 2, 3, \dots$, one can write

$$\text{at } M = 1, \quad \bar{C} \bar{q}_1 = \bar{T}_i \quad (A31)$$

$$\text{at } M = 2, \quad \bar{C} \bar{q}_2 = \bar{T}_i + \bar{E} \mid_{\text{at } M=2} - \bar{F} \mid_{\text{at } M=2} \quad (A32)$$

$$\text{at } M = 3, \quad \bar{C} \bar{q}_3 = \bar{T}_i + \bar{E} \mid_{\text{at } M=3} - \bar{F} \mid_{\text{at } M=3} \quad (A33)$$

$$\text{at } M - 1, \quad \bar{C} \bar{q}_{M-1} = \bar{T}_i + \bar{E} \mid_{\text{at } M-1} - \bar{F} \mid_{\text{at } M-1} \quad (A3, M-1)$$

$$\text{at } M, \quad \bar{C} \bar{q}_M = \bar{T}_i + \bar{E} \mid_{\text{at } M} - \bar{F} \mid_{\text{at } M} \quad (A3M)$$

By adding all these equations together, (A31) through (A3M), and noticing that

$$\bar{E} \mid_{\text{at } M} = \bar{F} \mid_{\text{at } M-1} + \bar{\phi}_1 \bar{q}_{M-1} \quad (\text{A4})$$

it can be shown that

$$\bar{C} \left[\sum_{i=1}^M \bar{q}_i \right] = M \bar{T}_i + \bar{\phi}_1 \sum_{i=1}^{M-1} \bar{q}_i - \bar{F} \mid_{\text{at } M} \quad (\text{A5})$$

or

$$\bar{q}_M + \sum_{i=1}^{M-1} \bar{q}_i = M \bar{C}^{-1} \bar{T}_i + \bar{C}^{-1} \bar{\phi}_1 \sum_{i=1}^{M-1} \bar{q}_i - \bar{C}^{-1} \bar{F} \mid_{\text{at } M} \quad (\text{A6})$$

substituting for \bar{C} , \bar{F} , and $\bar{C}^{-1} \bar{T}_i$ from (2.5.8a), (2.5.8d), and (A2), respectively yields

$$\bar{q}_M = M \bar{q}_1 + \bar{B} \left[\sum_{i=1}^{M-1} \bar{q}_i \right] - \bar{C}^{-1} \bar{F} \quad (\text{A7})$$

Where the matrix \bar{B} is defined as

$$\bar{B} = \bar{H}^{-1} \bar{\phi}_1 \quad (\text{A8})$$

Equation (A7) is the same as (2.5.1b) and is valid for $M \geq 2$. Notice that the vector \bar{F} is a function of time and should be calculated at each time step.

APPENDIX B

EVALUATION OF $I(r^+, b^+)$ GIVEN BY (3.4.5b)

A new method is developed to evaluate the values of $I(r^+, b^+)$ given by

$$I(r^+, b^+) = \sum_{i=1}^{\infty} \frac{J_0(\lambda_i r^+/b^+) J_1(\lambda_i/b^+)}{[\lambda_i J_0(\lambda_i)]^2} \quad (B1)$$

To evaluate this term effectively the summation is divided into two different parts:

$$I(r^+, b^+) = I_1(r^+, b^+) + I_2(r^+, b^+) \quad (B2a)$$

where

$$I_1(r^+, b^+) = \sum_{i=1}^{I_{\max}-1} \frac{J_0(\lambda_i r^+/b^+) J_1(\lambda_i/b^+)}{[\lambda_i J_0(\lambda_i)]^2} \quad (B2b)$$

and

$$I_2(r^+, b^+) = \sum_{i=I_{\max}}^{\infty} \frac{J_0(\lambda_i r^+/b^+) J_1(\lambda_i/b^+)}{[\lambda_i J_0(\lambda_i)]^2} \quad (B2c)$$

The first term in (B2a), I_1 , is evaluated by direct series expansion. The second term (the correction term or the tail of the summation), I_2 , can be simplified in the following manner.

For large values of λ_i one can write [34]

$$\lambda_i \approx i \pi + \frac{\pi}{4} \quad (B3)$$

$$J_0(\lambda_i) \approx \left(\frac{2}{\pi\lambda_i}\right)^{1/2} \cos\left(\lambda_i - \frac{\pi}{4}\right) = \left(\frac{2}{\pi\lambda_i}\right)^{1/2} (-1)^i \quad (\text{B4})$$

$$J_0(\lambda_i r^+ / b^+) \approx \left(\frac{2b^+}{\pi\lambda_i r^+}\right)^{1/2} \cos\left(\lambda_i r^+ / b^+ - \frac{\pi}{4}\right) \quad (\text{B5})$$

and

$$\begin{aligned} J_1(\lambda_i / b^+) &\approx \left(\frac{2b^+}{\pi\lambda_i}\right)^{1/2} \cos\left(\lambda_i / b^+ - \frac{3\pi}{4}\right) \\ &= \left(\frac{2b^+}{\pi\lambda_i}\right)^{1/2} \sin\left(\lambda_i / b^+ - \frac{\pi}{4}\right) \end{aligned} \quad (\text{B6})$$

Substituting (B3) through (B6) into (B2c) yields

$$I_2(r^+, b^+) \approx 2 \sum_{i=I_{\max}}^{\infty} \frac{b^+}{(r^+)^{1/2}} \frac{\cos\left(\lambda_i r^+ / b^+ - \frac{\pi}{4}\right) \sin\left(\lambda_i / b^+ - \frac{\pi}{4}\right)}{\lambda_i^2}$$

or

$$\begin{aligned} I_2(r^+, b^+) &\approx \frac{b^+}{(r^+)^{1/2}} \sum_{i=I_{\max}}^{\infty} \frac{\sin\left(\frac{1-r^+}{b^+} \lambda_i\right)}{\lambda_i^2} \\ &\quad - \frac{\cos\left(\frac{1+r^+}{b^+} \lambda_i\right)}{\lambda_i^2} \end{aligned} \quad (\text{B7})$$

From the composite midpoint rule in numerical analysis one can show that

$$\sum_{i=I_{\max}}^{\infty} f(\lambda_i) = \frac{1}{\pi} \int_{\lambda_{\max}}^{\infty} f(\lambda) d\lambda + \frac{f(\lambda_{\max})}{2} \quad (\text{B8})$$

Introducing (B8) into (B7) yields

$$I_2(r^+, b^+) \approx \frac{b^+}{\pi(r^+)^{1/2}} \left[\int_{\lambda_{\max}}^{\infty} \frac{\sin A\lambda}{\lambda^2} d\lambda - \int_{\lambda_{\max}}^{\infty} \frac{\cos B\lambda}{\lambda^2} d\lambda \right] + \frac{J_0(\lambda_{\max} r^+/b^+) J_1(\lambda_{\max}/b^+)}{[\lambda_{\max} J_0(\lambda_{\max})]^2} \quad (B9)$$

where

$$A = \frac{1-r^+}{b^+}, \quad B = \frac{1+r^+}{b^+} \quad (B10, a, b)$$

The integrals on the right hand side of (B9) can be evaluated as

$$\int_{\lambda_{\max}}^{\infty} \frac{\sin A\lambda}{\lambda^2} d\lambda = \frac{\sin(A\lambda_{\max})}{\lambda_{\max}} - A \text{Ci}(A\lambda_{\max}) \quad (B11a)$$

$$\int_{\lambda_{\max}}^{\infty} \frac{\cos B\lambda}{\lambda^2} d\lambda = \frac{\cos(B\lambda_{\max})}{\lambda_{\max}} + B \text{Si}(B\lambda_{\max}) - \frac{B\pi}{2} \quad (B11b)$$

where $\text{Si}(\cdot)$ and $\text{Ci}(\cdot)$ are the sine and cosine integrals given by equations (5.2.8) and (5.2.9) of [34], respectively. Finally, substituting (B11a) and (B11b) into (B9) gives,

$$I_2(r^+, b^+) \approx \frac{1+r^+}{2(r^+)^{1/2}} + \frac{b}{\pi(r^+)^{1/2}} \left[\frac{\sin(A\lambda_{\max}) - \cos(B\lambda_{\max})}{\lambda_{\max}} \right] - \frac{1}{\pi(r^+)^{1/2}} [(1-r^+) \text{Ci}(A\lambda_{\max}) + (1+r) \text{Si}(B\lambda_{\max})] + \frac{J_0(\lambda_{\max} r^+/b^+) J_1(\lambda_{\max}/b^+)}{[\lambda_{\max} J_0(\lambda_{\max})]^2} \quad (B12)$$

As it can be seen from (B12), the correction term, I_2 , can readily be evaluated providing λ_{\max} , r^+ , and b^+ are known. To compare the new method presented here with the direct series expansion method, $I(r^+, b^+)$ was evaluated for values of $r^+ = .1$ and $b^+ = 10$ with four decimal places accuracy. It was found that the number of terms needed in the direct series expansion approach is about 6-7 times larger than those used in the new alternative method. This in turn reduces the size of the numerical calculations and computer time.

APPENDIX C

EVALUATION OF THE INTEGRAL IN EQUATION (6.3.11)

The integral in equation (6.3.11) can be written as

$$I = \int_Z^{\infty} \frac{1}{u^2} e^{-u^2} \operatorname{erfc} \left(\frac{u}{p} \right) du \quad (C1)$$

Integrating equation (C1) by parts, by letting

$$dw = \frac{1}{u^2} du \quad (C2a)$$

$$v = e^{-u^2} \operatorname{erfc} \left(\frac{u}{p} \right) \quad (C2b)$$

yields

$$\begin{aligned} I &= -\frac{1}{u} e^{-u^2} \operatorname{erfc} \left(\frac{u}{p} \right) \Big|_Z^{\infty} - \frac{2}{p(\pi)^{1/2}} \int_Z^{\infty} \frac{1}{u} e^{-u^2(1 + \frac{1}{p^2})} du \\ &- 2 \int_Z^{\infty} e^{-u^2} \operatorname{erfc} \left(\frac{u}{p} \right) du = \frac{1}{Z} e^{-Z^2} \operatorname{erfc} (X) \\ &- \frac{Z}{p(\pi)^{1/2}} \int_Z^{\infty} \frac{1}{u} e^{-u^2(1 + \frac{1}{p^2})} du - 2 \int_Z^{\infty} e^{-u^2} \operatorname{erfc} \left(\frac{u}{p} \right) du \end{aligned} \quad (C3)$$

where (6.3.10c) was used ($p = Z/X$).

By using the substitution of $u^2(1 + \frac{1}{p^2}) = y$ and interchanging the order of integration, the first integral in (C3) can be written as

$$II = \int_Z^{\infty} e^{-u^2(1 + \frac{1}{p^2})} du = \frac{1}{Z} \int_{Z^2+X^2}^{\infty} \frac{e^{-y}}{y} dy = \frac{1}{Z} E_1 (X^2+Z^2) \quad (C4)$$

It now remains to find an expression for the second integral on the

right hand side of (C3). By using the relation $\operatorname{erfc}(\cdot) = 1 - \operatorname{erf}(\cdot)$, the integral can be written as

$$\begin{aligned} \text{III} &= \int_Z^{\infty} e^{-u^2} du - \int_Z^{\infty} e^{-u^2} \operatorname{erfc}\left(\frac{u}{p}\right) du \\ &= \frac{(\pi)^{1/2}}{2} \operatorname{erfc}(Z) - \int_Z^{\infty} e^{-u^2} \operatorname{erf}\left(\frac{u}{p}\right) du \end{aligned} \quad (\text{C5})$$

By using the substitution of $\frac{u}{p} = y$ and interchanging the order of integration of the integral on the right hand side of (C5) one can write

$$\text{III} = \frac{(\pi)^{1/2}}{2} \operatorname{erfc}(Z) - p \int_X^{\infty} e^{-p^2 y^2} \operatorname{erf}(y) dy \quad (\text{C6})$$

substitute (C5) and (C4) into (C3) yields

$$\begin{aligned} \text{I} &= \frac{(\pi)^{1/2}}{Z} \operatorname{ierfc}(Z) - \frac{e^{-Z^2}}{Z} \operatorname{erf}(X) - \frac{1}{p(\pi)^{1/2}} E_1(X^2+Z^2) \\ &\quad + 2p \int_X^{\infty} e^{-p^2 y^2} \operatorname{erf}(y) dy \end{aligned} \quad (\text{C7})$$

Finally, using (C7) into (6.3.11) yields

$$\begin{aligned} T(X,Z) &= (\pi)^{1/2} \operatorname{ierfc}(Z) - e^{-Z^2} \operatorname{erf}(X) \\ &\quad - \frac{X}{(\pi)^{1/2}} E_1(X^2+Z^2) + 2pZ \int_X^{\infty} e^{-p^2 y^2} \operatorname{erf}(y) dy \end{aligned} \quad (\text{C8})$$

which is the same as equation (6.3.12).

LIST OF REFERENCES

LIST OF REFERENCES

1. Ozisik, M. N., Boundary Value Problems of Heat Conduction, International Textbook Co., Scranton, Pennsylvania, 1968.
2. Myers, E. G., Analytical Methods in Conduction Heat Transfer, McGraw-Hill, New York, 1971.
3. Zienkiewicz, O. C., The Finite Element Method, Third Edition, McGraw-Hill Book Co., London, 1977.
4. C. A. Brebbia, (Ed.), Recent Advances in Boundary Element Methods, Pentech Press, London, 1978.
5. P. K. Bannerjee and R. Butterfield, (Eds.), Developments in Boundary Element Methods - 1, Applied Science Publishers, London, 1979.
6. T. A. Cruse and F. J. Rizzo, (Eds.), Boundary-Integral Equation Method: Computational Applications in Applied Mechanics, American Society of Mechanical Engineers, New York, 1975.
7. C. A. Brebbia, The Boundary Element Method for Engineers, Pentech Press, London, 1978.
8. C. A. Brebbia and S. Walker, (Eds.), Boundary Element Techniques in Engineering, Butterworths & Co., London, 1980.
9. Schneider, G. E., "Thermal Constriction Resistance Due to Arbitrary Contacts on a Half-Space-Numerical Solution of the Dirichlet Problem," Progress in Astronautics and Aeronautics: Thermophysics and Thermal Control, Vol. 65, edited by R. Viskanta, New York, 1979, pp. 103-119.
10. Schneider, G. E. and LeDain, B. L., "The Boundary Integral Equation Method Applied to Steady Heat Conduction with Special Attention Given to the Corner Problem," AIAA paper No. 79-0176, presented at the 17th Aerospace Sciences Meeting, New Orleans, La., Jan. 15-17, 1979.
11. Khader, M. S., "Heat Conduction with Temperature Dependent Thermal Conductivity," presented at the 19th National Heat Transfer Conference, ASME paper No. 80-HT-4, 1980.
12. Khader, M. S. and Hanna, M. C., "An Iterative Boundary Integral Numerical Solution for General Steady Heat Conduction Problems," Journal of Heat Transfer, Vol. 103, pp. 26-31, Feb. 1981.

13. Rizzo, F. J. and Shippy, D. J., "A Method of Solution for Certain Problems of Transient Heat Conduction," AIAA Journal, Vol. 8, No. 11, Nov. 1970, pp. 2004-2009.
14. Shaw, R. P., "An Integral Equation Approach to Diffusion," International Journal of Heat and Mass Transfer, Vol. 17, pp. 693-699, 1974.
15. Chang, Y. P., Kang, C. S., and Chen, D. J., "The Use of Fundamental Green's Functions for the Solution of Problems of Heat Conduction in Anisotropic Media," Journal of Heat and Mass Transfer, Vol. 16, 1973, pp. 1905-1918.
16. Wrobel, L. C. and Brebbia, C. A., "A Formulation of the Boundary Element Method for Axisymmetric Transient Heat Conduction," International Journal of Heat and Mass Transfer, Vol. 24, No. 5, pp. 843-850, 1981.
17. Yovanovich, M. M., and Martin, K. A., "Some Basic Three-Dimensional Influence Coefficients for the Surface Element Method," AIAA paper No. 80-1491, AIAA 15th Thermophysics Conf., July 14-16, 1980, Snowmass, Co.
18. Keltner, N. R., Beck, J. V., "Unsteady Surface Element Method," J. of Heat Transfer, Vol. 103, No. 4, pp. 759-764, Nov. 1981.
19. Beck, J. V. and Keltner, N. R., "Transient Thermal Contact of Two Semi-Infinite Bodies over a Circular Area," Paper No. AIAA-81-1162, presented at AIAA 16th Thermophysics Conf., June 23-25, 1981, Palo Alto, CA, to be published in the Progress in Aeronautics and Astronautics Progress Series 1982.
20. Kays, W. M. and Crawford, M. E., Convective Heat and Mass Transfer, Second Edition, McGraw-Hill Book Co., New York, 1980.
21. Colladay, R. S., "Inverse Problems Related to Transient Convection in the Thermal Entrance Region between Parallel Plates," Ph.D. Dissertation, Department of Mechanical Engr., Mich. State University, 1969.
22. Carslaw, H. S. and Jaeger, J. C., Conduction of Heat in Solids, Cambridge University Press, Cambridge, 1959.
23. Strong, A. B., Schneider, G. E. and Yovanovich, M. M., "Thermal Constriction Resistance of a Disk with Arbitrary Heat Flux - Finite Difference Solution in Oblate Spheroidal Coordinates," AIAA progress in Astronautics and Aeronautics, "Heat Transfer with Thermal Control Application," MIT Press, Vol. 39, 1975, Editor, Dr. M. M. Yovanovich, University of Waterloo.
24. Normington, E. G. and Blackwell, J. U., "Transient Heat Flow from Constant Temperature Spheroids and the Thin Circular Disk," Quarterly Journal of Mechanics and Applied Mathematics, Vol. 17, Part 1, pp. 65-72, 1964.

25. Blackwell, J. H., "Transient Heat Flow from a Thin Circular Disk Small-Time Solution," Journal Australian Math. Soc., Vol. 14, pp. 433-442, 1972.
26. Keltner, N. R., "Transient Heat Flow in Half-Space Due to an Isothermal Disk on the Surface," J. Heat Transfer, Vol. 95, Ser. 3, No. 3, pp. 412-414, 1973.
27. Keltner, N. R., Heat Transfer in Intrinsic Thermocouples Application to Transient Measurement Errors, Report SC-RR-72-0719, Sandia National Laboratories, Albuquerque, NM, January 1973.
28. Schneider, G. E., Strong, A. B. and Yovanovich, M. M., "Transient Heat Flow from a Thin Circular Disk," AIAA 10th Thermophysics Conference, Denver, Colorado, May 27-29, 1975, AIAA paper No. 75-707.
29. Marder, B. M. and Keltner, N. R., "Heat Flow from a Disk by Separation of Variables," Numerical Heat Transfer, Vol. 4, pp. 485-497, 1981.
30. Heasley, J. H., "Transient Heat Flow between Contacting Solids," Int. J. Heat Mass Transfer, Vol. 8, 147-154, 1965.
31. Schneider, G. E., Strong, A. B., and Yovanovich, M. M., "Transient Thermal Response of Two Bodies Communicating through a Small Circular Contact Area," Int. J. Heat Mass Transfer, Vol. 20, pp. 301-108, 1977.
32. Sadhal, S. S., "Transient Thermal Response of Two Solids in Contact over a Circular Disk," Int. J. Heat Mass Transfer, Vol. 23, pp. 731-733. 1980.
33. Beck, J. V., "Large Time Solutions for Temperatures in a Semi-Infinite Body with a Disk Heat Source," Int. J. Heat Mass Transfer, Vol. 24, pp. 155-164, 1981.
34. Abramowitz, M. and Stegun, I. A., Handbook of Mathematical Functions with Formulas, Graphs and Mathematical Tables, National Bureau of Standards, Applied Mathematics Series, Vol. 55, 1964.
35. Beck, J. V., "Transient Temperatures in a Semi-Infinite Cylinder Heated by a Disk Heat Source," Int. J. Heat Mass Transfer, Vol. 24, No. 10, pp. 1631-1640, 1981.
36. Burnett, D. R., "Transient Measurement Errors in Heated Slabs for Thermocouples Located at an Insulated Surface," Journal of Heat Transfer, Trans. ASME, Series C. Volume 83, p. 505, 1961.
37. Larson, M. B., "Time-Temperature Characteristics of Thin-Skinned Models as Affected by Thermocouple Variables," University of North Dakota, 1967. Published as NASA-CR-91453.

38. Larson, M. B. and E. Nelson, "Variables Affecting the Dynamic Response of Thermocouples Attached to Thin-Skinned Models," Journal of Heat Transfer, Trans. ASME, Series C., Volume 91, p. 166, 1969.
39. Henning, C. D. and R. Parker, "Transient Response of an Intrinsic Thermocouple," Journal of Heat Transfer, Trans. ASME, Series C, Volume 39, p. 146, 1967.
40. R. Parker, "Rapid Phase Transformations in Titanium Induced by Pulse Heating," Transactions of the Metallurgical Society of AIMI, pp. 1545-1549, August, 1965.
41. Shewen, E. C., "A Transient Numerical Analysis of Conduction between Contacting Circular Cylinders and Halfspaces Applied to a Biosensor," MS Thesis, University of Waterloo, 1976.
42. Geidt, W. H. and Nunn, R. H., comments given in reference [39].
43. Bickle, L. W., "A Time Domain Deconvolution Technique for the Correction of Transient Measurements," Report SC-RR-710658, Sandia Laboratories.
44. Bickle, L. W. and Keltner, N. R., "Techniques for Improving Effective Response Times of Intrinsic Thermocouples," Report SC-RR-710146, Sandia Laboratories (Sept. 1971).
45. Sadhal, S. S., "Unsteady Heat Flow Between Solids with Partially Contacting Interface," J. of Heat Transfer, Vol. 103, pp. 33-35, Feb. 1981.
46. Schapery, R. A., "Approximate Methods of Transform Inversion for Viscoelastic Stress Analysis," Proceedings of the Fourth U.S. National Congress of Applied Mechanics, pp. 1075-1085, 1961.
47. Jaeger, J. C., "Approximations in Transient Surface Heating," Australian Journal of Scientific Res., Ser. A, S, pp. 1-9, 1952.
48. Grimado, P. B., "The Transient Temperature Field in a Composite Semi-Space Resulting from an Incident Heat Flux," Quarterly of Applied Mathematics, Vol. XXXI, No. 4, Jan. 1974.
49. Rosser, J. Barkley, Theory and Applications of $\int_0^z e^{-x^2} dx$ and $\int_0^z e^{-p^2 y^2} dy \int_0^y e^{-x^2} dx$ Mapleton House, Brooklyn, NY, 1948.
50. Beck, J. V., "Average Transient Temperature within a Body Heated by a Disk Heat Source," Heat Transfer, Thermal Control and Heat Pipes, W. B. Oland, Ed., Vol. 70, Progress in Astronautics and Aeronautics, pp. 3-24, 1980.

MICHIGAN STATE UNIVERSITY LIBRARIES



3 1293 03145 6720